CHAPTER ONE

Introduction

1.1. Background

Extrusion is a continuous process where solid polymeric materials, either pellets or powders, are sheared and heated as they are conveyed through either a single or a twin-screw extruder to become a pressurized melt. The pressurized melt flows through a properly shaped orifice or extrusion die, and then is pulled (with a little pressure) as it is cooled and shaped to a final product called the extrudate shown in Fig (1.1).

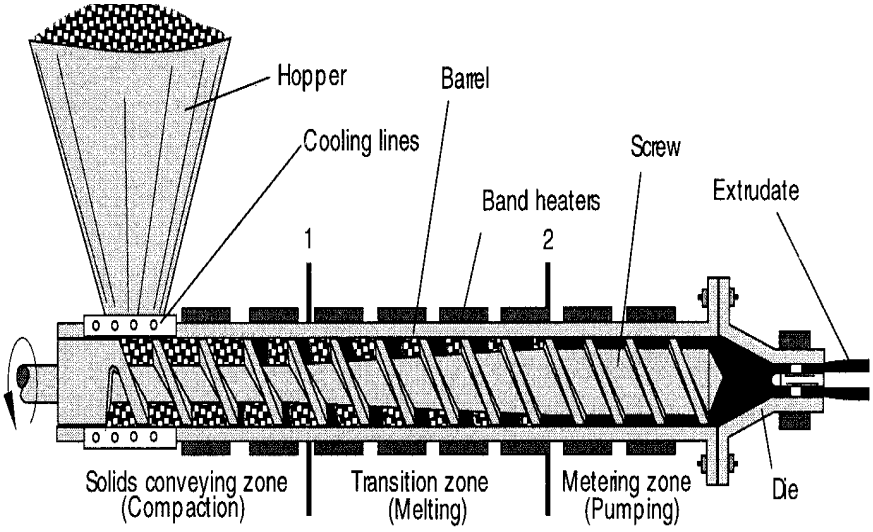

Fig. 1.1: Single screw extruder processing

Several unique products are made by extrusion and the dies needed to make these products are classified as: 1) sheet dies; 2) flat-film and blown-film dies; 3) pipe and tubing dies; 4) profile extrusion dies; and 5) co-extrusion dies. Furthermore, each product type has unique hardware downstream of the die to shape and cool the extruded melt (Kostic and Reifschneider, 2006) .

The plastics engineer has therefore to deal with the melt rheology, which describes the flow behavior and deformation of the melt. Thus, the design of machines and dies for polymer extrusion processing requires quantitative description of the properties related to polymer melt flow. Starting from the relationships for Hookean solids, formulae describing viscous shear flow of the melt are treated first and formulae describing extrusion machinery and dies design(Osswald and Hernández-Ortiz, 2006).

The complete master curve (rheogram) depicting the variation of the melt viscosity over the industrially relevant range of shear rates and temperature is essential in the design of polymer processing equipment, process optimization, and troubleshooting.

The flow parameter that is readily accessible to most processers is the melt flow index (MFI). The MFI is either specified by the thermoplastics raw material supplier or can be easily measured using a relatively inexpensive apparatus. It is a single-point viscosity measurement at a relatively low shear rate and temperature(Shenoy and Saini, 1996).

The method of the applicability of MFI instrument for rheological measurements by the determination of viscosity of thermoplastic polymer melts then drawing the master curve (viscosity vs. shear rate) of polymer(MFI, 2007).

Die design for a new product is developed on the basis of previous experience and experimentation. In many case costly experiments and in-plant trials can be replaced by numerical simulation.Several commercial polymer flow simulation programs are used for extrusion die design today. For example: Ansys Polyflow, Flow 2000,NEXTRUCAD Dieflow, HyperXtrude,Compuplast .

Numerical simulation has the potential to uncover important interior details of the extrusion process, such as velocity, shear stress, pressure, and temperature fields in the region of interest, which is not possible to do experimentally.(Kostic and Reifschneider, 2006)

The carried research and obtained data will be the basis of modeling of extrusion process using Ansys Polyflow program. It enables simulation flow viscous and viscoelastic behavior. This program use equations of conservation of mass, momentum and energy, and also of various rheological models describing material properties and behavior during processing. (Pepliński and Mozer, 2011)

Ansys Polyflow is a finite-element computational fluid dynamics (CFD) program designed primarily for simulating applications where viscous and viscoelastic flows play an important role. The flows can be isothermal or non-isothermal, two- or three-dimensional, steady-state or time-dependent. Ansys Polyflow is used primarily to solve flow problems in polymer and rubber processing, food rheology, glasswork furnaces, and many other rheological applications. The calculation of such flows is based on non-Newtonian fluid mechanics, characterized by a wide variety of fluid models and strong nonlinearities. The development of Ansys Polyflow is intimately linked to progresses in numerical simulation of non-Newtonian fluid mechanics; the most recent and best-performing algorithms are incorporated in Ansys Polyflow on a regular basis. The selection of constitutive models available in Ansys Polyflow is also based on current research in the area, it can also be used to solve chemically reacting flows. Transport of species as well as chemical reactions that act as sources or sinks of materials can be included. It is possible to detect contact during ANSYS POLYFLOW simulations. This capability makes ANSYS

POLYFLOW useful for blow molding, thermoforming, and compression molding simulations. A major advantage is that access to a library of non-Newtonian materials is maintained for all contact problems. ANSYS POL YFLOW also provides additional capabilities for glass furnaces, such as bubbling, radioactive correction, and electrical heating.

It can perform a number of complex calculations such as multi domain simulations, co-extrusion of several fluids, three-dimensional extrusion, and implicit and time-dependent calculation of free surfaces (Ansys, 2012)

1.2. Statement of problem

The problem of this work is how to choose the best viscosity model or master curve (viscosity versus shear rate) with minimum error in actual fitting data of melt viscosity and shear rate obtained from MFI instrument.

Several authors have shown that a master curve can be generated especially for many individual types of polymers by plotting $\mu \times MFI$ versus $\dot{\gamma}/MFI$ on a log-log scale (Vlachopoulos and Strutt, 2003)

Therefore, at the first part of the research a proposed of a new easy technique has been developed to use of least square procedures (percentage roots mean square error PRMSE) and Ansys Polyflow software to select best viscosity model for polypropylene.

The technique help designers and engineers to design or simulate the plastic machines and molds and dies in order to get accurate results.

Some authors have shown that how to simulate single screw extrusion using Polyflow to different zones. The melting zone (Feng and Qu). Sold convening and metering zones for Starch-Based Snack Products (Yamsaengsung and Noomuang, 2010)

others authors show how to use Polyflow for the design ,the balance and optimization of different extruder dies (profiles die (Vaddiraju et al.,

2004),(Pepliński and Mozer, 2011), Slit die(Fedi-Soetaredjo et al., 2003), flat-film dies(Patrick C. Lee, 2011), Co extrusion die(Dooley et al.)and blow molding die(Pepliński and Mozer, 2010)

But none of them study the extruder maximum output and pressure drop across the die. There are many parameters that can affect to the extruder output and the pressure drop .in this research these subject are studied using computer packages and analytical calculations and the results of the two methods are compared.

1.3. Objectives

- To select the optimum viscosity model that fit the experimental data obtained for PP113 product of Khartoum Petrochemical Company at isothermal conditions 230^{o}C.
- To use viscosity obtained from the model in the analytical calculations as well as in the simulation software.
- To perform analytical solution for single extruder metering zone and for the extruder with the die coupled to it was accomplished.
- To study the effect on die characteristic line due to entrance angle, die land and die radius was studied.
- To study the effect on extruder characteristic line due to flight width, flight clearance, flight depth, screw speed and screw length and the effect of the nose on this line.
- Selected the optimum operation point
- Compare the results of analytical calculation and computer simulation.

CHAPTER TWO

Literature Review

2.1. Polymer materials

Plastic materials have become an essential part in all aspect of today's recent life. Plastics are replacing most of the materials today due to good mechanical, chemical and thermal properties. Plastics are found on various products ranging from housing appliances, telecommunication equipment, electronics product, clothing and commercial market. One of the reasons for the great popularity of plastics in a wide variety of industrial applications is the great range of properties exhibited by plastics and their ease of processing(Yunus and Yusri, 2010).

2.2. Extrusion operation

An extruder is a plastics manufacturing unit operation that is used to produce thermoplastic polymers with a uniform cross section, such as pipe, hose, sheet, film and profiles. Since extruders also produce the polymer pellets that are used by other polymer processing operations (such as film blowing, injection molding and blow molding), almost all plastic material produced worldwide has passed through an extruder at least once

The plastic, usually in the form of granules or powder, is fed from a hopper on to the screw. It is then conveyed along the barrel where it is heated by conduction from the barrel heaters and shear due to its movement along the screw flights(Muccio, 1994)

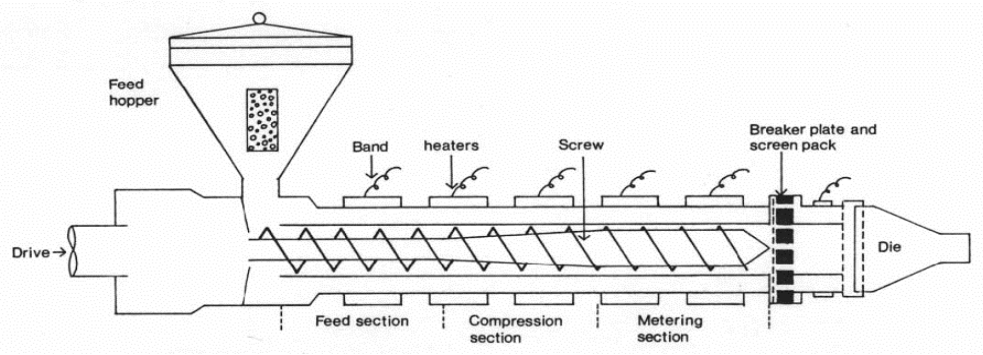

Fig. 2.1: Extruder Sections(Vaddiraju et al., 2004)

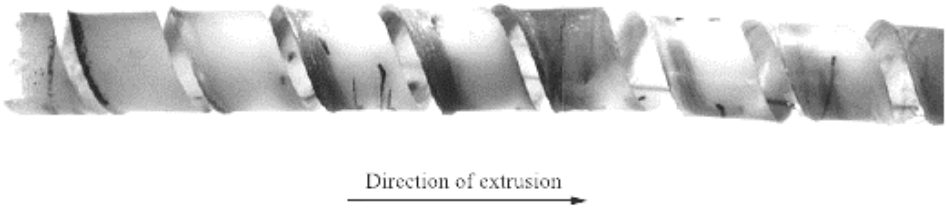

Fig. 2.2: Polymer melt in screw(Vaddiraju et al., 2004)

2.3. Extrusion Screws

2.3.1 Single Extrusion Screw

1. Screw

The screw is machined out of a solid rod. Like a shaft with helical screw on it, each turn of the helix is called a flight.

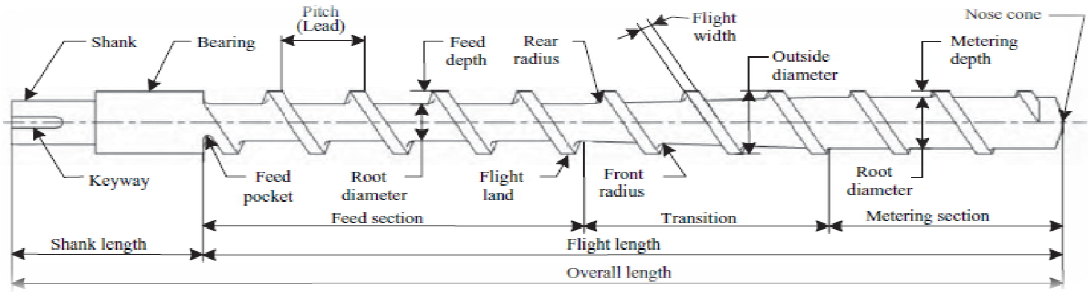

Fig. 2.3: Single screw section(SULAIMAN, 2011)

Important parameter = L/D of the screw (length of the flighted portion of the screw/ inside diameter of the barrel), it is measures the capability of the screw to mix materials and ability of the screw to melt hard-to-melt material. Typical L/D ratios are 16:1 to 32:1.

Barrel diameter is constant over the entire length of the extruder

The root is the measure of the diameter of the shaft of the screw (the root diameter can vary along the length of screw)

The flight rise above the shaft creating a flight depth (difference between top of the flight and the root diameter)

As the root diameter changes, the flight depth will correspondingly change (if the root diameter is small, the flight depth are large and vice versa.(SULAIMAN, 2011)

2. Screw zones

The extruder screw has three geometrically different zones whose functions can be described as follows:

a) Feed zone: transport and preheating of the solid material
b) Transition zone :compression and plastication of the polymer
c) Metering zone melt conveying, melt mixing and pumping of the melt to the die.

3. Deferent screw types

To perform these processing operations optimally screws of varied geometry are used.

a. Higher melting capacities compared to the three zone screws are achieved with screws having shearing and mixing devices.
b. Barrier type screws enable the separation of solids polymer from the melt, and thus lead to lower and constant melt temperatures over a wide range of screw speeds.

c. Devolatilizing screws are applied to extract volatile components from the melt.

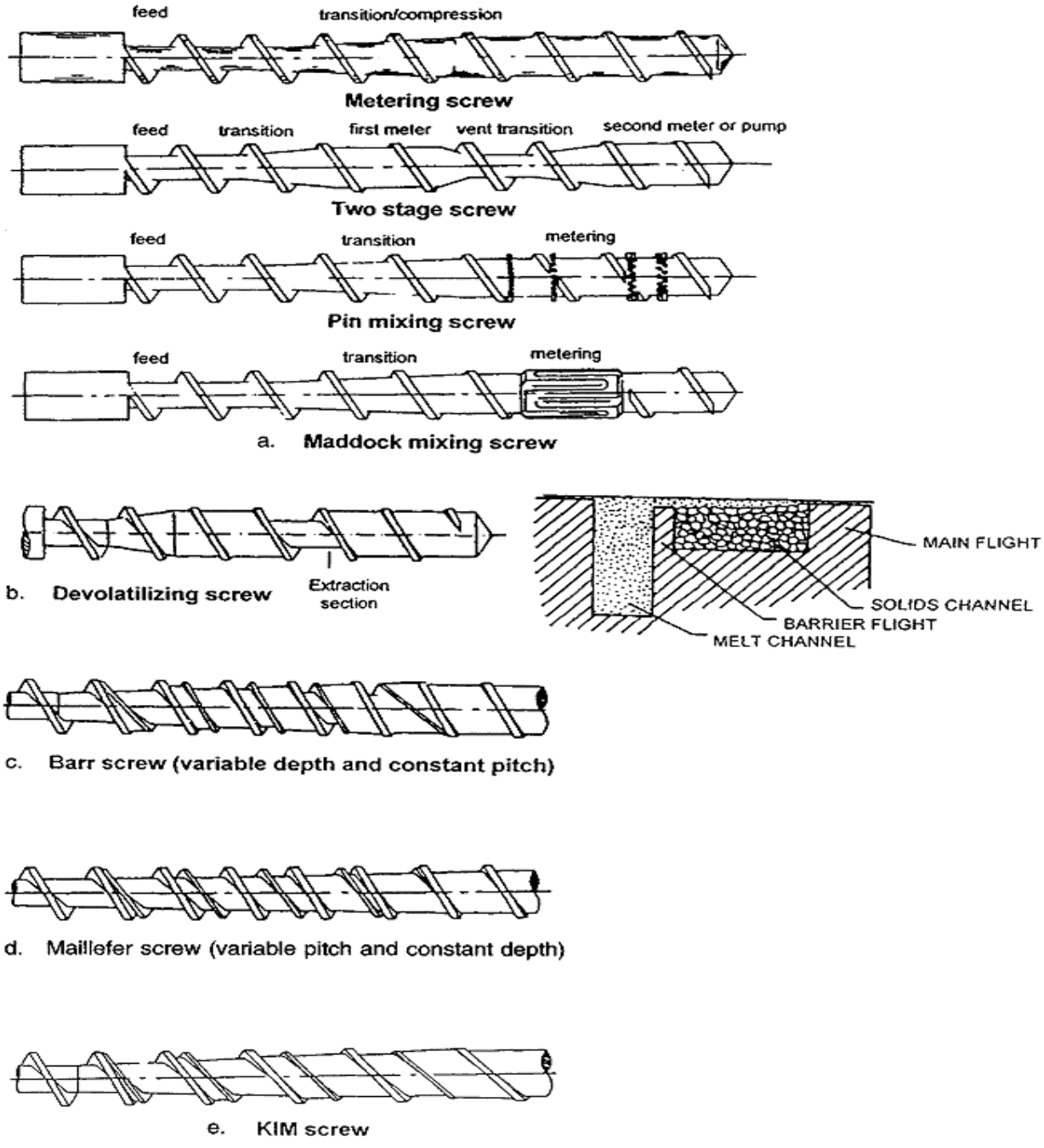

Fig. 2.4: Geometries of some single screws(Rao and O'Brien, 1998)

2.3.2 Twin screw extruders

Are mainly used in the compounding of polymers, for example, in the pelletizing and compounding of poly vinyl chloride.

The positive conveying characteristics of the twin screw extruders are achieved by forcing the material to move in compartments formed by the two screws and the barrel.

The degree of intermeshing between the flight of one screw and the channel of the other screw, sense of rotation and speed distinguish the different kinds of screws from one another.

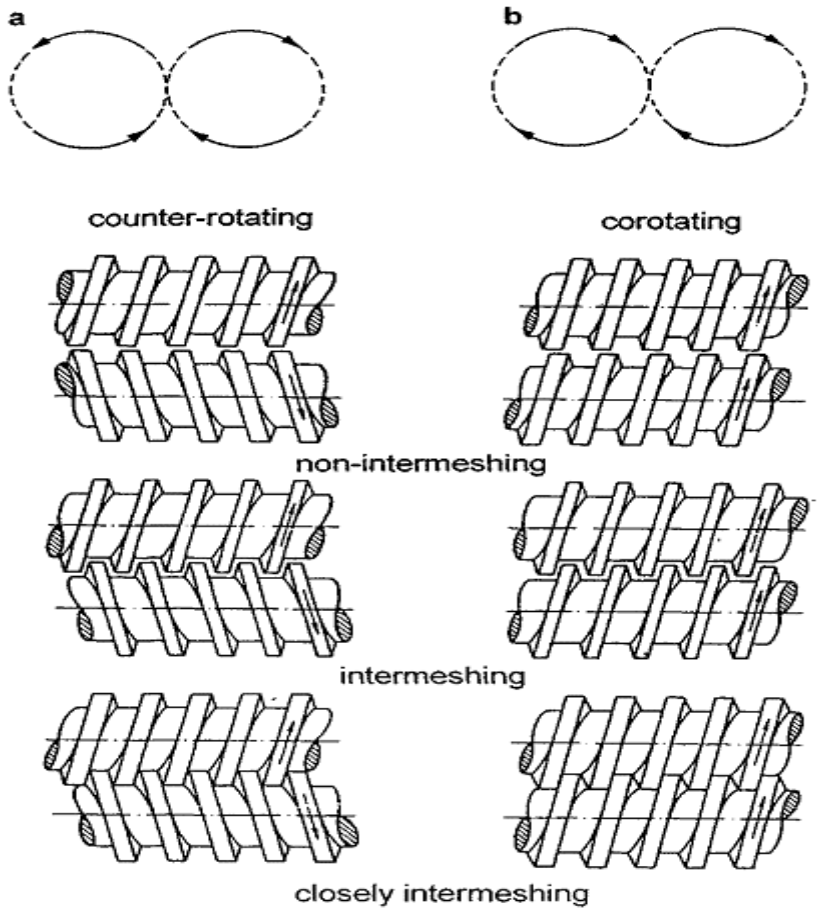

Fig. 2.5: Geometries of some twin screws(Rao and O'Brien, 1998)

2.4. Extrusion processing parameters

The factors affecting extrusion can be classified into

2.4.1 Resin-dependent parameters.

Resin-dependent parameters are not constants which one obtains bymeasuring the physical properties of the polymeric materials. The melt temperature and pressure are important which affect thequality of the product, and depend not only on the type of the resin but also onthe grade of the resin used, values of melt temperature and pressures for different materials in blown film, pipe extrusion, flat film extrusion, sheet extrusion and wire coating located in this reference.

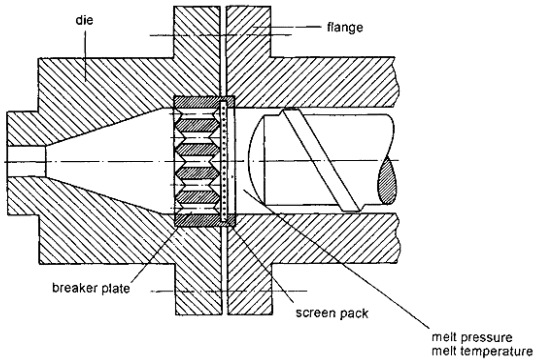

Fig. 2.6: Position of measurement of melt pressure and melt temperature(Rao and O'Brien, 1998)

2.4.2 Machine related parameters

They are more influenced by the geometry of the machine such as extrusion screw and die than by resin properties. For single screw extrusion illustrate the influence of the geometry of machinery on the target quantities of the process.

2.5. Single-screw extrusion the extruder output

Depending on the type of extruder the output is determined either by the geometry of the solids feeding zone alone as in the case of a grooved extruder or the solids and melt zones to be found in a smooth barrel extruder.

2.5.1 Extruder output according to Feeding zone

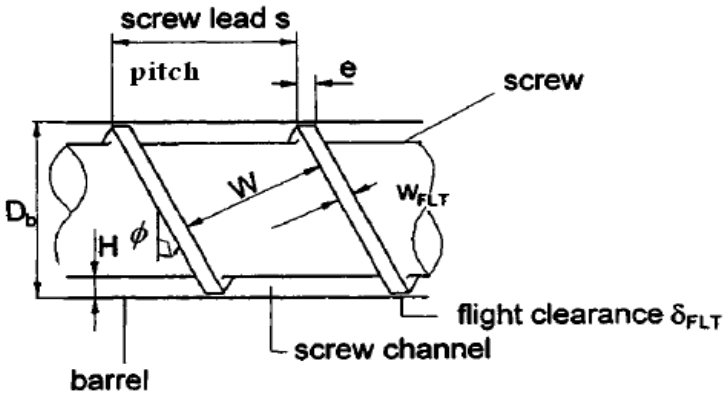

Fig. 2.7: Screw parts(Rao and O'Brien, 1998)

$$\dot{m_{feed}}\left(\frac{kg}{h}\right) = 60 \times \rho_b . N . \mu_F . \pi^2 . H . D_b (D_b - H) \frac{W}{W + w_{FLT}} . sin\emptyset cos\emptyset \quad ---(2.1)$$

$$\emptyset = tan^{-1}\frac{s}{\pi D} = tan^{-1}\frac{pitch\ or\ lead}{\pi D} \quad ---(2.2)$$

Where:

Helix angle $\emptyset$

Barrel diameter D_b

Screw lead (pitch) s

Number of flights v

Flight width at direction of flow W_{FLT}

Channel width at direction of flow W

Flight depth of the feed zone H

Conveying efficiency μ_F

Screw speed N

Bulk density of the polymer ρ_b

The conveying efficiency μ_F as defined here is the ratio between the actual extrusion rate and the theoretical maximum extrusion rate attainable under the assumption of no friction between the solid polymer and the screw. It depends on

- the type of polymer,
- bulk density,
- barrel temperature,
- Friction between the polymer, barrel and the screw(Rao and O'Brien, 1998).

2.5.2 Extruder output according to metering zone

The metering zone to develop the pressure needed to force the melt through the shaping die.

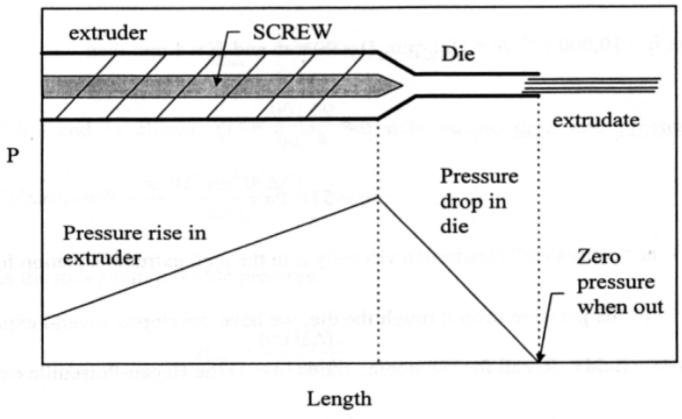

Fig. 2.8: Pressure buildup in screw

The derivation of the equation for output assumes that in the metering zone the melt has a constant viscosity and its flow is isothermal in

a wide shallow channel. These conditions are most likely to be approached in the metering zone.

The output from the extruder as consisting of three components flow

1) **Drag flow**
2) **pressure flow**
3) **Leakage flow**

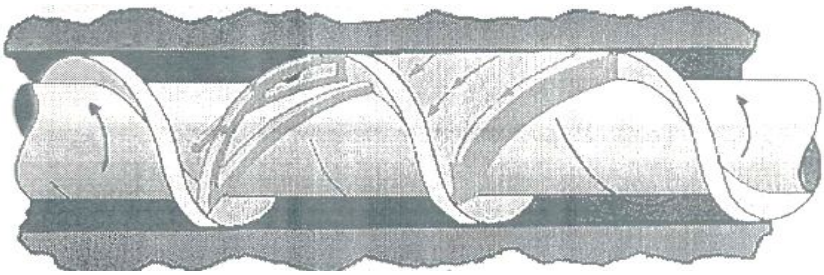

Fig. 2.9: Flow path along a channel

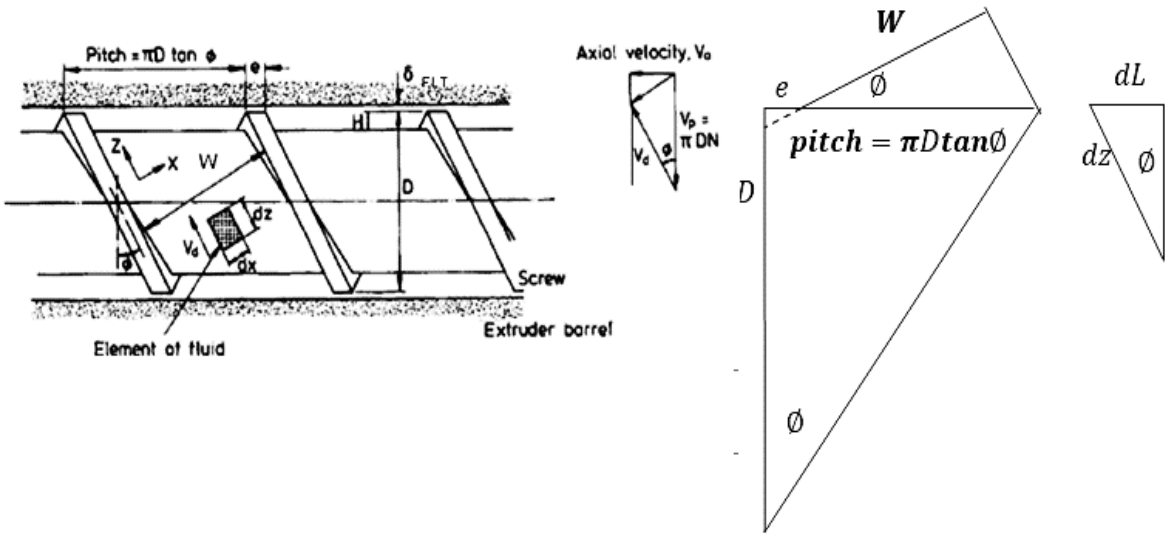

Fig. 2.10: Flow in metering zone

1) **Drag flow**

Derivation of drag flow: Consider the flow of the melt between parallel plates as shown in below Fig.

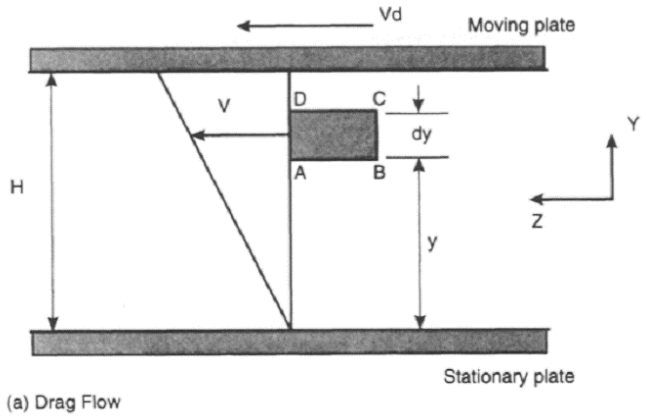

Fig. 2.11: Drag flow analysis

AB = dz, element width = dx and channel width = W

- For the small element of fluid ABCD the volume flow rate *d Q* is given by:

$$dQ = V.dy.dx - - - (2.3)$$

- Assuming the velocity gradient is linear, then

$$V = V_d\left[\frac{y}{H}\right] - - - (2.4)$$

- Substitute Eq (2.4) in Eq (2.3)and integrating over the channel depth, H, then the total drag flow, Q_d, is given by Eq (2.5).

$$Q_d = \int_0^H \int_0^W \frac{V_d y}{H}.dy.dx$$

$$Q_d = \frac{1}{2}WHV_d - - - (2.5)$$

This may be compared to the situation in the extruder where the fluid is being dragged along by the relative movement of the screw and barrel.

- The Drag velocity

$$V_d = \pi DNcos\emptyset_b - - - (2.6)$$

Where N is the screw speed (in revolutions per min).

$$W = (\pi Dtan\emptyset - e)cos\emptyset - - - (2.7)$$

- Substitute Eq (2.6) and Eq (2.7)in Eq (2.5).

$$Q_d = \frac{1}{2}(\pi D tan\emptyset - e) cos\emptyset . H . \pi DN cos\emptyset - - - (2.8)$$

$$Q_d = \frac{1}{2}\pi^2 D^2 NH sin\emptyset cos\emptyset \left(1 - \frac{e}{\pi D tan\emptyset}\right) - - - (2.9)$$

The shear rate in the metering zone:

$$\dot{\gamma} = \frac{dV}{dy} = \frac{V_P}{H} = \frac{\pi DN}{H} - - - (2.10)$$

The shear stress (Newtonian fluid) in the metering zone:

$$\tau = \mu \times \dot{\gamma} = \mu \times \frac{dV}{dt} = \mu \times \frac{V_P}{H} = \mu \times \frac{\pi DN}{H} - - - (2.11)$$

2) Pressure flow :

- Consider the element of fluid shown in below Fig. The forces are:

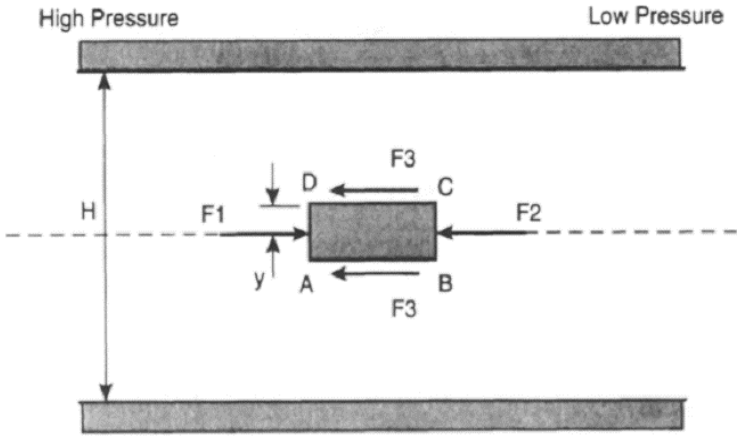

Fig. 2.12: Pressure flow analysis

$$F_1 = P_1 \cdot 2y . dx - - - (2.12)$$

$$F_2 = P_2 \cdot 2y . dx - - - (2.13)$$

$$F_3 = \tau_y \cdot dz . dx - - - (2.14)$$

Where P is pressure and τ is the shear stress acting on the element. For steady flow these forces are in equilibrium so they may be equated as follows:

$$F_1 = F_2 + 2F_3 - - - (2.15)$$

- Substitute Eqs(2.13,14 and 15) in Eq(2.16) This reduces to:

$$P_1 \cdot 2y.dx = P_2 \cdot 2y.dx + 2\tau_y \cdot dz.dx$$

$$y\frac{P_1 - P_2}{dz} = y\frac{dP}{dz} = \tau_y - - - (2.16)$$

- But Newton low for viscosity is:

$$\tau_y = \mu\frac{dV}{dy} - - - (2.17)$$

- substitute Eq(2.18) in Eq(2.17)

$$y\frac{dP}{dz} = \mu\frac{dV}{dy} - - - (2.18)$$

- Integrating Eq(2.18)

$$\int_0^V dV = \frac{1}{\mu}\int_{H/2}^{y} ydy$$

$$V = \frac{1}{\mu}\frac{dP}{dz}\left(\frac{y^2}{2} - \frac{H^2}{8}\right) - - - (2.19)$$

For the element of fluid of depth, *d y,* at distance, y, from the center line (and whose velocity is V) the elemental flow rate, *dQ,* is given by

$$dQ = VdA = 2VWdy - - - (2.20)$$

- Eq(2.20) be integrated to give the pressure flow, Q p

$$Q_p = 2W\int_0^{H/2}\left(\frac{1}{\mu}\frac{dP}{dz}\left(\frac{y^2}{2} - \frac{H^2}{8}\right)\right)dy$$

$$Q_p = -\frac{1}{12\mu}\frac{dP}{dz}WH^3 - - - (2.21)$$

- From the triangle in Fig(2.9)

$$\sin \emptyset = \frac{dL}{dz} \quad so \quad \frac{dP}{dL} = \sin \emptyset - - - (2.22)$$

The Eq (2.21) is reduced to the expression for Q_p after substitute Eq (2.22) becomes

$$Q_p = -\frac{\pi DH^3 \sin \emptyset^2}{12\mu}\left(1 - \frac{e}{\pi D tan\emptyset}\right).\frac{dP}{dL} - - - (2.23)$$

3) Leakage flow :

- The leakage flow may be considered as flow through a wide slit which has a depth, δ_{FLT}, a length (e cos$\emptyset_b$) and a width of *($\pi D/cos\emptyset_b$)*. Since this is a pressure flow, the derivation is similar to that described in (Pressure flow). For convenience therefore the following substitutions may be made in Eq(2.21)

$$Q_p = -\frac{1}{12\mu}\frac{dP}{dz}WH^3 - - - (2.21)$$

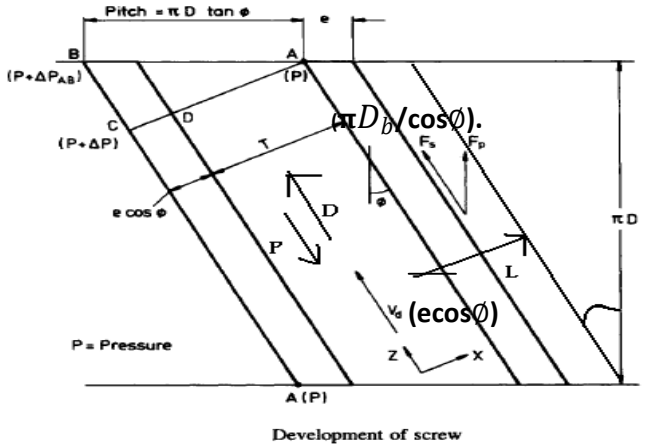

Development of screw

Fig. 2.13: Leakage flow analysis

$$H = \delta_{FLT} - - - (2.24)$$

$$W = \frac{\pi D}{cos\emptyset} - - - (2.25)$$

$$pressure\ gradient = \frac{dP}{ecos\emptyset} - - - (2.26)$$

So the leakage flow $Q_L, is\ given\ by$

$$Q_L = -\frac{\pi^2 D^2 {\delta_{FLT}}^2}{12\mu.e} tan\emptyset \frac{dP}{dL} - - - (2.27)$$

4) The total output and conditions

- The total output is the combination of drag flow, back pressure flow and leakage.

$$Q_{Total} = Q_d + Q_p + Q_L - - - (2.28)$$

$$Q_{Total} = \frac{1}{2}\pi^2 D^2 NHsin\emptyset cos\emptyset \left(1 - \frac{e}{\pi D tan\emptyset}\right) - \frac{\pi D H^3 \sin\emptyset^2}{12\mu}\left(1 - \frac{e}{\pi D tan\emptyset}\right).\frac{dP}{dL} - \frac{\pi^2 D^2 {\delta_{FLT}}^2}{12\mu.e} tan\emptyset \frac{dP}{dL} - - - (29)$$

Where:

D: Flight diameter

H: Flight depth

e: Flight width

δ_{FLT}: Flight clearance

L: Length of metering zone

Q_d, Q_p, Q_L: Volume flow rate of drag, pressure and Leakage flow, respectively

dP: Pressure difference across the metering zone

μ: Melt viscosity

N: Screw speed (rev/s)

- For many practical purposes sufficient accuracy is obtained by neglecting the leakage flow term and consider (e) is small
- In addition the pressure gradient is often considered as linear so

$$\frac{dP}{dL} = \frac{P}{L} - - - (2.30)$$

$$Q_{Total} = \frac{1}{2}\pi^2 \mathrm{D}^2 NH sin\emptyset cos\emptyset - \frac{\pi \mathrm{D} H^3 sin^2\emptyset}{12\mu} . \frac{P}{L} - - - (2.31)$$

Where 'L' is the length of the extruder.

- In the above analysis, it is the melt flow which is being considered and so the relevant pressure gradient will be that in the metering zone.
- If all other physical dimensions and conditions are constant then the variation of output with screw flight angle at the barrel, Øcan be studied. As shown in Fig (2.14). the maximum output would be obtained if the screw flight angle was about 35° In practice a screw flight angle of 17.65678715 ° is frequently used because
    1. This is the angle which occurs if the pitch of the screw is equal to the diameter and so it is convenient to manufacture.
    2. For a considerable portion of the extruder length, the screw is acting as a solids conveying device and it is known that the optimum angle in such cases is 17 ° to 20 °(Crawford, 1998).

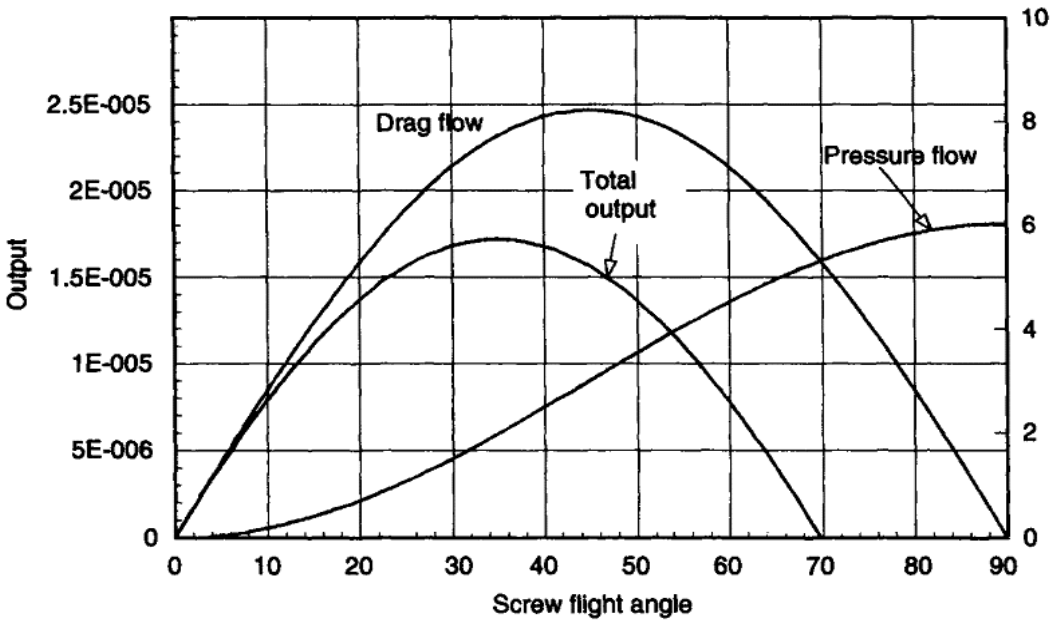

Fig. 2.14: Variation of drag flow and pressure flow

2.6. Single-screw extrusion and die characteristics

2.6.1 The extruder characteristic

From Total output Eq (2.31) it may be seen that there are two interesting situations to consider.

$$Q_{Total} = \frac{1}{2}\pi^2 \mathrm{D}^2 NH sin\emptyset cos\emptyset - \frac{\pi \mathrm{D} H^3 sin^2\emptyset}{12\mu} \cdot \frac{P}{L} - - - (2.31)$$

I. One is the case of free discharge where there is no pressure build up at the end of the extruder ($\frac{dP}{dL} = 0$) and e is small so

$$Q_{Total} = Q_d = Q_{max} = \frac{1}{2}\pi^2 D^2 NH sin\emptyset cos\emptyset - - - (2.32)$$

II. Where the pressure at the end of the extruder is large enough to stop the output ($Q_{Total} = 0$) and e is small(Crawford, 1998).

$$\therefore P_{max} = \frac{6\mu\pi \mathrm{D} NL}{H^2 tan\emptyset} - - (2.33)$$

With the help of Eq (2.29) the effect of different parameters on the extruder output is presented in Fig (2.15) by changing one variable at a time and keeping all other variables constant.

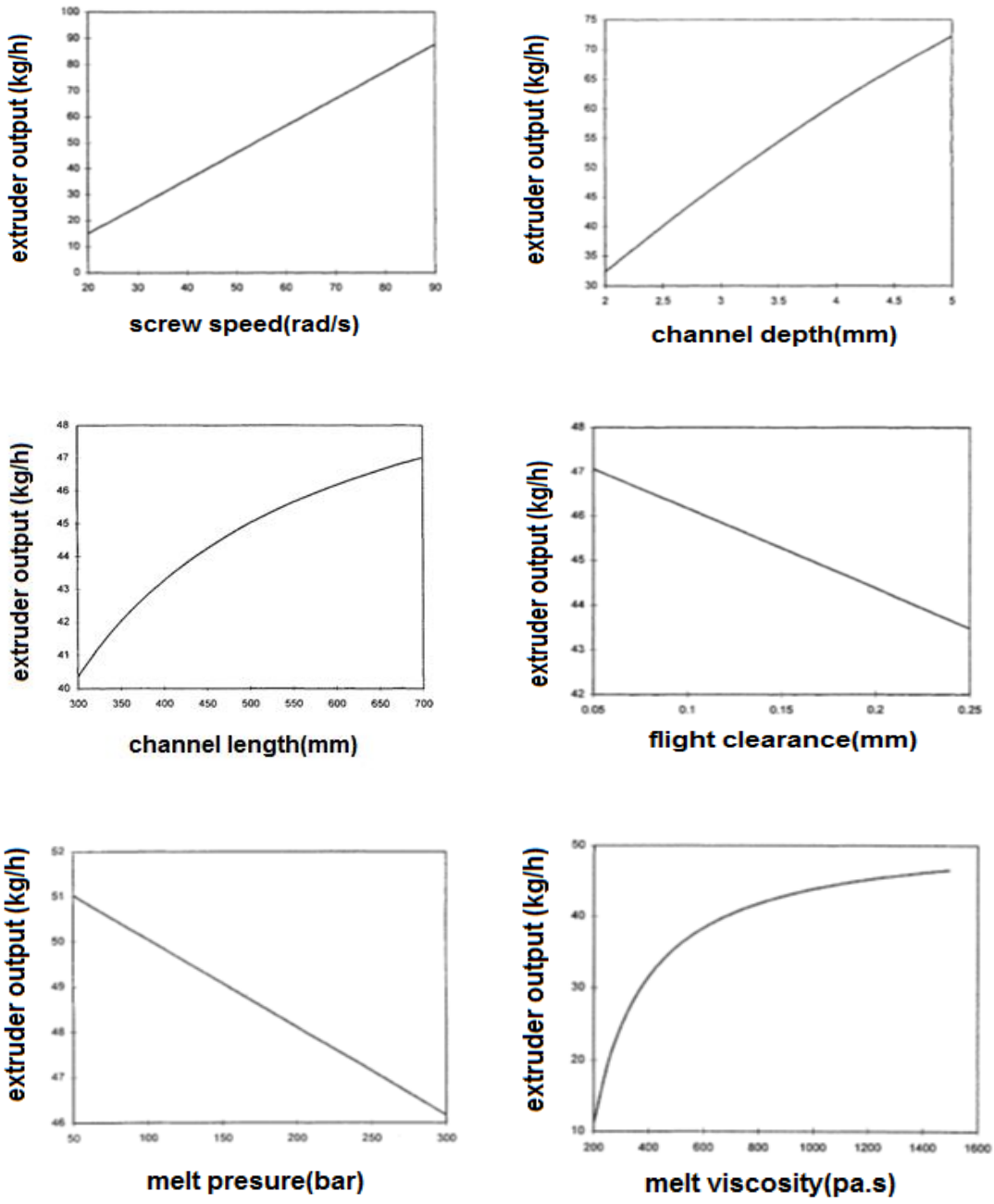

Fig. 2.15: The effect of different parameters on the extruder output(Rao and O'Brien, 1998)

III. Important: The performance of an extruder is affected by the resistance to flow offered by the die. We cannot separate extruder design from die design. In general the die restricts the flow

somewhat, but not completely. Combining Eq(2.31) we get the extruder characteristic

We have 1 equation and 2 unknowns to solve for (dP andQ_{Total})

We need a 2nd equation - this comes from the die(Eng, 2002).

2.6.2 Die Characteristics

The die in its simplest form is just a flow channel within a piece of metal. The Types of dies are capillary dies (filaments, yarns), flat dies (sheet), dies to produce hollow tubes (pipe, films) and profile dies (irregular cross sections).

The Problems in die design are concerned with obtaining the desired shape (swell of polymer distorts the shape), uniform thickness, uniform temperature and avoiding surface defects. The derivation of equations of tapered and non-tapered dies assumed the polymer melt, is a Newtonian, isothermal, uncompressible and no slip on the die wall.

1. **Analysis of Circular die:**

For a Newtonian fluid we might express the behavior of the die as

$$Q = \frac{\pi {R_1}^4}{8\mu L_1}.\Delta p = \left(\frac{\pi {R_1}^4}{8\mu L_1}\right)\frac{2L_1\tau_1}{R_1} - - - (2.33)$$

Where:

R_1 : Radius of the die

L_1 : length of the die

ΔP : Pressure drop over the die

μ : Viscosity

Q : Volumetric flow rate

K : Function of the die geometry

For Isothermal Flow through Circular Tube newton or non –newton fluid see (Appendix A).

2. Analysis of Tapered circular die:

In many practical situations involving the flow of polymer melts through dies and along channels, the cross-sections are tapered. In these circumstances, tensile stresses will be set up in the fluid and their effects superimposed on the effects due to shear stresses as analyzed above. Cog swell has analyzed this problem for the flow of a power law fluid along coni-cylindrical. The flow in these sections is influenced by three factors:

(1) Entry effects given suffix at point 2

(2) Shear effects given suffix S

(3) Extensional effects given suffix E

Each of these will contribute to the behavior of the fluid although since each results from a different deformation mode, one effect may dominate depending on the geometry of the situation.

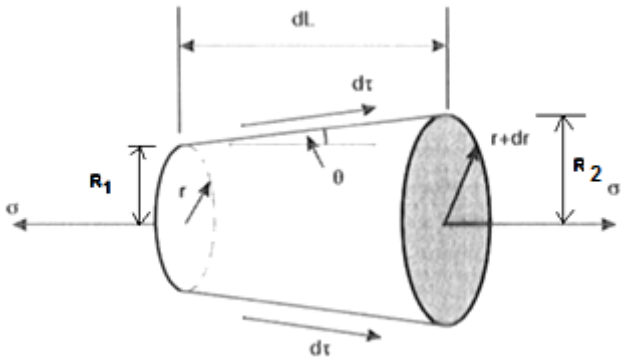

Fig. 2.16: Tapered circular die

i. **Pressure drop due to shear, Δp_s**

$$\Delta p_s = \frac{2\tau_1}{3tan\,\theta}\left(1-\left(\frac{R_1}{R_2}\right)^3\right) - - - (2.34)$$

$$\tau_1 = \mu_1.\dot{\gamma}_1 - - - (2.35)$$

Where:

τ_1 Shear stress

$\dot{\gamma}_1$ Shear rate

μ_1 Shear viscosity

ii. Pressure drop due to extensional flow Δp_E

$$\Delta p_E = \frac{2\sigma_1}{3}\left(1-\left(\frac{R_1}{R_2}\right)^3\right) - - - (2.36)$$

$$\sigma_1 = \lambda\frac{\tan(\theta)}{3}\left(\frac{4Q}{\pi {R_1}^3}\right) = \lambda\frac{\tan(\theta)}{3}\dot{\gamma}_1 = \lambda\,\dot{\varepsilon}_1 - - - (2.37)$$

Where :

λ tensile viscosity about three time of shear viscosity at low shear rate

$\dot{\varepsilon}$ tensile strain

iii. Pressure drop at die entry, P_2

When the fluid enters the die from a reservoir it will conform to a streamline shape such that the pressure drop is a minimum. This will tend to be of a coni-cylindrical geometry and the pressure drop, P_2, may be estimated by considering an infinite number of very short frustums of a cone.(Crawford, 1998)

$$P_2 = \frac{2\sqrt{2}}{3}\left(\frac{4Q}{\pi {R_2}^3}\right)(\mu_2\lambda)^{1/2} - - - (2.38)$$

The above mentioned study use the assumption of no-slip at the solid boundary, However, polymer melts can slip at solid interface when the wall shear stress exceeds a critical value so that there approximate analytical equations that are derived for the calculation of pressure drop of

power-law fluids for viscous flow through tapered dies for a wide range of wall-slip conditions and the predicted pressure drop values are compared with two-dimensional (2D) finite element calculations to identify contraction angles for which the analytical equations can be used(Hatzikiriakos and Mitsoulis, 2009).

Entrance pressure drop is a large one when a molten polymer flows through a Tapered die of a given angle(Bagley, 2004) .This pressure is required in order to calculate the true shear stress in capillary flow and also frequently the apparent extensional rheology of molten polymers, a method well practiced in industry. Therefore, it is important to understand the origin of this excess pressure and consequently to be able to predict it (Ansari et al., 2010) .

The Entrance pressure drop as a function of contraction angle at a given apparent shear rate under slip or no-slip boundary conditions. This was studied for a branched polypropylene (PP) melt both experimentally and theoretically. The entrance pressure was first determined experimentally as a function of the contraction angle ranging from 10^{o} to 150^{o}. It was found that at a given apparent shear rate, the pressure loss decreases with increasing contraction angle from 10^{o} to about 45^{o}, and consequently slightly increases from 45^{o} up to contraction angles of 150^{o}.(Mitsoulis et al., 2005)

The Entrance pressure drop in the capillary flow of several types of polyethylene were studied both experimentally and numerically under slip and no-slip conditions. These losses were first measured as a function of the contraction angle ranging from 15^{o} to 90^{o}. It was found that the excess pressure loss attains a local minimum at a contraction angle of about 30^{o} for all types of polyethylene examined(Ansari et al., 2010).

2.6.3 The operating point

The operating point is the Intersection of the Extruder Characteristic and the die characteristic. At the operating Point

$$Q_{Total(screw)} = Q_{die} \quad ---(2.39)$$

There Two solution methods using to solve Eq (2.39) Analytical solution and Graphical solution.

a) Analytical solution For capillary dies

The pressure at the operating point is given after substitute Eqs(2.30 and 2.33) in Eq (35).

$$\frac{1}{2}\pi^2 {D_b}^2 NH sin\emptyset_b cos\emptyset_b - \frac{\pi D_b H^3 \sin \emptyset_b^{\,2}}{12\mu}.\frac{P}{L} = \frac{\pi {R_1}^4}{8\mu L_1}.P$$

$$P_{op} = \frac{2\pi\mu {D_b}^2 NH sin\emptyset_b cos\emptyset_b}{\frac{{R_1}^4}{2L_1} + \frac{D_b H^3 sin^2\emptyset_b}{3L}} \quad ---(2.40)$$

$$Q_{op} = \frac{\pi {R_1}^4}{8\mu L_1}.P_{op} \quad ---(2.41)$$

b) Graphical solution

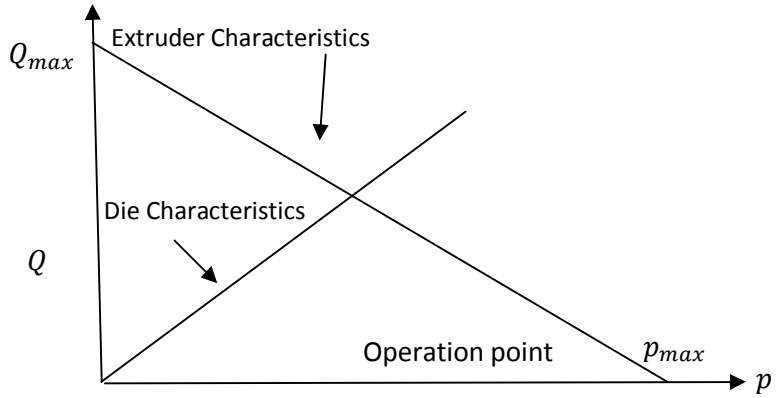

Fig. 2.17: Graphical solution for extruder die at operation point

With the help of Eq(2.40) the effect of different parameters on the extruder output at operation point is presented (Crawford, 1998),in

Fig(2.18) by changing one variable at a time and keeping all other variables constant .

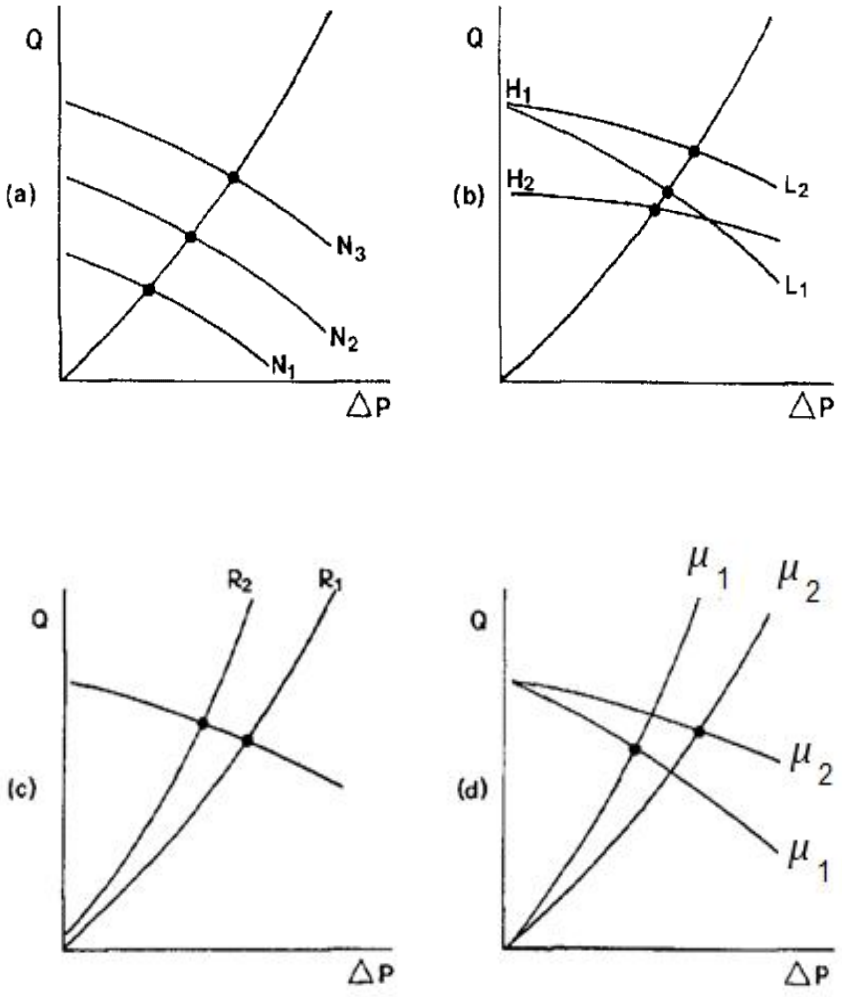

Fig. 2.18: Single-Screw Extrusion and die Effect of Process Variables

From the Fig (2.18)
(a) Effect of Screw Speed (N_3>N_2>N_1)
(b) Effect of Screw Channel Depth (H_1>H_2) and Metering Section Length (L_2>L_1).

(c) Effect of Die Radius (R_2>R_1).

(d) Effect of Viscosity (μ_2>μ_1)(Lafleur and Vergnes)

2.7. Polymer rheology

2.7.1 Introduction

Most polymer processes are dominated by the shear strain rate. Consequently, the viscosity used to characterize the fluid is based on shear deformation measurement devices.

Viscosity is the most important flow property, and it is the resistance to shearing, it can be measured by either capillary or rotational viscometers. In capillary viscometers like (Melt Flow Index Tester), the shear stress is determined from the pressure applied by a piston. The shear rate is determined from the flow rate (Strutt, 2001).

2.7.2 Rheology from melt flow index tester

MFI represents a point at specific shear rate and shear stress values on the viscosity versus shear rate curve at constant load and temperature(&D.R.SAIN, 2000).Melt index is the amount of melt which flows through the capillary of the measuring instrument under a defined time scale at a given temperature and pressure, the Fig(2.19) shows the schema of shows the schema of capillary plastometer.

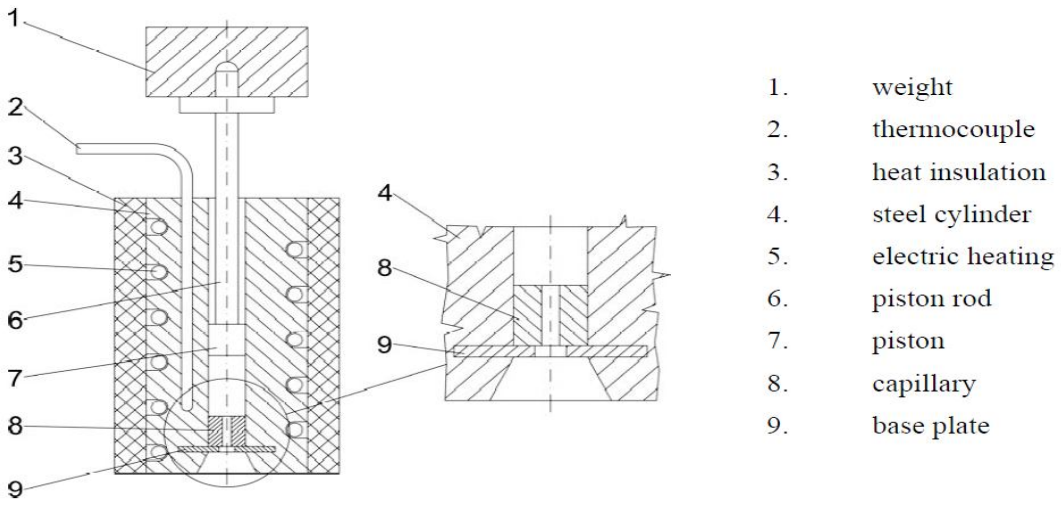

Fig. 2.19: Schema of capillary plastometer

By measuring the mass of melt, we can calculate the Melt Flow Index (MFI)

$$MFI_{[T,F]} = \quad m.S/t \quad - - - (2.41)$$

Where

MFI [g/10min] melt flow index

T [^{0}C] test temperature

F [dyne] weigh force

S [s] factor of standard time (10 minutes=600s), S=600

t [s] time needed for V amount of materials to flow through the capillary

m [g] amount of materials flowing through the capillary under t time (Budapest University of Technology and Economics, 11. February 2007).

Where dimensions as per ASTM D1238:

Piston radius $R_P = 0.4775cm$

Capillary radius $R_C = 0.10475cm$

Capillary length $L_C = 0.8cm$

Weigh force F = test load L (kg) $\times 9.80665 \times 10^5$ dyn $- - - (2.42)$

The equations for master curve from MFI tester

Mass flow rate (&D.R.SAIN, 2000).

$$\dot{m}(g/s) = MFI/600 - - - (2.43)$$

Melt density

$$\rho_m(g/cm^3) = m/\pi R_P{}^2 l - - - (2.44)$$

Where

m [g] amount of materials flowing through the capillary under t time.

l [cm] distant of piston move down during materials flowing through the capillary under t time(Corp, 2013).

Volume flow rate

$$Q(cm^3/s) = \dot{m}/\rho_m \quad - - - (2.45)$$

Shear rate

$$\dot{\gamma}(s^{-1}) = 4Q/\pi R_c{}^3 \quad - - - (2.46)$$

Shear stress

$$\tau(dyne/cm^2) = R_c F/2\pi R_P{}^2 L_c \quad - - - (2.47)$$

Viscosity (&D.R.SAIN, 2000).

$$\mu\ (dyne/cm^2 . s\ ) = \frac{\tau}{\dot{\gamma}} \quad - - - (2.48)$$

2.7.3 General behavior of polymer melts

In a fluid under stress, the ratio of the shear stress, τ ,to the rate of strain $\dot{\gamma}$ is called the shear viscosity,μ and is analogous to the modulus of a solid. In an ideal (Newtonian) fluid the viscosity is a material constant. However, for plastics the viscosity varies depending on the stress, strain rate, temperature etc. A typical relationship between shear stress and shear rate for a plastic is shown in Fig (2.20).

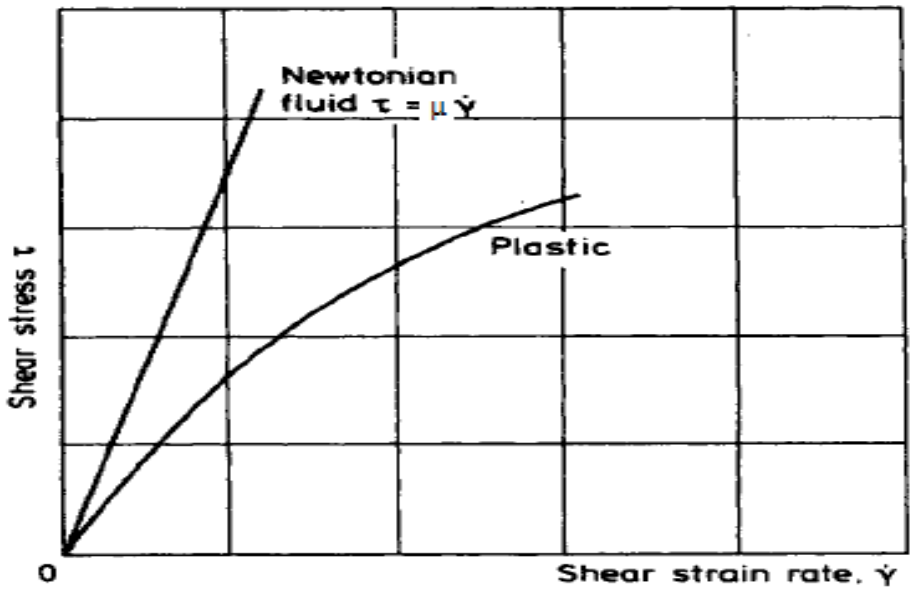

Fig. 2.20: Relations between shear stress and shear rate

2.7.4 The viscosity - shear rate relationship

As a starting point it is useful to plot the relationship between shear stress and shear rate as shown in Fig (2.20) since this is similar to the stress-strain characteristics for a solid. However, in practice it is often more convenient to rearrange the variables and plot viscosity against strain rate as shown in Fig (2.21). Logarithmic scales are common so that several decades of stress and viscosity can be included. Fig (2.21) also illustrates the effect of temperature on the viscosity of polymer melts. When a fluid is flowing along a channel which has a uniform cross-section then the fluid will be subjected to shear stresses only. To define the flow behavior we may express the fluid viscosity, μ, as the ratio of shear stress, τ(Crawford, 1998).

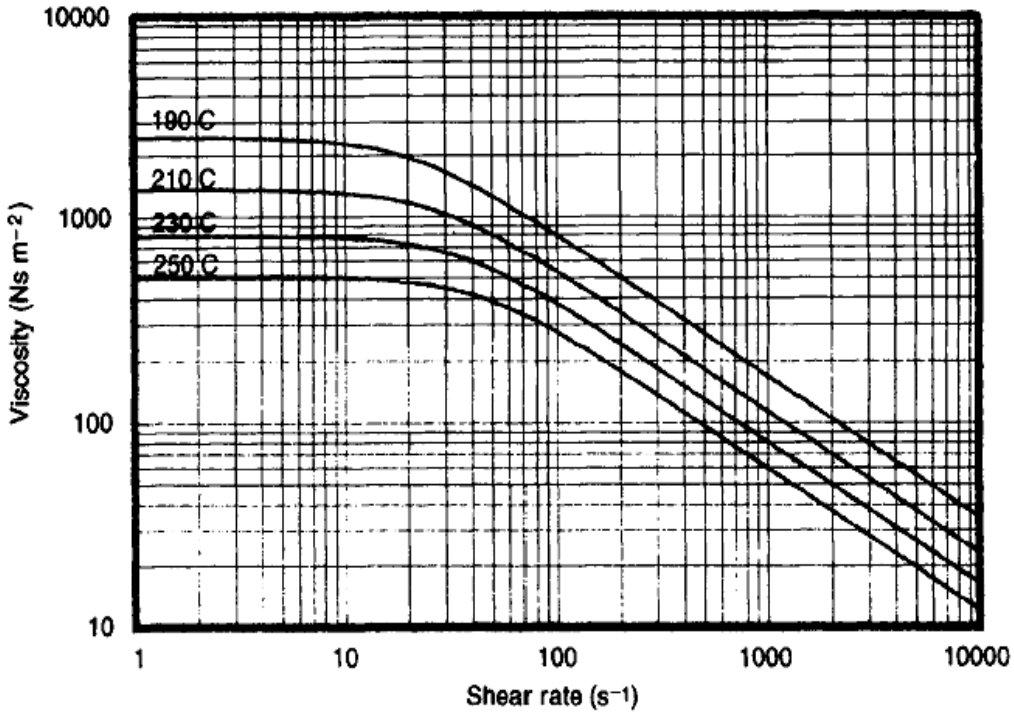

Fig. 2.21: Viscosity curves for polypropylene

2.7.5 Numerical computation method to fit experimental data

Least-square procedures are widely used in numerical computations. Here the quality of the fit between the observed μ^*_{obs} and predicted μ^*_{fit} viscosity values was quantified using a modified least square procedure called the percentage root-mean-square error function (%RMSE):

$$\%\text{RMSE} = \frac{100}{\text{N}} \sqrt{\sum_{i=1}^{N} \left(\frac{\mu^*_{obs} - \mu^*_{fit}}{\mu^*_{obs}}\right)^2} \quad ---(2.49)$$

Where N is the number of data points:

The best-fit is used to find the smallest error (based on the %RMSE value) between viscosity measurements and the modeled viscosity(Borg and Pääkkönen, 2009).

2.7.6 Extrudate swell

Extrudate swell is also known as Barus effect. When a polymer melt is extruded through a die the cross-sectional area of the extrudate is greater than that of the die.

$$B_{SR} = \frac{D_{extrudate}}{D_{die}} = \sqrt{\frac{area\ of\ swoollen\ extrudate}{area\ of\ capillary}} \quad ---(2.50)$$

The general explanation for die swell is related to the recoverable elastic deformation developed during flow through the die(Crawford, 1998).

Extrudate swell is also linked with velocity profile development

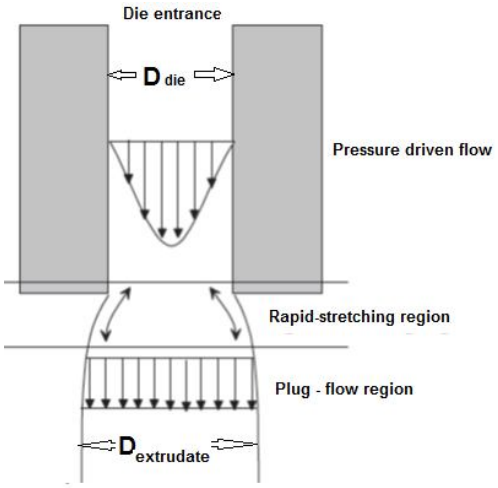

Fig. 2.22: Velocity profiles and die swell relationship

Extrudate swell is so important to quality of the products by control the size and shape of the extruded, to determine quantity of the productivity of the extruded products. And associated with the occurrences of sharkskin and melt fracture.

In general information in extrudate swell most techniques rely on direct measurement of the size of the melt extruded from the die.

- Extrudate swell increases: as the die length decreases, as the shear rate or shear stress increase, and the molar mass of the polymer increases.
- In other side Extrudate swell can be minimized by reducing increasing die temperature and die land length or reducing the shear rate or shear stress.

Factors affecting the extrudate swell

Residence flow time, Die temperature, Shear rate, Die length or die land, L/D radio, Additives, Molar mass, Flow patterns, Die geometry and number of flow channel, Magnetic field and Radial profiles(Sombatsompop, 1999).

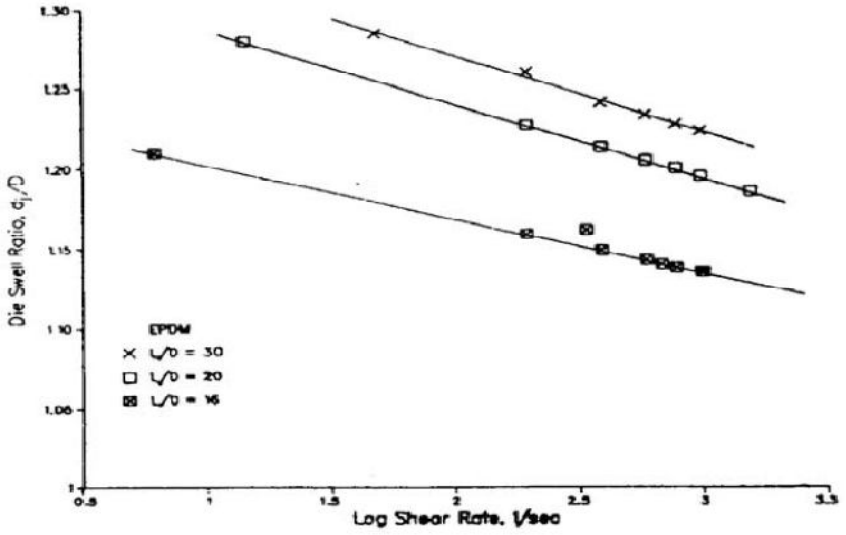

Fig. 2.23: Die swell ratio (dj/D), versus shear rate ($\dot{\gamma}$), for ethylene ,propylene , and Dine Elastomer extrudate in capillary dies at 80°C (Musameh and Jodeh, 2009)

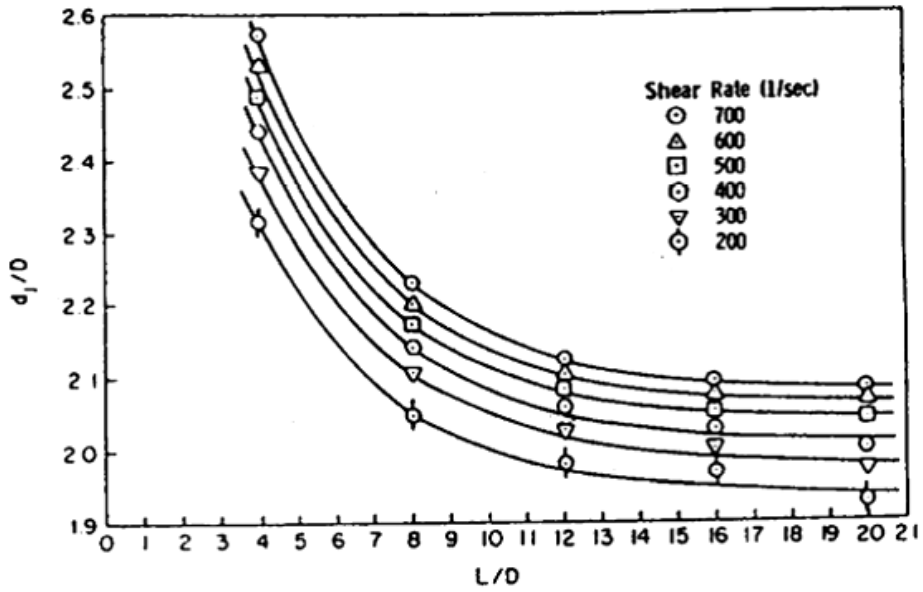

Fig. 2.24: Die swell ratio (dj/D), versus capillary length ratio (L/D), for high-density polyethylene at 180°C and various shear rate(Musameh and Jodeh, 2009)

2.8. Polymer processing modeling using numerical methods

2.8.1 Introduction

In most polymer processes the quality of the final part is greatly dependent on the melting. The optimization of the equipment and manufacturing process, as done today, is time consuming and expensive.

Quantifying flow and heat transfer is an even more intimidating task. Obviously these barriers make numerical simulation of polymer processes a viable alternative when optimizing and analyzing the process.

The advent of more powerful computers and efficient numerical techniques are now beginning to make it possible to simulate three-dimensional problems of complex geometry with non-linear material behavior.

The general techniques used for the modeling and simulation of polymer processes and background on numerical techniques and basic modeling in polymer processing are will be present.

2.8.2 Modeling

In order to be able to predict and model complex polymer flows, one must first have a basic understanding of the mathematics that govern the flow. Regardless of the complexity of the flow, it must satisfy certain physical laws. These laws can be expressed in mathematical terms as the conservation of mass, the conservation of momentum, and the conservation of energy. In addition to these three conservation equations, there may also be one or more constitutive equations that describe material properties, i.e. shear rate and viscosity. Since these equations may also be coupled together, i.e. temperature dependent viscosity, the solution can become even more complex. The goal of the modeler is to take a physical problem, apply these mathematical equations and solve them to predict the flow

phenomena. Although analytical solutions to the conservation equations for some simple two-dimensional shapes are available, when more complex two-dimensional problems or three-dimensional analysis are required, numerical methods are required.

There are three basic classes of numerical techniques that are commonly used to solve complex fluid flow problems (Fig.2.25). They are: the finite difference method (FDM), the finite element method (FEM), and the boundary element method (BEM). Each of these methods has its own advantage and disadvantages and, therefore, one may be preferred for certain type of process or material. Each technique has been adapted in some form for specific problems encountered in polymer processing.

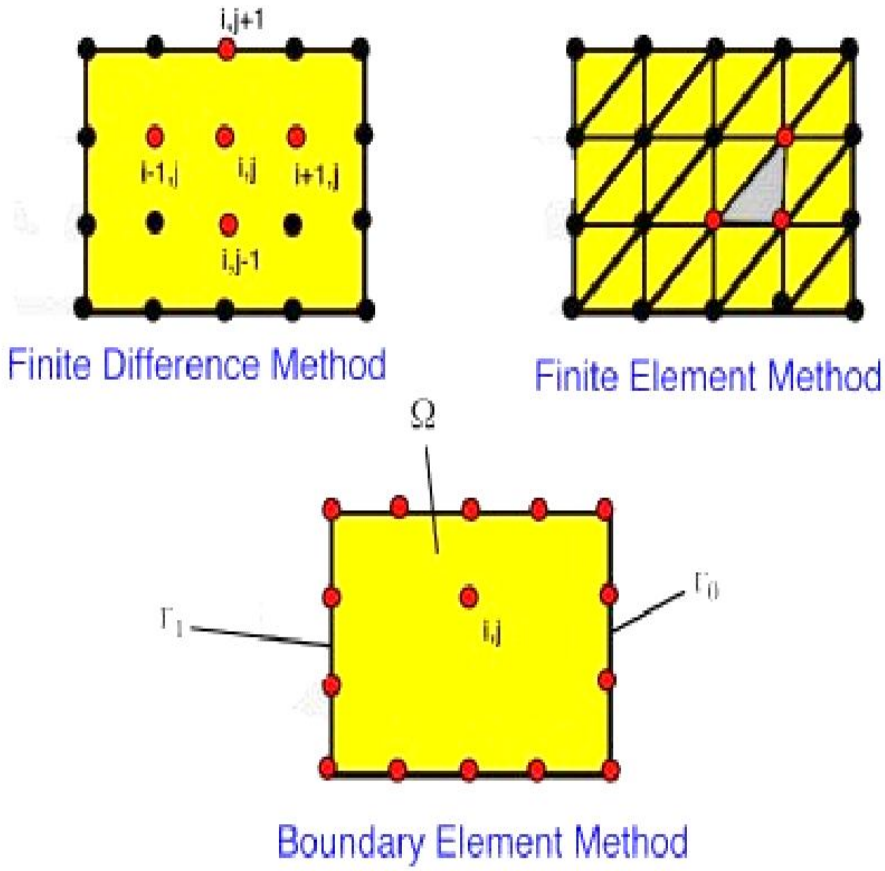

Fig. 2.25: Comparison between various numerical techniques

a) Finite Difference Method

The finite difference method is the simplest to use and understand. Fig (2.25) shows the grid that would be constructed to represent the geometry of a two dimensional domain. Once the grid is created, the governing differential equations are rewritten in a discretized form and then applied at each nodal point. The resulting system of algebraic equations can then be solved for by standard Gaussian elimination or more elaborate numerical algorithms. Because of the simplicity of the method, it can implement in a wide variety of problems. The method discretizes the governing equations at the start of the analysis, and it lends itself to model non-linear problems.

The finite difference method is also easy to program and computer simulations can provide quick computation times. The first consideration when implementing the FDM is that it is best suited for cases that have relatively simple geometries. Even though more complex geometries can be modeled with special differential equations or coordinate transformations, there are still limitations that exist, and the other methods presented often prove to be more efficient.

b) Finite Element Method

The finite element method has become the basis for most commercial structural dynamic and fluid flow simulation programs. Like FDM, FEM is a domain method in which the entire geometry to be modeled must be discretized into nodes and elements. The mesh shown in Fig (2.25) represents the discretization required for FEM to model a two dimensional geometry. Although several different methods are available to obtain the final equations, the Galerkin method of weighted residuals is normally preferred in fluid flow problems. Once the mesh has been created, the governing differential equations are then expressed in integral form and

numerically integrated to obtain an algebraic system of equations. Because of the nature of the finite element method, it is capable of modeling much more complex geometries than FDM. It can also provide quite accurate solutions to the field variables, such as fluid velocities or pressures, for a wide variety of problems that include non-linear flows. However, higher order derivative solutions, such as velocity gradients, tend to be less accurate. Without complex adaptive meshing techniques, FEM is also difficult to use for problems with moving solid boundaries. Since the governing equations are approximated with the Galerkin method, they have a certain amount of intrinsic error even before numerical errors are accounted for, which is carried throughout the computation. This can cause the FEM to become unstable in highly non-linear situations. Although this can be partially alleviated by special up winding techniques it nonetheless increases the amount of computation effort. In addition, since the solution is computed only at the nodes and the velocity field must be interpolated, the tracking of particles in the flow field in not easily accomplished with FEM.

FEM is extensively used when simulating processes that are highly non-linear such as flow of viscoelastic materials. For example, Fig (2.26) shows predicted extrudate swell of HDPE flowing through a converging die.

FEM has also proved to be ideal when simulating mold filling processes, fiber orientation, shrinkage, and war page of thin plastic parts.

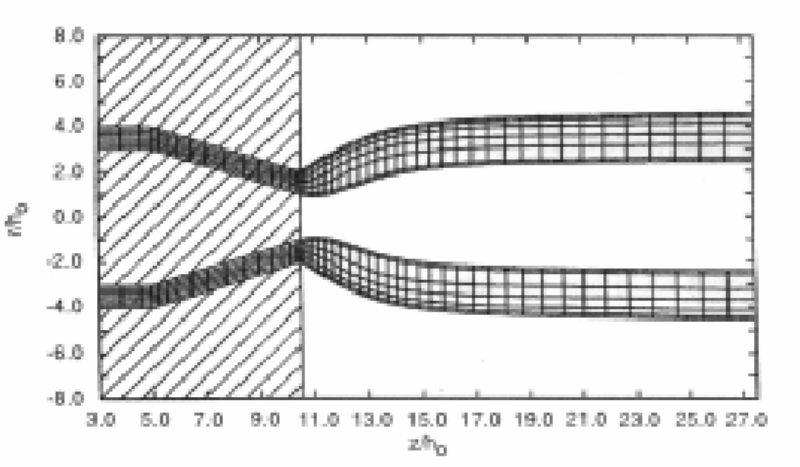

Fig. 2.26: Predicted extrudate swell of HDPE flowing through a converging die

c) Boundary Element Method

BEM only requires that the boundary or surfaces of the geometry be discretized. A two-dimensional geometry only requires a discretization of the curve that makes up the boundary of the part. In essence, the order of analysis being made is reduced by one. Figure 9 compares FEM and BEM discretization of a two dimensional model of an internal batch mixer.

Because of the relatively complex mathematics involved with BEM, it has been relatively slow to gain the same level of acceptance that FEM did in the engineering community, and has been primarily used by mathematicians. The formulation of the boundary element method begins with a different form of the governing equations, which are expressed in terms of domain integrals. These integrals are manipulated by Green-Gauss transformations until they are reduced to boundary integrals. The integrals are then numerically evaluated to yield an algebraic system of equations. Interestingly, up to the point of evaluating the integrals, no approximations have been made in the governing equations. Thus, the boundary element

method, unlike the FDM or FEM, does not introduce any error to the solution until the boundary is discretized

The BEM solution is exact up until the geometry is meshed. Another advantage of BEM is that the accuracy of higher order derivatives is excellent. This becomes extremely important when trying to calculate heat transfer effects or track particles. Here, the boundary element is well suited to track particles in the flow of material since the solution at any location in the fluid can be obtained quite easily and very accurately(Osswald and Gramann, 2001).

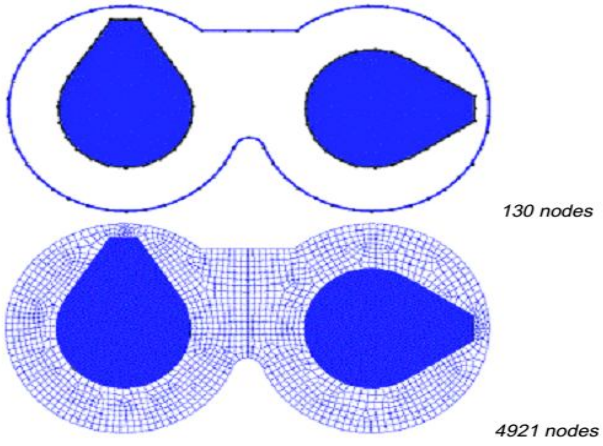

Fig. 2.27: BEM and FEM discretization of a 2D (completely filled) internal batch mixer

2.9. Polymer processing simulation using ansys Polyflow software

2.9.1 Introduction

Polyflow is specialized computation fluid dynamic (CFD) software from Fluent Inc. It is a useful tool to investigate and simulate CFD research problems such as extrusion and molding in polymer processing. Being a

specialized CFD simulation tool for polymer processing, Polyflow has the following special features:

i. A robust CFD solver for complex non-Newtonian rheologies including viscoelastic flow, which is very common in polymer processing.
ii. A direct coupled, unstructured solver using the Finite Element technique.
iii. Advanced techniques to deal with deforming mesh, complex motion of solid parts (screws) and detection of contact between free surface and molds.

Using Polyflow, users can run simulations with all types of element, even with hybrid mesh and non-conformal mesh. This capability makes the analysis for problems on complex geometry less difficult. In addition, the following special capabilities of Polyflow are pretty useful in running simulations for polymer processing or glass forming:

i. Various 2D and 3D remeshing techniques which is able to predict the free surfaces for the free flow of liquid materials.
ii. Rich embedded rheological models, including a total of 10 type of non-Newtonian models, 9 kind of viscoelastic models and 8 different temperature dependence models, which can easily be applied for different types of polymer processes.
iii. Moving boundaries with specification of normal force, normal velocity or interface tension that enables to address the common process boundary conditions in injection molding and extrusion.

The use of the special capabilities and physical models provided in Polyflow enables the saving of a lot of time and efforts in defining and running a polymer processing or glass forming simulation.

Even though it is also possible for users to do similar simulations using the generic software, however, it will take much more efforts and time to create the necessary physical models by writing some codes.

Polyflow is suitable not only for polymer processing simulations, it can also be used for rubber and plastic processing. The actual industry application examples include extrusion/co-extrusion, wire/cable coating, inverse die design (die shape prediction from final product), and blow/injecting molding and so on, for any kind of viscoelastic materials (Junhong, 2003).

2.9.2 Ansys Polyflow in Workbench user interface

ANSYS Polyflow fluid flow systems in ANSYS Workbench to set up and solve a 3D extrusion problem .When working in Workbench, your work in POLYFLOW is automatically saved as needed.For example, whenever you close POLYDATA, run POLYFLOW, or save your Workbench Project, your unsaved data is automatically saved.

Ansys Polyflow Project schematic consists of five sections, Design Modular, Meshing, Setup, Solution and Result.

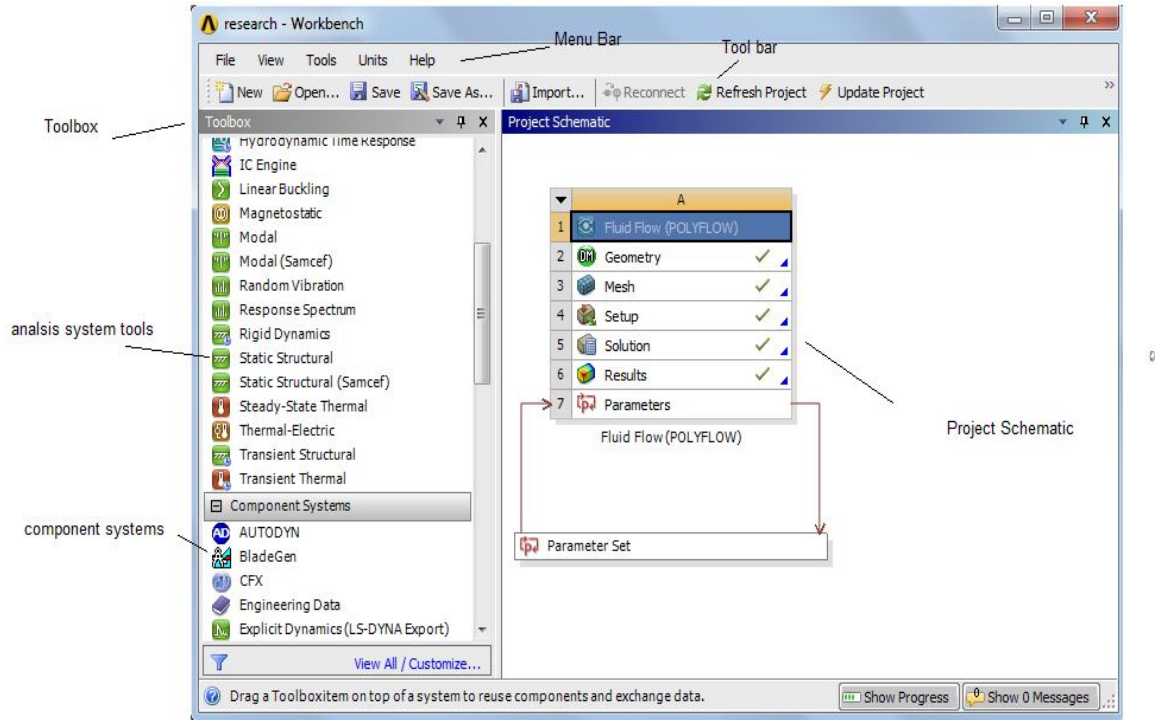

Fig. 2.28: Polyflow in workbench graphical user interface

Design Modular: can import geometry from Solid works or other CAD 3D software or using a module Design Modeler start by creating a sketch in 2D and modified then can perform features like Extrude, Revolve, and Sweep on it to generate 3D model.

Meshing: ANSYS Meshing, applied to the model, finite element mesh and determines the characteristics and parameters. There are several possible choices in the types of networks in this module: automatic, square (Fig 2.28a), triangular (Fig2 .29b), mixed referred to as a square – triangle (Fig 2.28c).Starting with the default mesh generation (automatic) method. This will give us mesh that ANSYS mesher thinks appropriate for our geometry. Or another type of mesh then assign to boundaries names and in statistical see numbers of Nodes and element.

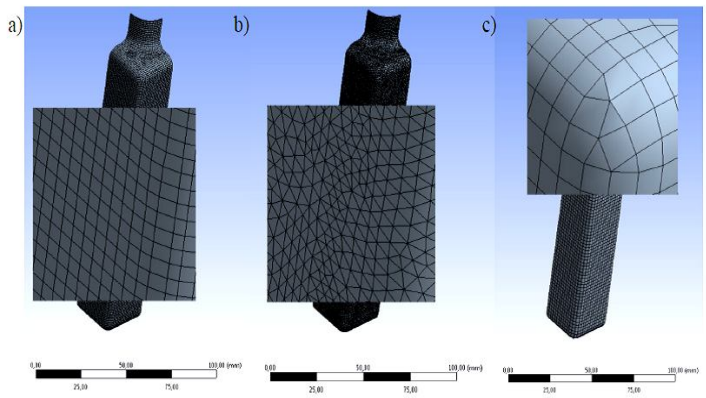

Fig. 2.29: Types of finite element mesh: a) square grid, b) triangular mesh, c) net mixed(Gupta et al., 2013)

Setup (Polydata): Used for assigning different parameters value and mathematical expressions into use. For example define the tasks FEM or mixed, steady- state , time –depending problems , isothermal or non-isothermal , enter the state of boundary condition assigned before in mesh step and enter materials properties and it units. Remesh method for inverse extruder (ie.profile dies) and free jets tasks (ie.swell).and finally unites of calculation results.

Solution:*by* the means of mathematical iteration and energy equations used to get the relations of different parameters for effectiveness.

Result: Contours of different parameters are graphically represented and their relations with the dependent variables at every mesh of the structural geometry. And added expressions as output parameters to design points.

Ansys (polyman) is an environment layer built on top of the programs used in the ANSYS POLYFLOW package, it package is an interactive graphical program that allows to visualize material data, including steady shear viscosity and steady elongational viscosity. It computes material properties from constitutive equations and numerical parameters, for

isothermal and non-isothermal generalized Newtonian, differential viscoelastic, and integral viscoelastic fluids. It can also compare them with experimental curves (i.e., fitting). Several viscosity laws are available for generalized Newtonian flows. The isothermal viscosity laws *(* Constant, Power Law, Bird-Carreau Law, Cross Law, Modified Cross Law, Bingham Law, Modified Bingham Law, Herschel-Bulkley Law, Modified Herschel-Bulkley Law, Log-Log Law and Carreau-Yasuda Law) (Release, 2012).

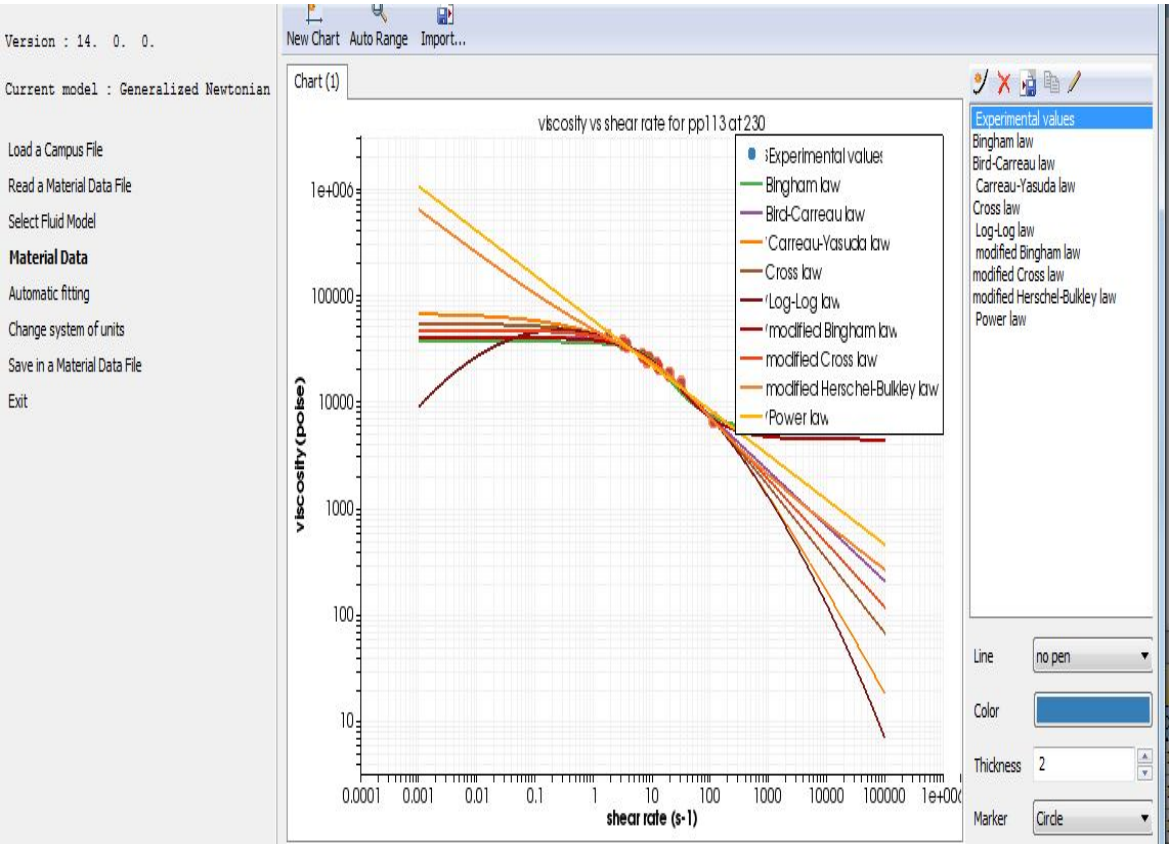

Fig. 2.30: Polyflow (polyman) experimental data fitting for rheological models (Prepared by the researcher)

For Basic Equations, Shear-Rate and Temperatures Dependent Viscosity Laws in Polyflow see Appendix (D), and Boundary Conditions Appendix (E).

2.9.3 Flowchart for Numerical Simulation using Polyflow

Ansys Polyflow consist of few interdependent modules used to prepare analyze geometry define data, calculations and presents results. Typical flowchart for numerical simulation was presented on Fig (2.31) (Pepliński and Mozer, 2011).

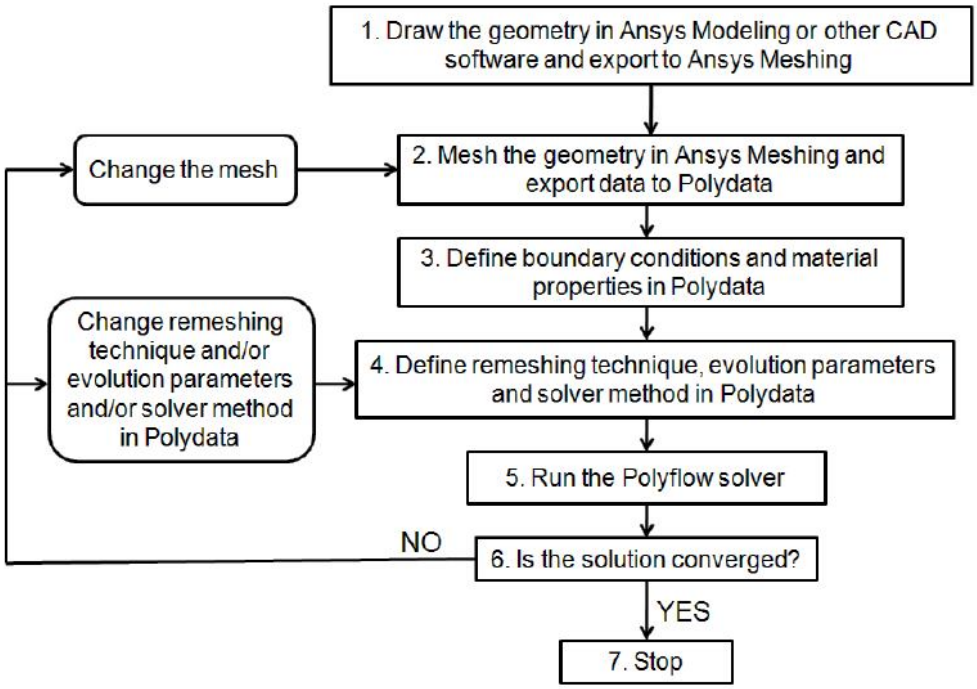

Fig. 2.31: Flowchart for numerical simulation using Ansys Polyflow

2.10. Simulation flow of polymer in circular die using Polyflow

The is example prepared by the researcher to calculate pressure drop and shear rate vs flow rate at values (10, 20,30,40,50 and 60 cm^3/s)

Design Modular: creating a sketch in 2D (XY plan) and generate 3D model by revolve tools (see Fig 2.32).

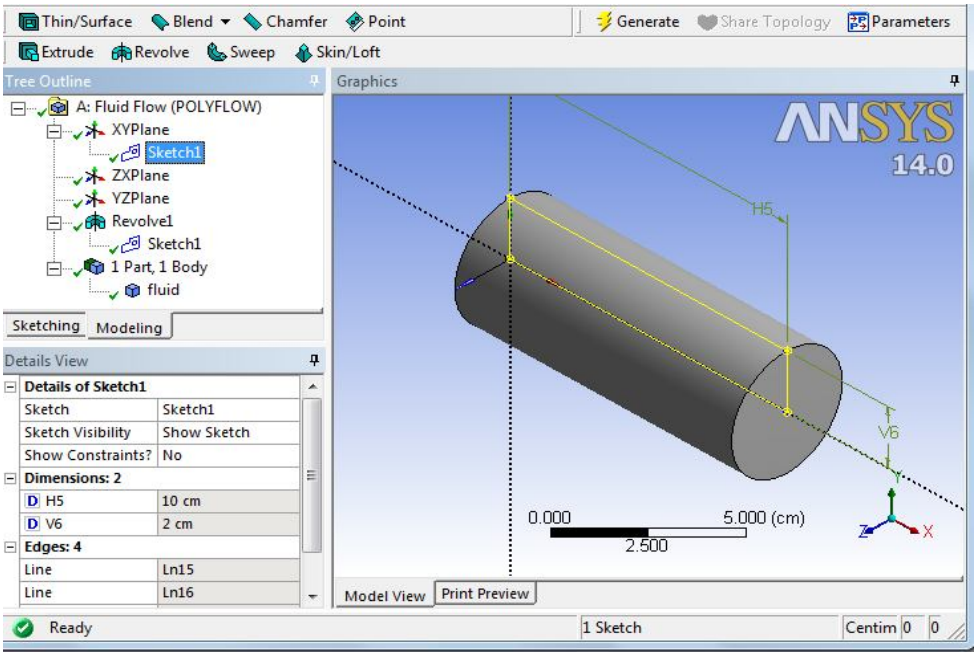

Fig. 2.32: Geometry of circular die in Polyflow

Meshing: Starting with the default mesh generation (automatic) and define the names of boundary.

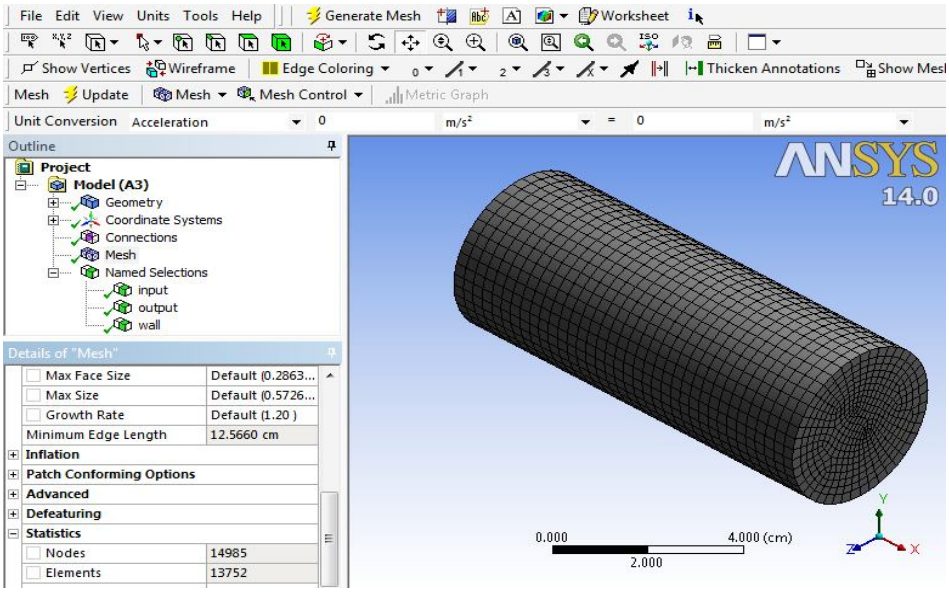

Fig. 2.33: Meshing geometry for circular die in Polyflow

Setup (Polydata): the task is FEM, steady- state, isothermal, the boundary set input face inflow =10cm^3/s, output=outflow, wall = zero normal

velocity and zero surface velocity condition, enter materials data (type of viscosity model) with it units.

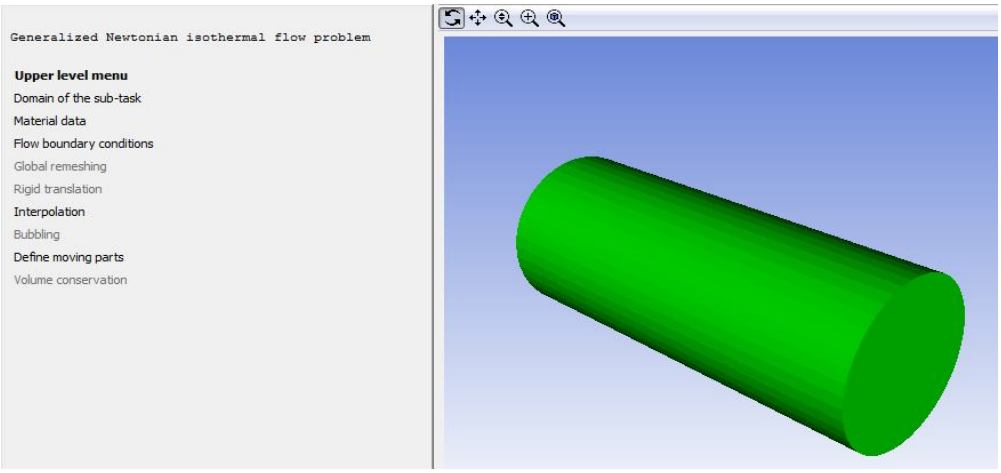

Fig. 2.34: Step materials and boundary for circular die in Polyflow (polydata)

Solution and **Result:**Contours of different parameters are graphically represented and their relations with the dependent variables at every mesh of the structural geometry in Fig (2.35)

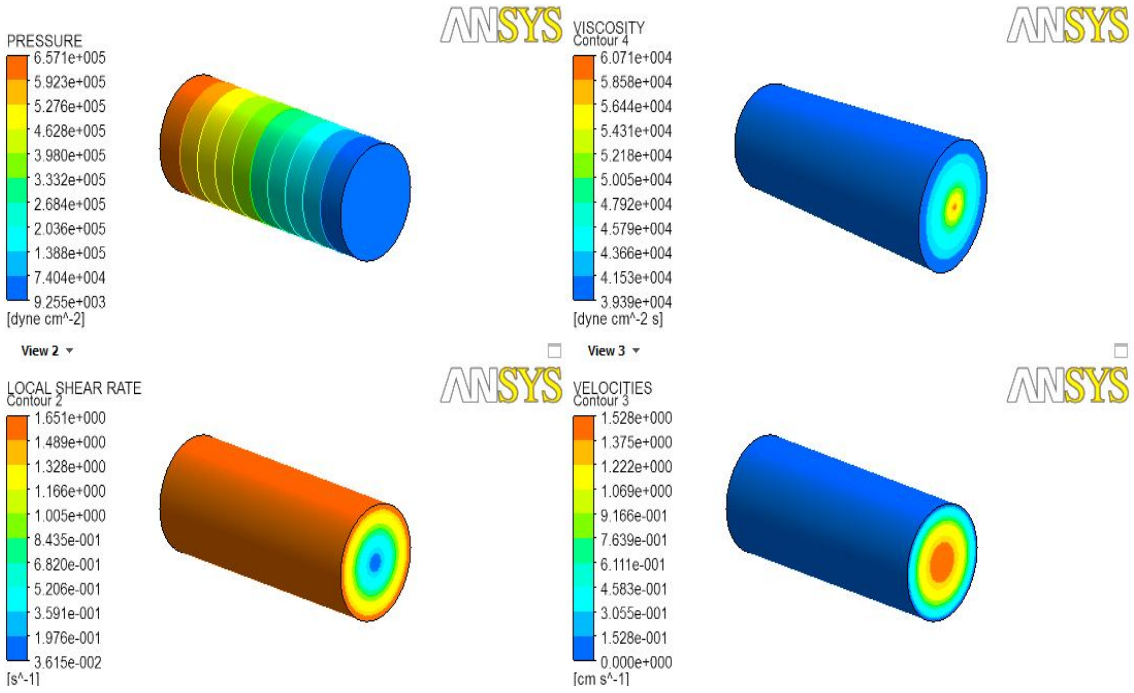

Fig. 2.35: Results for circular die in Polyflow (CFD Post)

Fig (2.36) shown Generate results for multiple design points using the Parameter and Design Points view and chart how the maximum shear rate and Pressure drop varies with the inlet flow rate.

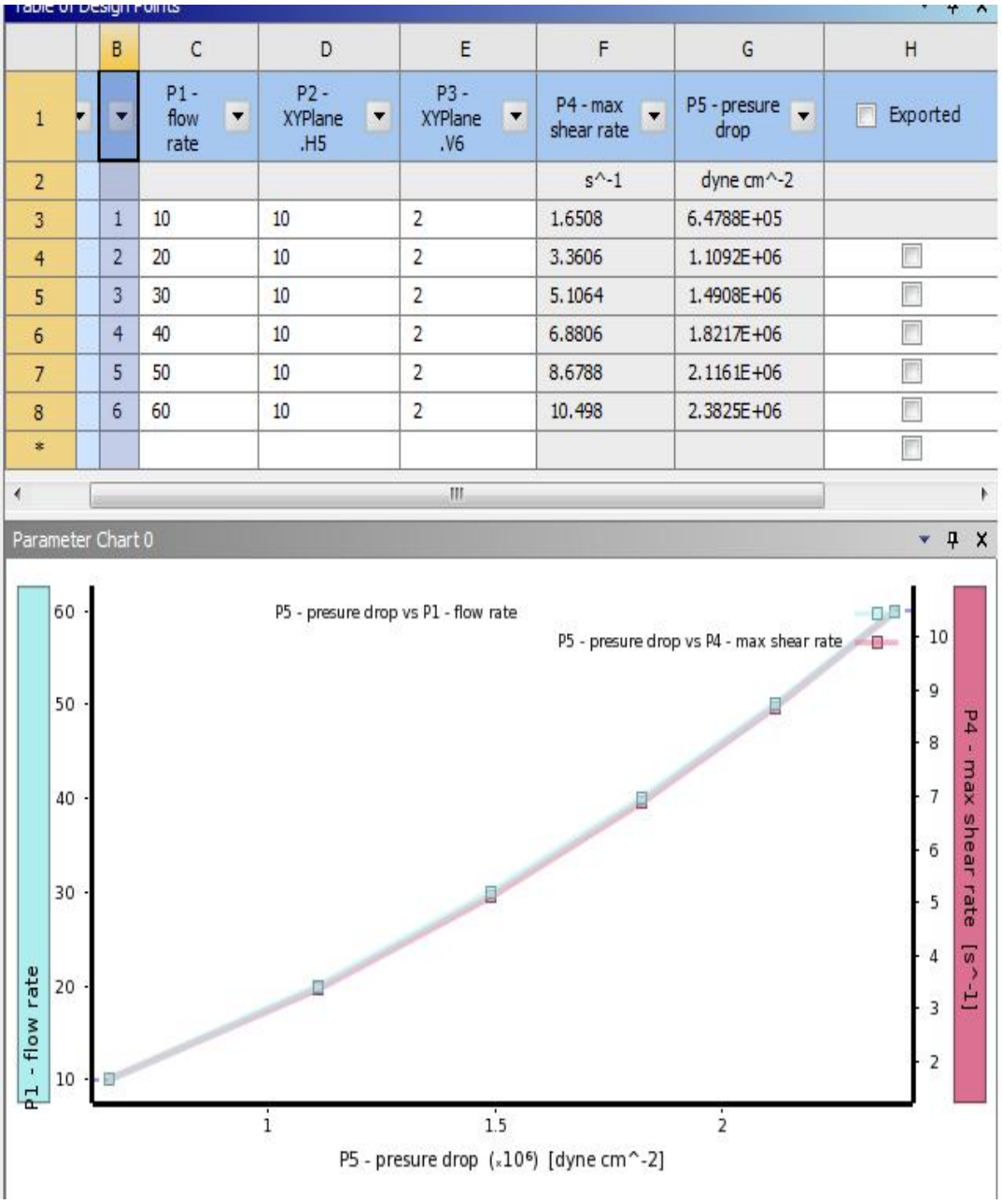

	B	C	D	E	F	G	H
1		P1 - flow rate	P2 - XYPlane .H5	P3 - XYPlane .V6	P4 - max shear rate	P5 - presure drop	Exported
2					s^-1	dyne cm^-2	
3	1	10	10	2	1.6508	6.4788E+05	
4	2	20	10	2	3.3606	1.1092E+06	
5	3	30	10	2	5.1064	1.4908E+06	
6	4	40	10	2	6.8806	1.8217E+06	
7	5	50	10	2	8.6788	2.1161E+06	
8	6	60	10	2	10.498	2.3825E+06	
*							

Fig. 2.36: Design points and chart at different inflow to pressure drop and maximum shear rate

CHAPTER THREE

Materials and Methods

3.1. Materials

To estimate the best viscosity model (viscosity versus shear rate) at isothermal condition for experimental data can be obtained from melt flow index tester for Polypropylene after fitted data in ansys Polyflow (polymat) and applied statistical analysis like Percentage Root Mean Square Error (%PRMSE).

Polypropylene properties (MFI =2 - 4 g/10min 2.16kg/230^{0}C), manufactured by Khartoum petrochemical company (PP113) for extrusion applications was used in this work. The eleven samples with average 5 grams weighting, the different MFI values were obtained at loads from 0.74kg to 8.165kg and constant temperature 230^{0}C(see in Fig 3.1 and appendix B)

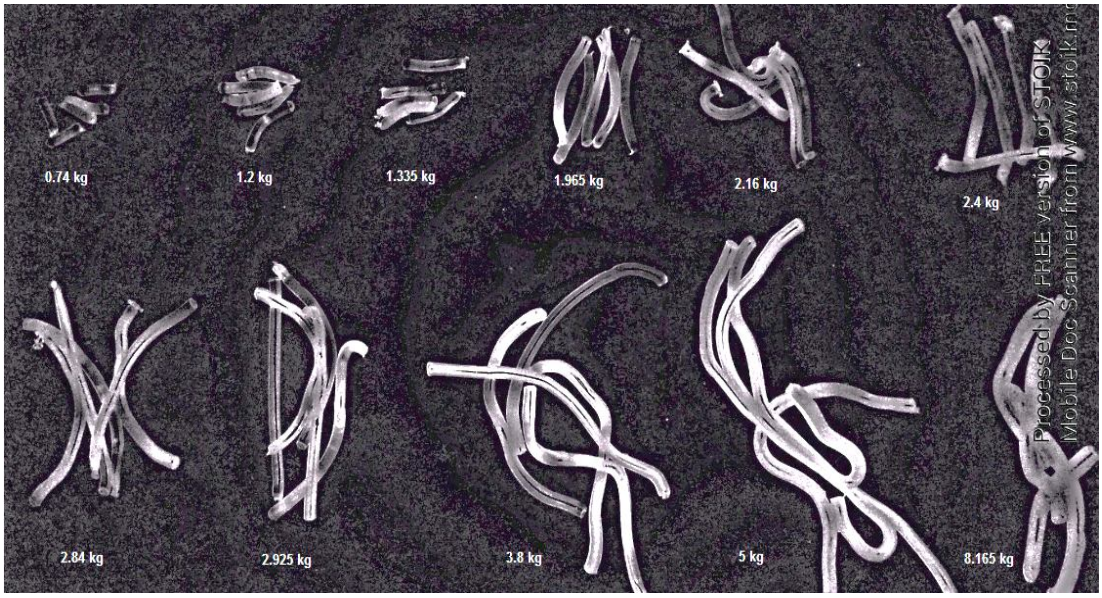

Fig. 3.1: Experimental melt extrudate from MFI for PP113 at different load

Table (4.1) lists all calculated equations from Eq (2.41) to Eq (2.48).The experimental data on shear stress is plotted against shear rate, (Fig 4.1) In case is plotted against viscosity at log scale (Fig 4.2),the Experimental viscosity (obs) with fitted viscosity (fit) for ten non Newton viscosity models fitting in POLYMAT against experimental shear rate lists in Table (4.2) and. Fig(4.3), the method of PRMSE Eq (2.49) was described in Table (4.3).

3.2. Methods to Analytical and Simulation of Single Screw Extruder Metering zone and die characteristics for polypropylene using Ansys Polyflow

After the viscosity model was obtained for PP in Eq (4.1), the analysis and simulation of the problem can be divided in to three parts as follows:

1. The combined die section (Tapered and non-tapered)
2. The single screw extruder without and with nose models.
3. The die characteristics at operating point.

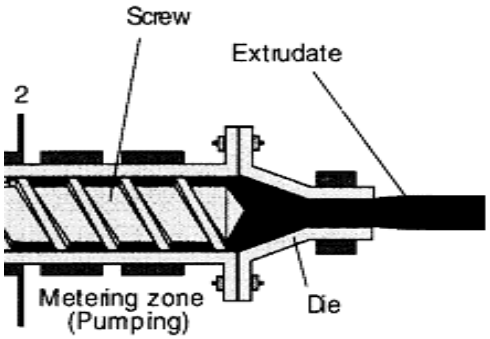

Fig. 3.2: Single extruder metering zone and die

3.2.1 The combined die section (Tapered and non-tapered)

Tapered die is very important in polymer processing, such as profile extrusion, film blowing and tube extrusion. The calculation of pressure drop for polymer melt flow through it, is important to the plastic engineering. The theoretical Pressure drop for non –tapered die as function of shear stresses but in tapered the tensile stresses will be set up in the fluid and their effects superimposed on the effects due to shear stresses this problem was analyzed for the flow fluid along coni-cylindrical. The flow is influenced by three factors Shear, Extensional and Entrance effects.

The derivation of equations of tapered and non-tapered dies assumed the polymer melt, is a Newtonian, isothermal, uncompressible and no slip on the die wall. (Crawford, 1998)

3.2.1.1 Die model

Analytically: The Die combined with non- Tapered circular section and Tapered circular section shown in Fig (4.5).The total pressure drop in die combination of two section Eq (2.33 to 2.38) at the steady –state the Flow rate constant the total pressure drop is:

$$\Delta p_{Total} = \Delta p_{circular} + \Delta p_s + \Delta p_E + \Delta p_2$$

$$\Delta p_{Total} = \frac{2L_1\tau_1}{R_1} + \frac{2\tau_1}{3tan\theta}\left(1-\left(\frac{R_1}{R_2}\right)^3\right) + \frac{2\sigma_1}{3}\left(1-\left(\frac{R_1}{R_2}\right)^3\right) + \frac{2\sqrt{2}}{3}\left(\frac{4Q}{\pi {R_2}^3}\right)(\mu_2\lambda)^{1/2} \quad ---(3.1)$$

Where:

$R_1 = 0.5\ \text{cm}, L_1 = 1\text{cm}, \mu_1 = \text{from Eq}(4.1), \tau_1 = \mu_1.\dot{\gamma}_1 = \mu_1.\frac{4Q}{\pi {R_1}^3}$,

$R_2 = 3.1\text{cm}, \lambda = 3 \times \mu_1$, $\dot{\varepsilon_1} = \frac{\dot{\gamma}_1}{3}\tan(\theta), \sigma_1 = \lambda\,\dot{\varepsilon_1}, Q = 5\ \frac{\text{cm}^3}{\text{s}}$

Analytical Effect of angle on Pressure Drop: The optimum angle for design when pressure drop is minimum for derivative Eq (3.1):

$$\frac{d\Delta p_{Total}}{d\theta} = -\frac{2\tau_1}{3}\left(\frac{1+tan^2\,\theta}{tan^2\,\theta}\right)\left(1-\left(\frac{R_1}{R_2}\right)^3\right)+\frac{2\lambda\left(\frac{\dot{\gamma}_1}{3}(1+tan^2\,\theta)\right)}{3}\left(1-\left(\frac{R_1}{R_2}\right)^3\right)=0$$

$$=-\frac{2\tau_1}{3}\left(\frac{1+tan^2\,\theta}{tan^2\,\theta}\right)\left(1-\left(\frac{R_1}{R_2}\right)^3\right)+\frac{2\frac{\lambda}{3}\left(\dot{\gamma}_1(1+tan^2\,\theta)\right)}{3}\left(1-\left(\frac{R_1}{R_2}\right)^3\right)$$

$$=0$$

$$=-\frac{2\mu_1\dot{\gamma}_1}{3}\left(\frac{1+tan^2\,\theta}{tan^2\,\theta}\right)\left(1-\left(\frac{R_1}{R_2}\right)^3\right)$$

$$+\frac{2\mu_1\dot{\gamma}_1\left((1+tan^2\,\theta)\right)}{3}\left(1-\left(\frac{R_1}{R_2}\right)^3\right)=0$$

$$\left(\frac{1+tan^2\,\theta}{tan^2\,\theta}\right)=(1+tan^2\,\theta)$$

$$tan^2\,\theta=1\ \therefore\theta=45$$

Calculate the values of pressure drop by applying Eq (3.1) at different angles (10, 20, 30, 40, 45, 50, 60,70and 80^o) when die radius 0.5cm and land 1cm shown in the Table (4.4) and Fig (4.7).

Analytical Effect of Die land on Pressure Drop: The relationship between pressure drop and die land can be derived from Eq (3.1) to Eq (3.2):

$$\frac{d\Delta p_{Total}}{dL_1}=\frac{2\tau_1}{R_1}---(3.2)$$

Calculate the values of pressure drop by applying Eq (3.1) at different die land (0.5, 1, 2, and 5cm) shown in the table (4.6) and Fig (4.9).

Analytical Effect of Die radius on Pressure Drop: The relationship between pressure drop and die radius can be derived from Eq (3.1) to Eq (3.3):

$$\Delta p_{Total}=$$

$$\frac{2L_1\tau_1}{R_1}+\frac{2\tau_1}{3\tan\theta}\left(1-\left(\frac{R_1}{R_2}\right)^3\right)+\frac{2\sigma_1}{3}\left(1-\left(\frac{R_1}{R_2}\right)^3\right)+\frac{2\sqrt{2}}{3}\left(\frac{4Q}{\pi {R_2}^3}\right)(\mu_2\lambda)^{1/2}---(3.1)$$

$$\Delta p_{Total} = \frac{2L_1\mu_1}{R_1}\left(\frac{4Q}{\pi {R_1}^3}\right) + \frac{2\mu_1}{3\tan\theta}\left(\frac{4Q}{\pi {R_1}^3}\right)\left(1-\left(\frac{R_1}{R_2}\right)^3\right) + \frac{2\lambda}{9}\left(\frac{4Q}{\pi {R_1}^3}\right)\left(1-\left(\frac{R_1}{R_2}\right)^3\right) + \frac{2\sqrt{2}}{3}\left(\frac{4Q}{\pi {R_2}^3}\right)(\mu_2\lambda)^{1/2}$$

$$\Delta p_{Total} = \frac{8QL_1\mu_1}{\pi}\left(\frac{1}{{R_1}^4}\right) + \frac{8Q\mu_1}{3\pi\tan\theta}\left(\frac{1}{{R_1}^3}\right)\left(1-\left(\frac{R_1}{R_2}\right)^3\right) + \frac{8\lambda Q}{9\pi}\left(\frac{1}{{R_1}^3}\right)\left(1-\left(\frac{R_1}{R_2}\right)^3\right) + \frac{2\sqrt{2}}{3}\left(\frac{4Q}{\pi {R_2}^3}\right)(\mu_2\lambda)^{1/2}$$

$$\Delta p_{Total} = \frac{8QL_1\mu_1}{\pi}\left(\frac{1}{{R_1}^4}\right) + \frac{8Q\mu_1}{3\pi\tan\theta}\left(\frac{1}{{R_1}^3}\right) - \frac{8Q\mu_1}{3\pi\tan\theta}\left(\frac{1}{{R_2}^3}\right) + \frac{8\lambda Q}{9\pi}\left(\frac{1}{{R_1}^3}\right) - \frac{8\lambda Q}{9\pi}\left(\frac{1}{{R_2}^3}\right) + \frac{2\sqrt{2}}{3}\left(\frac{4Q}{\pi {R_2}^3}\right)(\mu_2\lambda)^{1/2}$$

$$\Delta p_{Total} = \frac{8QL_1\mu_1}{\pi}\left(\frac{1}{{R_1}^4}\right) + \frac{8Q\mu_1}{3\pi\tan\theta}\left(\frac{1}{{R_1}^3}\right) + \frac{8\lambda Q}{9\pi}\left(\frac{1}{{R_1}^3}\right) - \frac{8Q\mu_1}{3\pi\tan\theta}\left(\frac{1}{{R_2}^3}\right) - \frac{8\lambda Q}{9\pi}\left(\frac{1}{{R_2}^3}\right) + \frac{2\sqrt{2}}{3}\left(\frac{4Q}{\pi {R_2}^3}\right)(\mu_2\lambda)^{1/2}$$

$$\Delta p_{Total} = C_1\left(\frac{1}{{R_1}^4}\right) + C_2\left(\frac{1}{{R_1}^3}\right) + C_3\left(\frac{1}{{R_1}^3}\right) + C_4 \quad ---(3.3)$$

where

$$C_1 = \frac{8QL_1\mu_1}{\pi}, C_2 = \frac{8Q\mu_1}{3\pi\tan\theta}, C_3 = \frac{8\lambda Q}{9\pi}, C_4 = -\frac{8Q\mu_1}{3\pi\tan\theta}\left(\frac{1}{{R_2}^3}\right) - \frac{8\lambda Q}{9\pi}\left(\frac{1}{{R_2}^3}\right) + \frac{2\sqrt{2}}{3}\left(\frac{4Q}{\pi {R_2}^3}\right)(\mu_2\lambda)^{1/2}$$

Calculate the values of pressure drop by applying Eq (3.1) at different die radii (0.5, 0.6, 0.7, 0.8, 1, 1.5 and 2cm) shown in the table (4.8) and Fig (4.11).

Simulation model:

Model: creating a sketch on the XY Plane to half of theoretical model was shown in Fig (4.5) and set dimensions then revolve the sketch to complete 3D model, see Fig (4.6).

Meshing: automatically generate medium meshing and assign to three face as boundary input, output and wall.

Setup (Polydata): the task is FEM, steady- state, isothermal, enter materials data (type of viscosity model Eq (4.1) the boundary set as:

Boundary 1: Input =inflow (5 cm^3/s)

Boundary 2: Output=outflow,

Boundary 3: Wall = zero normal velocity and zero surface velocity condition V_n=0 Vs=0

Solution and Result: Contours of output parameters (shear rate, pressure drop) are graphically represented at every mesh of the structural geometry.

Generate results for multiple design points for study effect of die dimensions (angle, die land L1 and radius R1) at the values of analytical considered to the parameters (pressure drop was taken between average pressure at Die inlet and average pressure at Die outlet, average velocity, maximum and minimum shear rate) using the parameter and Design Points view. The results shown in Tables (4.5, 4.7 and 4.9) and Figs (4.8, 4.10 and 4.12).

3.2.1.2 Die and free jet

Analytically: In section (2.7.6) the swell ratio of the polymer melt is extruded through a die the cross-sectional area of the extrudate is greater than that of the die.

$$B_{SR} = \frac{D_{extrudate}}{D_{die}} = \sqrt{\frac{area\ of\ swoollen\ extrudate}{area\ of\ capillary}} \quad - - - (2.50)$$

Extrudate swell increases: as the die length decreases, as the shear rate or shear stress increase, and the molar mass of the polymer increases.

Factors affecting the extrudate swell ,Residence flow time, Die temperature, Shear rate, Die length or die land, L/D radio, Additives, Molar mass, Flow patterns, Die geometry and number of flow channel.

Simulation model:

Model: added to die model was designed the Extrude tools to output face to complete 3D model content two parts Die and Free Jet, see Fig(4.13).

Meshing: automatically generate medium meshing and assign to four faces as boundary input, output and wall and free surface.

Setup (Polydata): the task is FEM, steady- state, isothermal, enter materials data (type of viscosity model Eq 4.1) the boundary set as:

Boundary 1: Input =inflow (5cm3/s)

Boundary 2: Output= normal and tangential force imposed f_n=0 fs=0

Boundary 3: Wall = zero normal velocity and zero surface velocity condition

Boundary 4: free surface =free surface

Solution and Results: plans of velocity are graphically represented when the generate results for multiple design points for study effect of die land values (0.5, 1, 2 and 5cm) at constant radius 0.5cm, L/D ratio at radii (0.5, 0.6, 0.7, 0.8, 1, 1.5 and 2cm) at constant die land 5cm to output parameters (pressure drop was take between average pressure at Die inlet and average pressure at Die outlet, swell ratio equal square area at free jet _outlet over area of die outlet, maximum and minimum

shear rate) the results shown in tables (4.10),(4.11) and Figs (4.14),(4.15),(4.16),(4.17).

3.2.2 The single screw extruder without and with nose models

Analytically: total flow rate in single screw extruder in the metering zone.

$$Q_{Total} = Q_d - Q_p$$

$$Q_{Total} = \frac{1}{2}\pi^2 D^2 NHsin\emptyset cos\emptyset - \frac{\pi DH^3 sin^2\emptyset}{12\mu}.\frac{P}{L} - - - (2.31)$$

Where:

D: Flight diameter =6cm

H: screw depth =0.6cm

L: Length of metering zone = one flight =6cm

Q_d, Q_p: Volume flow rate of drag, pressure flow

p: Pressure difference across the metering zone

μ: Melt viscosity =from viscosity model at shear rate of metering zone Eq (4.1)

N: Screw speed (rev/s) =60RPM=1rev/s

$\emptyset$: flight angle =Square pitch (pitch=Diameter) $= 17.65678715$

e: Flight width =0.6 cm

δ_{FLT}: Flight clearance=0.1cm

And the shear rate in the metering zone:

$$\dot{\gamma} = \frac{\pi DN}{H} - - - (2.10)$$

And two situations

$$Q_T = Q_d = Q_{max} = \frac{1}{2}\pi^2 D^2 NHsin\emptyset cos\emptyset - - - (2.32)$$

$$P_{max} = \frac{6\mu\pi \mathrm{D}NL}{H^2 tan\emptyset} - -(2.33)$$

Screw model:

Model: creating three sketches to the flight, screw roots and barrel (melt) on the XY Plane and set dimensions the flight sketch was sweep and revolves another sketches to complete 3D model, the flight and roots bodies combined to describe screw body then subtract it from melt body, the final body a sign to fluid, see Fig (4.18).

Meshing: automatically generate medium meshing and assign to four faces as boundary input, output, barrel, screw

Setup (Polydata): the task is FEM, steady- state, isothermal, enter materials data (type of viscosity model Eq (4.1) the boundary set as:

Boundary 1: input = normal and tangential force imposed f_n=0 ,fs=0

Boundary 2: output= normal and tangential force imposed f_n=0 ,fs=0

Boundary 3: barrel = zero normal velocity and zero surface velocity condition V_n=0 ,Vs=0

Boundary 4: screw = angular velocity (rad/s)

Solution and Results: Contours of output parameters (shear rate, pressure drop) are graphically represented at every mesh of the structural geometry.

Generate results for multiple design points for study effect of screw parameters (flights width (e), flight clearance (δ_{FlT}), depth (H), rotation speed (N), and metering length (L)) at the values of the parameters (maximum pressure drop was taken between max pressure at screw and min pressure at screw, Postprocessor of Flow rate at screw output, maximum and minimum shear rate) using the parameter and Design Points view.

Nose model:

Model: anothersketchfor nose body added to screw model, the final body a sign to fluid and longer than screw by 1cm, see Fig (4.19).

Meshing: automatically generate medium meshing and assign to four faces as boundary input, output, barrel, screw

Setup (Polydata): the task is FEM, steady- state, isothermal, enter materials data (type of viscosity model Eq (4.1) the boundary set as:

Boundary 1: input = normal and tangential force imposed f_n=0 ,fs=0

Boundary 2: output= normal and tangential force imposed f_n=0 ,fs=0

Boundary 3: barrel = zero normal velocity and zero surface velocity condition V_n=0 ,Vs=0

Boundary 4: screw = angular velocity (rad/s)

Solution and Results: Contours of output parameters (shear rate, pressure drop) are graphically represented at every mesh of the structural geometry.

Generate results for multiple design points for study effect of screw parameters (flights width (e), flight clearance (δ_{FlT}), depth (H), screw speed (N), and metering length (L)) at the values of the parameters (maximum pressure drop was taken between max pressure at screw and min pressure at screw, Postprocessor of Flow rate at screw output, maximum and minimum shear rate) using the parameter and Design Points view.

Analytical extruder line Q_{max}, P_{max}

$$\dot{\gamma}_H = \frac{\pi DN}{H} = \frac{\pi \times 6 \times \left(\frac{60}{60}\right)}{0.6} = 31.4159 \text{ which gives} \mu = 13864.4 \text{ poise}$$

$$Q_T = Q_{max} = \frac{1}{2}\pi^2 \times 6^2 \times \left(\frac{60}{60}\right) \times 0.6 \times sin17.65678715 cos17.65678715 = 30.808\,\text{cm}^3/s$$

$$P_{max} = \frac{6 \times 13864.4 \times \pi \times 6 \times \left(\frac{60}{60}\right) \times 6}{(0.6)^2 tan17.65678715} = 8.209 \times 10^7 \frac{dyne}{cm^2}$$

$$\dot{\gamma}_{\delta t} = \frac{\pi DN}{\delta t} = \frac{\pi \times 6 \times \left(\frac{60}{60}\right)}{0.1} = 188.4956 \approx \mu = 4647.652 \text{ poise}$$

$$Q_T = Q_{max} = 30.808\,\text{cm}^3/s$$

$$P_{max} = 2.752 \times 10^7 \frac{dyne}{cm^2}$$

The simulation of maximum flow rate and pressure in screw and nose in Figs (4.20), (4.21), (4.22), (4.23).

Effect of different flight width to the maximum output: Calculated and simulation of maximum output at different flight width (e=0.6, 0.5, 0.4, 0.3, and 0.2cm)are shown in tables (4.12),(4.13),(4.14) and Fig (4.24).

Effect of different flight clearance to the maximum output: Calculated and simulation of maximum output at different flight width (δ_{FlT} =0.1, 0.09, 0.08, 0.07, 0.06 and 0.05cm) are shown in tables (4.15),(4.16), (4.17) and Fig (4.25).

Effect of different flight depth to the maximum output: Calculated and simulation of maximum output at different depth (H =0.6, 0.5, 0.4, and 0.3cm) are shown in tables (4.18), (4.19), (4.20) and Fig (4.26).

Effect of different screw speed to the maximum output: Calculated and simulation of maximum output at different speed (N=30, 45, 60, 75 and 90 RPM) are shown in tables (4.21), (4.22),(4.23) and Fig (4.27).

Effect of screw length to the maximum output: Calculated and simulation of maximum output at different screw length (L=6, 12, 18, 24 and 39 cm) are shown in tables (4.24),(4.25),(4.26) and Fig (4.28).

3.2.3 The die characteristics at operating point

Analytically : the operation point is the intersection between extruder line and die line, Eq (2.40),(2.41) described the operating pressure and operating flow rate in screw and circular die section.

$$P_{op} = \frac{2\pi\mu D^2 NH sin\emptyset_b cos\emptyset_b}{\frac{{R_1}^4}{2L_1} + \frac{DH^3 sin^2\emptyset_b}{3L}} - - - (2.40)$$

$$Q_{op} = \frac{\pi {R_1}^4}{8\mu L_1} . P_{op} - - - (2.41)$$

$$Q_{op} = \frac{\pi {R_1}^4}{8L_1} . \frac{2\pi D^2 NH sin\emptyset_b cos\emptyset_b}{\frac{{R_1}^4}{2L_1} + \frac{DH^3 sin^2\emptyset_b}{3L}} - - - (2.41)$$

Operation point model:

Model: the die and nose models were design before in Figs (4.6), (4.19) combined them see Fig (4.29).

Meshing: automatically generate medium meshing and assign to four faces as boundary input, output, barrel, screw

Setup (Polydata): the task is FEM, steady- state, isothermal, enter materials data (type of viscosity model Eq 7) the boundary set as:

Boundary 1: input = normal and tangential force imposed f_n=0 ,fs=0

Boundary 2: output= normal and tangential force imposed f_n=0 ,fs=0

Boundary 3: barrel = zero normal velocity and zero surface velocity condition V_n=0 ,Vs=0

Boundary 4: screw = angular velocity (rad/s)

Solution and Results: Contours of output parameters (shear rate, pressure drop) are graphically represented at every mesh of the structural geometry.

Generate results for multiple design points for study effect of screw parameters (flights width (e), flight clearance (δ_{FlT}), depth (H), screw speed (N) and screw length (L)) at the values of the parameters (maximum pressure drop was taken between max pressure at screw and min pressure at screw, Postprocessor of Flow rate at screw output, maximum and minimum shear rate) using the parameter and Design Points view.

Analytical extruder line Q_{max}, P_{max}

Calculated maximum extruder output and maximum pressure at high shear rate in die radius 0.5cm, and die land 1cm.

$$Q_T = Q_{max} = \frac{1}{2}\pi^2 \times 6^2 \times \left(\frac{60}{60}\right) \times 0.6 \times sin17.65678715 cos17.65678715$$
$$= 30.808\,\text{cm}^3/s$$

$$\dot{\gamma}_{die} = \frac{4Q_{max}}{\pi R_1{}^3} = \frac{4 \times 30.808}{\pi \times (0.5)^3} = 303.80491 \quad \approx \mu = 3210.257701 \text{ poise}$$

$$P_{max} = \frac{6 \times 3210.257701 \times \pi \times 6 \times \left(\frac{60}{60}\right) \times 7}{(0.6)^2 tan17.65678715} = 2.2 \times 10^7 \frac{dyne}{cm^2}$$

The simulation maximum output and pressure for different operating points at die radii (R1=0.5, 0.6, 0.7, 0.8, and 1cm) and die land 1cm in tables (4.27), (4.28), and Figs (4.30),(4.31).

Effect of different flight width on operating points: Calculated extruder line and simulation of operating points at different flight width (e=0.6, 0.4, and 0.2cm) are shown in tables (4.29), (4.30) and Fig (4.32).

Effect of different clearance on operating points: Calculated extruder line and simulation of operating points at different flight width (δ_{FlT} =0.1, 0.08, and 0.06cm) are shown that in tables (4.31), (4.32) and Fig (4.33).

Effect of different flight depth on operating points: Calculated extruder line and simulation of operating points at different depth (H =0.6, 0.5, and 0.4cm) are shown in tables (4.33), (4.34) and Fig (4.34).

Effect of different screw speed on operating points: Calculated extruder line and simulation of operating points at different speed (N=30, 60, and 90 RPM) are shown in tables (4.35), (4.36) and Fig (4.35).

Effect of screw length on operating points: Calculated extruder line and simulation of operating points at different screw length (L=7, 13, and 19 cm) are shown in tables (4.37), (4.38) and Fig (4.36).

CHAPTER FOUR

Results and Discussion

4.1. Material

Table (4.1) and (Fig. 4.1) it is obvious that the plastic melt is non Newton fluid. In case is plotted against viscosity at log scale (Fig.4.2) it is obvious that the viscosity decrease with increase shear rate. Table (4.2) and. Fig (4.3), (Fig.4.2) Table (4.3), it is obvious that the best model (Carreau Yasuda law) according to PRMSE method. Fig (4.4), without taking into account the slight differences between it and (log log law and cross law). By substitute the model parameter from Appendix C in the equation in appendix D, Eq (D.15)

$$\mu = \mu_\infty + (\mu_0 - \mu_\infty)(1 + (\beta\dot{\gamma})^a)^{\frac{n-1}{a}} - - - (4.1)$$

Where

μ_∞= infinite-shear-rate viscosity =$0.01445808\ poise$

μ_0= zero-shear-rate viscosity =$67380.02\ poise$

β = natural time (i.e., inverse of the shear rate at which the fluid changes from Newtonian to power-law behavior) =0.03531332 sec

a = index that controls the transition from the Newtonian plateau to the power-law region = 0.4534786

n = power-law index = 0.5375814E-05

4.2. The combined die section (Tapered and non-tapered)

Die: The analytical derivation for the taper angle to obtain minimum pressure drop is $45^\circ$the same result was obtained when calculating the different types of pressure drops for range of taper angle 10° to80°.The taper angle don't affect the value of strain shear rate, on the other hand when using poly flow software the taper angle that gives minimum pressure drop is between $45^\circ \sim 50^\circ$,see Fig(4.7).The same result was obtain experimentally by (Mitsoulis et al., 2005) .This study shows that the shear strain rate for minimum pressure drop is not affected by taper angle while the software ,the shear strain rate varies as the taper angle is increased, see Table (4.5) and Fig(4.8).

The pressure gradient across die land Eq (3.2) is equal to $2.2 \times 10^6 \text{dyne.cm}^{-1}$. The software gives a value of $2.4529 \times 10^6 \text{dyne.cm}^{-1}$.Both results were obtained when varying die land 0.5, 1, and 5 cm, see Tables (4.6), (4.7) and Fig(4.9).

When studying the relation between the die radius and pressure drop using both calculation Eq (3.3) and software .the pressure drop is

inversely related to die radius .At a radius of 2cm and above the results tend to be identical, seeTables (4.8), (4.9) and Fig(4.11).

Die and Free Jet: in table (4.10) and Fig (4.14),(4.15) it is obvious that the swell ratio decreased by small amount when die land was increased at linear pressure drop gradient, in table (4.11) and Fig(4.16),(4.17) it is obvious the swell ratio decreased by high amount when L/D was increase at non- linear pressure drop gradient.

4.3. The single screw extruder without and with nose models

The extruderline: Fig (4.20) shown that the maximum output is equal 30.8077 cm^3/s and the maximum pressure at the shear rate in flight depth $31.4s^{-1}$ and at flight clearance $188.4s^{-1}$, in this figure the screw and nose simulation appeared as single points, the flow rate was not affected but the pressure was, when the nose combined to the screw the pressure drop increased as a result of the length increased from 6cm to 7cm. the calculated pressure at flight clearance and flight depth were high compared to the simulation, the shear rate of $188.4s^{-1}$ calculated at flight clearance give pressure that approached to simulation results, in Fig (4.21) the simulation give a value of $203\ s^{-1} - 207\ s^{-1}$.

Flight width: in table (4.12) the calculated maximum extruder output equal 30.808 when flight width was varied, the simulation of screw and nose was described in tables (4.13), (4.14) it is obvious that there is small difference in flow rate between them, the flow rate was increased and pressure decreased at flight width decreased. Finally the difference between the results of analytical and simulations in Fig (4.24) tend to be equal.

Flight clearance: in table (4.15) the calculated maximum extruder output equal 30.808 cm^3/s was obtained. When flight clearance was varied, the simulation of screw and nose was described in tables (4.16), (4.17) it is obvious that there is small difference in flow rate between them, the output and pressure was increased as flight clearance decreased. Finally the difference between analytically and simulations in Fig (4.25) tend to be equal.

Flight depth: in table (4.18) the maximum extruder output decreased as screw depth decreased analytically. The simulation of screw and nose was described in tables (4.19), (4.20) it is obvious that there is small different in flow rate between them, the pressure was increase at depth decreased. Finally the difference between analytical and simulations in Fig (4.26) diverge at deep depth with linear relationship.

Screw speed: in table (4.21) the maximum extruder output increased at screw speed increased analytically, the simulation of screw and nose was described in tables (4.23), (4.24) it is obvious that there small different in flow rate between them, the pressure was increase at screw speed was increased, finally the difference between analytically and simulations in Fig (4.27) diverge at high speed with linear relationship.

Screw length: in table (4.24) the calculated maximum extruder output equal 30.808 cm^3/s was obtained. When screw length was varied, the simulation of screw and nose was described in tables (4.25),(4.26) it is obvious that there is a fluctuation in flow and pressure at length was varied. Finally the difference between analytically and simulations was not constant, in Fig (4.28) it is obvious that at 12cm (2 flight) give a maximum extruder output.

4.4. The die characteristics at operating point

The extruderline : Fig(4.30) shown the maximum output equal $30.8077\,cm^3/s$and the maximum pressure according to the shear rate at die $303.80491s^{-1}$ equal $2.2 \times 10^7\,dyne/cm^2$, table (4.27) described simulated nose that was give the maximum output $19.9736\,cm^3/s$,and pressure $7.5966 \times 10^6\,dyne/cm^2$ and operating points at different die radii from table (4.28) ,in Fig(4.30) it is obvious that the linear relationship of analytical and simulated the same intersected at maximum output and maximum pressure. Fig (4.31) shown interior values shear rate, pressure, viscosity, and velocity.

Flight width: in table (4.29) the constant calculated of maximum extruder output equal $30.8077\,cm^3/s$ and the maximum pressure $2.2 \times 10^7\,dyne/cm^2$ when flight width was varied, also described simulated nose that was give the maximum output with pressure and the values of operating points at different die radii and flight width from table(4.30) ,Fig(4.32) it is obvious that the linear relationship of analytical give maximum output and pressure ($30.8077\,cm^3/s$, $2.2 \times 1\,0^7\,dyne/cm^2$) and simulated the maximum output ($31.5\,cm^3/s$, $32.3\,cm^3/s$, $and\ 32.5\,cm^3/s$) and maximum Pressure ($2.11 \times 10^7\,dyne/cm^2$, $2.09 \times 10^7\,dyne/cm^2$, $and\ 2.08 \times 10^7\,dyne/cm^2$) at 0.6, 0.5, and 0.4 cm flight width respectively ,from the predictive linear equations the output increase and pressure decrease at flight width decrease, these good results but the designed flight width about 0.1 screw diameter(Muccio, 1994) is 0.6 cm to avoid screw corrosion it cannot by rehabilitated by wearing .

Flight clearance: in table (4.31) the constant calculated of maximum extruder output equal $30.8077\,cm^3/s$ and the maximum pressure equal

$2.2 \times 10^7\ dyne/cm^2$ when flight clearance was varied, also described simulated nose that was give the maximum output with pressure and the values of operating points at different die radii and flight clearance from table(4.32) ,Fig(4.33) it is obvious that the linear relationship of analytical give maximum output and pressure ($30.8077\ cm^3/s$, $2.2 \times 10^7\ dyne/cm^2$) and simulated the maximum output ($30.866\ cm^3/s, 29.531\ cm^3/s, and\ 28.188\ cm^3/s$) and maximum pressure($2.18 \times 10^7\ dyne/cm^2, 2.55 \times 10^7\ dyne/cm^2, and\ 3.18 \times 10^7\ dyne/cm^2$) at 0.1, 0.08, and 0.06 cm flight clearance respectively ,from the predictive linear equations the output decrease and pressure increase at flight clearance decrease, these obesity results at the simulation of screw and nose was obtained before.

flight depth: table (4.33) described the analytical calculated values of maximum extruder output and the maximum pressure at flight depth was varied, simulated nose that was give the maximum output with pressure ,and the values of operating points at different die radii and flight depth from table(4.34) , Fig (4.34) it is obvious that the linear relationship of analytical give maximum output ($30.8077\ cm^3/s, 25.6731\ cm^3/s, and\ 20.5385\ cm^3/s$) and maximum pressure($2.2 \times 10^7\ dyne/cm^2, 3.6555 \times 10^7\ dyne/cm^2, and\ 6.711 \times 10^7\ dyne/cm^2$) and simulated the maximum output ($30.897\ cm^3/s, 25.974\ cm^3/s, and\ 19.938\ cm^3/s$) and maximum pressure($2.16 \times 10^7\ dyne/cm^2, 2.43 \times 10^7\ dyne/cm^2, and\ 2.67 \times 10^7\ dyne/cm^2$) at 0.6, 0.5, and 0.4 cm flight depth respectively ,from

the predictive linear equations the maximum extruder output analytically and simulation tended to the same values but analytically pressure high amount than simulation values at flight depth decreased less than 0.1cm.

Screw speed: table (4.35) described the analytical calculated values of maximum extruder output and the maximum pressure at flight depth was varied, simulated nose without die that was give the maximum output with pressure ,and the values of operating points for different die radii and screw speed in table(4.36) , Fig (4.35) it is obvious that the linear relationship of analytical give maximum output ($15.4039\,cm^3/s\,, 30.8077\ cm^3/s\,,\ and\ 46.2116\,cm^3/s$) and maximum pressure ($1.82\times10^7\,dyne/cm^2\,,\ 2.2\times10^7\,dyne/cm^2\,,\ and\ 2.34\times10^7\,dyne/cm^2$) and simulated maximum output ($14.90\,cm^3/s\,, 30.112\,cm^3/s\,, and\ 45.06\,cm^3/s$) and maximum pressure($1.7\times10^7\,dyne/cm^2\,, 2.25\times10^7\,dyne/cm^2\,,\ and\ 2.6\times10^7\,dyne/cm^2$) at 30, 60, and 90 rev/minscrew speed respectively ,from the predictive linear equations the maximum extruder output and pressure analytically and simulation tended to the same values .

Screw length: table (4.37) described the analytical calculated values of maximum extruder output and the maximum pressure at screw length was varied, simulated nose without die that was give the maximum output with pressure ,and the values of operating points for different die radii and screw length in table(4.38) ,

Fig (4.36) it is obvious that the linear relationship of analytical give three equal maximum output of ($30.8077\,cm^3/s$) and maximum pressure ($2.2\times10^7\,dyne/cm^2\,, 4.12\times10^7\,dyne/cm^2\,, and\ 6.02\times$

$10^7\ dyne/cm^2$) and simulated maximum output ($30.897\ cm^3/s$, $29.532\ cm^3/s\ , and\ 24.538\ cm^3/s$) and maximum pressure($2.15 \times 10^7\ dyne/cm^2\ , 3.53 \times 10^7\ dyne/cm^2\ , and\ 8.15 \times 10^7\ dyne/cm^2$) at 7, 13, and 19 cm screw length respectively ,from the predictive linear equations the maximum extruder output analytically was constant and pressure increased at screw length was increased , in simulation the output was decreased and pressure increased at screw length was increased. The screw length was not effect in output analytically but in simulation it was.

Table 4.1: Experimental data for PP113 from MFI.

Sample	t(s)	load (g)	load(kg)	m(g)	MFI (g/10min)	load F (dyne)	distance of piston *l* (cm)	Melt density (g/cm^3)	Flow rate Q (cm^3/s)	shear rate at wall (s^{-1})	Shear Stress ($dyne/cm^2$)	Viscosity ($dyne/cm^2.s$)
1	150	325+415	0.74	0.1778	0.711	725692.1	0.325	0.76	0.001551553	1.719	66326.91541	38590.037
2	150	325+875	1.2	0.33	1.32	1176798	0.587	0.78	0.002803131	3.105	107557.1601	34637.603
3	150	325+960	1.335	0.335	1.34	1309187.775	0.688	0.68	0.003285442	3.640	119657.3406	32877.404
4	150	325+1640	1.965	0.6423	2.56	1927006.725	1.256	0.71	0.005976364	6.620	176124.8497	26603.303
5	150	325+875+960	2.16	0.765	3.06	2118236.4	1.51	0.71	0.007210781	7.988	193602.8882	24237.147
6	150	325+875+1200	2.4	0.8805	3.52	2353596	1.646	0.75	0.007855765	8.702	215114.3202	24719.108
7	150	325+875+1640	2.84	1.165	4.66	2785088.6	2.197	0.74	0.010491448	11.622	254551.9456	21902.464
8	150	325+960+1640	2.925	1.2225	4.9	2868445.125	2.416	0.71	0.011560843	12.807	262170.5778	20471.347
9	150	325+875+968+1640	3.8	1.839	7.36	3726527	3.666	0.70	0.017515959	19.404	340597.6737	17553.339
10	150	325+875+969+1640+1200	5	2.974	11.9	4903325	5.894	0.70	0.028155387	31.190	448154.8338	14368.736
11	30	325+875+969+1640+1200+3165	8.165	1.7692	42.48	8007129.725	3.497	0.71	0.100241737	111.044	731836.8437	6590.489

Table 4.2: Experimental (obs) with fitted (fit) viscosity for ten non Newton viscosity models

Exp	Power Low	Bird-Carreau Law	Cross Law	Log log law	Bingham law	Herschel-Bulkley law	modified Cross law	modified Bingham law	modified Herschel-Bulkley law	Carreau Yasuda law
38590.03724	45412.01182	37573.25705	38697.0458	38889.31757	34529.45607	37530.28061	38292.33019	36028.939	39884.70614	39049.84588
34637.6035	35427.97961	34582.28711	33900.29594	33895.84207	32914.25153	34842.51188	34028.3507	33395.295	33483.00355	33816.96347
32877.40406	33143.96077	33371.08834	32505.06136	32461.14219	32291.81347	33806.7486	32696.29091	32460.852	31941.30352	32369.08665
26603.30264	25783.08705	27570.69962	27014.40648	26920.01629	28819.08725	28027.98518	27198.15378	27950.197	26572.23246	26866.71516
24237.14692	23829.02123	25556.84069	25264.84754	25184.99908	27226.03045	25591.05334	25394.11631	26222.710	24983.60784	25155.0276
24719.10775	22987.34758	24640.1176	24469.98772	24400.42528	26393.65634	24543.35487	24570.78419	25392.755	24268.02355	24380.97127
21902.46398	20358.6245	21629.16973	21823.80309	21800.45089	22992.2191	21312.10258	21824.68595	22445.814	21881.05526	21812.45384
20471.34659	19545.83395	20664.28149	20955.34341	20949.76869	21612.1279	20326.27542	20924.63428	21426.022	21087.79172	20970.24093
17553.33874	16417.70576	16878.04388	17400.43453	17468.07348	16081.55464	16596.3475	17267.43118	17107.529	17729.05332	17510.00873
14368.73577	13452.10314	13287.17992	13760.88578	13876.43806	11999.83161	13165.44343	13597.07635	12823.126	14034.49033	13915.77655
6590.489347	7894.104651	6918.799807	6692.019625	6659.555721	7167.423352	7085.08718	6736.920983	6804.221	6615.603709	6648.867404

Table 4.3: Apply PRMSE for experimental (obs) and fitted (fit) viscosity models

	Exp	Power Low	Bird-Carreau Law	Cross Law	Log log law	Bingham law	Herschel-Bulkley law	modified Cross law	modified Bingham law	modified Herschel-Bulkley law	Carreau-Yasuda law
	0	0.031251423	0.000694231	7.6893E-06	6.01459E-05	0.011071998	0.000754157	5.95152E-05	0.004404556	0.001125556	0.000141972
	0	0.000520681	2.55042E-06	0.000453108	0.000458599	0.002475439	3.49964E-05	0.000309385	0.001286362	0.001111136	0.000561319
	0	6.57331E-05	0.000225478	0.00012826	0.000160302	0.000317244	0.000799022	3.03462E-05	0.000160525	0.000810681	0.000239042
	0	0.000950572	0.001322325	0.000238799	0.00014173	0.006937196	0.002867907	0.000499972	0.00256328	1.36401E-06	9.80396E-05
	0	0.000283547	0.002964718	0.00179792	0.00152939	0.015207401	0.003120429	0.002278666	0.006711266	0.00094853	0.001434199
	0	0.004908061	1.02113E-05	0.000101567	0.000166208	0.004589125	5.05521E-05	3.60043E-05	0.000742676	0.000333004	0.000187119
	0	0.00496842	0.000155695	1.28983E-05	2.16933E-05	0.002475551	0.000726524	1.26104E-05	0.000615423	9.55423E-07	1.68887E-05
	0	0.002043958	8.88237E-05	0.000558975	0.000546172	0.00310536	5.02192E-05	0.000490292	0.002174795	0.000906768	0.000593915
	0	0.004185588	0.001480019	7.58786E-05	2.35953E-05	0.007030217	0.002972326	0.000265297	0.000645031	0.000100207	6.09338E-06
	0	0.004069617	0.005665794	0.001789599	0.001173866	0.027180526	0.007013022	0.002884126	0.011570775	0.00054112	0.000993759
	0	0.039125831	0.002481613	0.000237332	0.000109824	0.00766332	0.005632084	0.000493667	0.001051729	1.45214E-05	7.84628E-05
PRMSE	**0**	**2.762999791**	**1.116793623**	**0.668167867**	**0.602441657**	**2.697617225**	**1.408980586**	**0.779906843**	**1.624360456**	**0.697921528**	**0.599642512**

Table 4.4: Calculation pressure drop at different die angle

R_1 (cm)	L_1 (cm)	Angle (θ) degree	Q $(\frac{cm^3}{s})$	γ_1 (s^{-1})	γ_2 (s^{-1})	μ_1 $(\frac{dyne}{cm^2}.s)$	μ_2 $(\frac{dyne}{cm^2}.s)$	τ_1 $(\frac{dyne}{cm^2})$	λ $(\frac{dyne}{cm^2}.s)$	$\dot{\varepsilon}_1$ (s^{-1})	σ_1 $(\frac{dyne}{cm^2})$	$\Delta p_{circular}$ $(\frac{dyne}{cm^2})$	Δp_s $(\frac{dyne}{cm^2})$	Δp_E $(\frac{dyne}{cm^2})$	Δp_2 $(\frac{dyne}{cm^2})$	Δp_{Total} $(\frac{dyne}{cm^2})$
0.5	1.0	10.0	5.0	50.9	0.2	10685.7	53630.6	544216.2	32057.0	3.0	95960.0	2176865.0	2048969.0	63704.9	8353.8	**4297892.7**
0.5	1.0	20.0	5.0	50.9	0.2	10685.7	53630.6	544216.2	32057.0	6.2	198078.5	2176865.0	992632.0	131498.3	8353.8	**3309349.1**
0.5	1.0	30.0	5.0	50.9	0.2	10685.7	53630.6	544216.2	32057.0	9.8	314203.4	2176865.0	625770.1	208590.0	8353.8	**3019578.9**
0.5	1.0	40.0	5.0	50.9	0.2	10685.7	53630.6	544216.2	32057.0	14.2	456651.6	2176865.0	430566.9	303157.1	8353.8	**2918942.7**
0.5	1.0	45.0	5.0	50.9	0.2	10685.7	53630.6	544216.2	32057.0	17.0	544216.2	2176865.0	361288.5	361288.5	8353.8	**2907795.8**
0.5	1.0	50.0	5.0	50.9	0.2	10685.7	53630.6	544216.2	32057.0	20.2	648571.7	2176865.0	303157.1	430566.9	8353.8	**2918942.7**
0.5	1.0	60.0	5.0	50.9	0.2	10685.7	53630.6	544216.2	32057.0	29.4	942610.2	2176865.0	208590.0	625770.1	8353.8	**3019578.9**
0.5	1.0	70.0	5.0	50.9	0.2	10685.7	53630.6	544216.2	32057.0	46.6	1495221.8	2176865.0	131498.3	992632.0	8353.8	**3309349.1**
0.5	1.0	80.0	5.0	50.9	0.2	10685.7	53630.6	544216.2	32057.0	96.3	3086403.7	2176865.0	63704.9	2048969.0	8353.8	**4297892.7**

Table 4.5: Design points at different die angle

Table of Design Points

	A	B	C	D	E	F	G	H	I	J	K	L
1	Name		P3 - angle	P13 - R1	P12 - L1	P10 - flow rate	P7 - average velosity	P6 - presure drop	P8 - max velosity	P9 - max shear rate	P11 - min shear rate	Exported
2	Units						cm s^-1	dyne cm^-2	cm s^-1	s^-1	s^-1	
3	Current	1	10	0.5	1	5	7.952	6.1233E+06	10.928	67.343	0.028903	
4	DP 1	2	20	0.5	1	5	7.373	4.4093E+06	10.831	73.952	0.056358	☑
5	DP 2	3	30	0.5	1	5	8.0871	3.8908E+06	10.846	80.197	0.095681	☑
6	DP 3	4	40	0.5	1	5	7.6186	3.7744E+06	10.921	88.198	0.18004	☑
7	DP 4	5	45	0.5	1	5	7.852	3.7453E+06	11	88.53	0.26391	☑
8	DP 5	6	50	0.5	1	5	7.7419	3.7421E+06	11.037	91.254	0.33823	☑
9	DP 6	7	60	0.5	1	5	7.566	3.8582E+06	11.116	93.925	0.48874	☑
10	DP 7	8	70	0.5	1	5	7.727	4.3439E+06	11.321	112.97	0.47498	☑
11	DP 8	9	80	0.5	1	5	7.9736	6.9648E+06	11.822	190.58	0.49037	☑
*												☐

Table 4.6: Calculation pressure drop at different die land

R_1 (cm)	L_1 (cm)	Angle (θ) degree	Q $(\frac{cm^3}{s})$	$\dot{\gamma}_1$ (s^{-1})	$\dot{\gamma}_2$ (s^{-1})	μ_1 $(\frac{dyne}{cm^2}.s)$	μ_2 $(\frac{dyne}{cm^2}.s)$	τ_1 $(\frac{dyne}{cm^2})$	λ $(\frac{dyne}{cm^2}.s)$	$\dot{\varepsilon}_1$ (s^{-1})	σ_1 $(\frac{dyne}{cm^2})$	$\Delta p_{circular}$ $(\frac{dyne}{cm^2})$	Δp_s $(\frac{dyne}{cm^2})$	Δp_E $(\frac{dyne}{cm^2})$	Δp_2 $(\frac{dyne}{cm^2})$	Δp_{Total} $(\frac{dyne}{cm^2})$
0.5	0.5	45	5	50.93	0.214	10685.661	53630.599	5.44E+05	32056.98272	16.977	5.44E+05	1.09E+06	3.61E+05	3.61E+05	8.35E+03	**1.819E+06**
0.5	1	45	5	50.93	0.214	10685.661	53630.599	5.44E+05	32056.98272	16.977	5.44E+05	2.18E+06	3.61E+05	3.61E+05	8.35E+03	**2.908E+06**
0.5	2	45	5	50.93	0.214	10685.661	53630.599	5.44E+05	32056.98272	16.977	5.44E+05	4.35E+06	3.61E+05	3.61E+05	8.35E+03	**5.085E+06**
0.5	5	45	5	50.93	0.214	10685.661	53630.599	5.44E+05	32056.98272	16.977	5.44E+05	1.09E+07	3.61E+05	3.61E+05	8.35E+03	**1.162E+06**

Table 4.7: Design points at different die land

Table of Design Points

	A	B	C	D	E	F	G	H	I	J	K	L
1	Name		P12 - angle	P14 - L1	P13 - R1	P10 - flow rate	P7 - average velosity	P6 - presure drop	P8 - max velosity	P9 - max shear rate	P11 - min shear rate	Exported
2	Units						cm s^-1	dyne cm^-2	cm s^-1	s^-1	s^-1	
3	Current	1	45	0.5	0.5	5	7.8359	2.4768E+06	11.035	93.123	0.22448	
4	DP 1	2	45	1	0.5	5	7.7541	3.7479E+06	11	90.442	0.24497	☑
5	DP 2	3	45	2	0.5	5	7.6669	6.1754E+06	11.015	91.402	0.21087	☑
6	DP 3	4	45	5	0.5	5	7.5222	1.3533E+07	11.106	81.716	0.26696	☑
*												☐

Table 4.8: Calculation pressure drop at different die radius

R_1 (cm)	L_1 (cm)	Angle (θ) degree	Q $(\frac{cm^3}{s})$	$\dot{\gamma}_1$ (s^{-1})	$\dot{\gamma}_2$ (s^{-1})	μ_1 $(\frac{dyne}{cm^2}.s)$	μ_2 $(\frac{dyne}{cm^2}.s)$	τ_1 $(\frac{dyne}{cm^2})$	λ $(\frac{dyne}{cm^2}.s)$	$\dot{\varepsilon}_1$ (s^{-1})	σ_1 $(\frac{dyne}{cm^2})$	$\Delta p_{circular}$ $(\frac{dyne}{cm^2})$	Δp_s $(\frac{dyne}{cm^2})$	Δp_E $(\frac{dyne}{cm^2})$	Δp_2 $(\frac{dyne}{cm^2})$	Δp_{Total} $(\frac{dyne}{cm^2})$
0.5	1.0	45.0	5.0	50.9	0.2	10685.7	53630.6	544216.2	32057.0	17.0	544216.2	2176865.0	361288.5	361288.5	8353.8	**2907795.8**
0.6	1.0	45.0	5.0	29.5	0.2	14321.5	53630.6	422100.3	42964.6	9.8	422100.3	1407000.8	279359.9	279359.9	9671.2	**1975391.8**
0.7	1.0	45.0	5.0	18.6	0.2	17867.4	53630.6	331624.9	53602.2	6.2	331624.9	947499.7	218537.8	218537.8	10802.3	**1395377.6**
0.8	1.0	45.0	5.0	12.4	0.2	21225.3	53630.6	263915.4	63676.0	4.1	263915.4	659788.6	172919.8	172919.8	11773.7	**1017401.8**
1.0	1.0	45.0	5.0	6.4	0.2	27225.7	53630.6	173324.0	81677.0	2.1	173324.0	346648.0	111670.7	111670.7	13334.4	**583323.7**
1.5	1.0	45.0	5.0	1.9	0.2	38249.0	53630.6	72148.4	114747.1	0.6	72148.4	96197.9	42649.8	42649.8	15805.1	**197302.6**
2.0	1.0	45.0	5.0	0.8	0.2	45244.9	53630.6	36004.8	135734.7	0.3	36004.8	36004.8	17557.4	17557.4	17189.8	**88309.4**

Table 4.9: Design points at different die radius

Table of Design Points

	A	B	C	D	E	F	G	H	I	J	K	L
1	Name		P14 - angle	P13 - R1	P12 - L1	P10 - flow rate	P7 - average velosity	P6 - presure drop	P8 - max velosity	P9 - max shear rate	P11 - min shear rate	Exported
2	Units						cm s^-1	dyne cm^-2	cm s^-1	s^-1	s^-1	
3	Current	1	45	0.5	1	5	8.112	3.7406E+06	11.016	91.059	0.23734	
4	DP 1	2	45	0.6	1	5	5.2643	2.5019E+06	7.7573	52.307	0.26331	☑
5	DP 2	3	45	0.7	1	5	3.9865	1.7341E+06	5.7927	32.869	0.2824	☑
6	DP 3	4	45	0.8	1	5	3.2832	1.2121E+06	4.5006	20.837	0.15371	☑
7	DP 4	5	45	1	1	5	2.0309	6.9477E+05	2.9396	10.764	0.08341	☑
8	DP 5	6	45	1.5	1	5	0.80005	2.5369E+05	1.3371	3.5684	0.039372	☑
9	DP 6	7	45	2	1	5	0.43382	1.2951E+05	0.73234	1.9355	0.035344	☑
*												☐

Table 4.10: Swell ratio at different die land

Table of Design Points

	A	B	C	D	E	F	G	H	I	J
1	Name	Update Order	P3 - angle	P4 - flow rate	P13 - R1	P12 - L1	P6 - presure drop	P8 - max shear rate	P9 - min shear rate	P10 - swell ratio
2	Units						dyne cm^-2	s^-1	s^-1	
3	Current	1	45	5	0.5	0.5	2.8311E+06	77.11	0.3575	1.0821
4	DP 1	2	45	5	0.5	1	4.2235E+06	79.291	0.35786	1.065
5	DP 2	3	45	5	0.5	2	6.6588E+06	79.08	0.3572	1.0605
6	DP 3	4	45	5	0.5	5	1.4131E+07	76.643	0.36017	1.0596

Table 4.11: Swell ratio at different die L/D ratio

Table of Design Points

	A	B	C	D	E	F	G	H	I	J	K
1	Name	Update Order	P3...	P4 - flow rate	P11 - R1	P10 - L1	P12 - L/D	P7 - SR	P6 - presure drop	P8 - max shear rate	P9 - min shear rate
2	Units								dyne cm^-2	s^-1	s^-1
3	Current	1	45	5	0.5	5	5	1.0591	1.4195E+07	79.052	0.35399
4	DP 1	2	45	5	0.6	5	4.1667	1.0736	9.18E+06	44.515	0.3557
5	DP 2	3	45	5	0.7	5	3.5714	1.0866	6.1711E+06	27.869	0.30223
6	DP 3	4	45	5	0.8	5	3.125	1.0967	4.31E+06	17.892	0.35644
7	DP 4	5	45	5	1	5	2.5	1.113	2.2959E+06	8.7137	0.23741
8	DP 5	6	45	5	1.5	5	1.6667	1.1326	6.6768E+05	2.6492	0.05836
9	DP 6	7	45	5	2	5	1.25	1.1452	2.754E+05	1.2693	0.048331
*											

Table 4.12: Calculated maximum extruder output at different flight width

D (cm)	N (rev/s)	H (cm)	e (cm)	L (cm)	$Clearance$ (cm)	$shear\ rate$ (s^{-1})	$Viscosity$ $(poise)$	$P(\frac{dyne}{cm^2})$	$Q_d(\frac{cm^3}{s})$	$Q_p(\frac{cm^3}{s})$	$Q_T(\frac{cm^3}{s})$
6	*1*	*0.6*	*0.6*	*6*	*0.1*	*31.4159*	*13864.4*	*0*	*30.808*	*0*	*30.808*
6	*1*	*0.6*	*0.5*	*6*	*0.1*	*31.4159*	*13864.4*	*0*	*30.808*	*0*	*30.808*
6	*1*	*0.6*	*0.4*	*6*	*0.1*	*31.4159*	*13864.4*	*0*	*30.808*	*0*	*30.808*
6	*1*	*0.6*	*0.3*	*6*	*0.1*	*31.4159*	*13864.4*	*0*	*30.808*	*0*	*30.808*
6	*1*	*0.6*	*0.2*	*6*	*0.1*	*31.4159*	*13864.4*	*0*	*30.808*	*0*	*30.808*

Table 4.13: Design point of extruder output and pressure in screw at different flight width

Table of Design Points

	A	B	C	D	E	F	G	H	I
1	Name	Update Order	P13 - e	P14 - H	P17 - Rr	P19 - Rb	P18 - L	P2 - extruder outpout	P1 - D pmax
2	Units								dyne cm^-2
3	Current	1	0.6	0.6	2.4	3.1	6	19.896	6.7848E+06
4	DP 1	2	0.5	0.6	2.4	3.1	6	20.143	6.99E+06
5	DP 2	3	0.4	0.6	2.4	3.1	6	20.346	7.1336E+06
6	DP 3	4	0.3	0.6	2.4	3.1	6	20.242	6.8435E+06
7	DP 4	5	0.2	0.6	2.4	3.1	6	20.362	6.7325E+06
*									

Table 4.14: Design point of extruder output and pressure in nose at different flight width

Table of Design Points

	A	B	C	D	E	F	G	H
1	Name	Upd... Order	P14 - e	P16 - Rb	P15 - Rr	P13 - H	P1...	P11 - delta P
2	Units							dyne cm^-2
3	Current	1	0.6	3.1	2.4	0.6	19.974	7.5966E+06
4	DP 1	2	0.5	3.1	2.4	0.6	20.349	7.4497E+06
5	DP 2	3	0.4	3.1	2.4	0.6	20.61	7.4556E+06
6	DP 3	4	0.3	3.1	2.4	0.6	20.653	7.1049E+06
7	DP 4	5	0.2	3.1	2.4	0.6	20.982	7.3727E+06
*								

Table 4.15: Calculated maximum extruder output at different flight clearance

D (cm)	N (rev/s)	H (cm)	e (cm)	L (cm)	$Clearance$ (cm)	$shear\ rate$ (s^{-1})	$Viscosity$ $(poise)$	$P(\frac{dyne}{cm^2})$	$Q_d(\frac{cm^3}{s})$	$Q_p(\frac{cm^3}{s})$	$Q_T(\frac{cm^3}{s})$
6	*1*	*0.6*	*0.6*	*6*	*0.1*	*31.4159*	*13864.4*	*0*	*30.808*	*0*	*30.808*
6	*1*	*0.6*	*0.6*	*6*	*0.09*	*31.4159*	*13864.4*	*0*	*30.808*	*0*	*30.808*
6	*1*	*0.6*	*0.6*	*6*	*0.08*	*31.4159*	*13864.4*	*0*	*30.808*	*0*	*30.808*
6	*1*	*0.6*	*0.6*	*6*	*0.07*	*31.4159*	*13864.4*	*0*	*30.808*	*0*	*30.808*
6	*1*	*0.6*	*0.6*	*6*	*0.06*	*31.4159*	*13864.4*	*0*	*30.808*	*0*	*30.808*
6	*1*	*0.6*	*0.6*	*6*	*0.05*	*31.4159*	*13864.4*	*0*	*30.808*	*0*	*30.808*

Table 4.16: Design point of extruder output and pressure in screw at different flight clearance

Table of Design Points

	A	B	C	D	E	F	G	H	I	J
1	Name	Update Order	P13 - e	P14 - H	P17 - Rr	P19 - Rb	P1...	P20 - clearnce	P2 - extruder outpout	P1 - D pmax
2	Units									dyne cm^-2
3	Current	1	0.6	0.6	2.4	3.1	6	0.1	19.896	6.7848E+06
4	DP 1	2	0.6	0.6	2.4	3.09	6	0.09	19.881	7.257E+06
5	DP 2	3	0.6	0.6	2.4	3.08	6	0.08	19.836	7.7673E+06
6	DP 3	4	0.6	0.6	2.4	3.07	6	0.07	19.867	8.2001E+06
7	DP 4	5	0.6	0.6	2.4	3.06	6	0.06	19.944	8.4456E+06
8	DP 5	6	0.6	0.6	2.4	3.05	6	0.05	19.965	8.8638E+06
*										

Table 4.17: Design point of extruder output and pressure in nose at different flight clearance

Table of Design Points

	A	B	C	D	E	F	G	H	I
1	Name	Update Order	P14 - e	P16 - Rb	P15 - Rr	P13 - H	P1...	P10 - flow rate	P11 - delta P
2	Units								dyne cm^-2
3	Current	1	0.6	3.1	2.4	0.6	0.1	19.974	7.5966E+06
4	DP 1	2	0.6	3.09	2.4	0.6	0.09	20.049	7.6166E+06
5	DP 2	3	0.6	3.08	2.4	0.6	0.08	19.988	8.1754E+06
6	DP 3	4	0.6	3.07	2.4	0.6	0.07	19.957	8.6939E+06
7	DP 4	5	0.6	3.06	2.4	0.6	0.06	20.007	8.7953E+06
8	DP 5	6	0.6	3.05	2.4	0.6	0.05	20.097	9.9469E+06

Table 4.18: Calculated maximum extruder output at different screw depth

D (cm)	N (rev/s)	H (cm)	e (cm)	L (cm)	$Clearance$ (cm)	$shear\ rate$ (s^{-1})	$Viscosity$ $(poise)$	$P(\frac{dyne}{cm^2})$	$Q_d(\frac{cm^3}{s})$	$Q_p(\frac{cm^3}{s})$	$Q_T(\frac{cm^3}{s})$
6	*1*	*0.6*	*0.6*	*6*	*0.1*	*31.4159*	*13864.42*	*0*	*30.808*	*0*	*30.808*
6	*1*	*0.5*	*0.6*	*6*	*0.1*	*37.6991*	*12605.57*	*0*	*25.673*	*0*	*25.673*
6	*1*	*0.4*	*0.6*	*6*	*0.1*	*47.1239*	*11162.23*	*0*	*20.538*	*0*	*20.538*
6	*1*	*0.3*	*0.6*	*6*	*0.1*	*62.8319*	*9464.576*	*0*	*15.404*	*0*	*15.404*

Table 4.19: Design point of extruder output and pressure in screw at different depth

Table of Design Points

	A	B	C	D	E	F	G	H	I
1	Name	Update Order	P13 - e	P14 - H	P17 - Rr	P19 - Rb	P18 - L	P2 - extruder outpout	P1 - D pmax
2	Units								dyne cm^-2
3	Current	1	0.6	0.6	2.4	3.1	6	19.896	6.7848E+06
4	DP 1	2	0.6	0.5	2.5	3.1	6	16.294	7.9599E+06
5	DP 3	4	0.6	0.4	2.6	3.1	6	12.493	1.1827E+07
6	DP 4	5	0.6	0.3	2.7	3.1	6	8.7235	1.2484E+07

Table 4.20: Design point of extruder output and pressure in nose at different depth

Table of Design Points

	A	B	C	D	E	F	G	H
1	Name	Update Order	P14 - e	P16 - Rb	P15 - Rr	P13 - H	P10 - flow rate	P11 - delta P
2	Units							dyne cm^-2
3	Current	1	0.6	3.1	2.4	0.6	19.974	7.5966E+06
4	DP 1	2	0.6	3.1	2.5	0.5	16.298	8.9284E+06
5	DP 2	3	0.6	3.1	2.6	0.4	12.454	1.1599E+07
6	DP 3	4	0.6	3.1	2.7	0.3	8.665	1.3178E+07

Table 4.21: Calculated maximum extruder output at different screw speed

D (cm)	N (rev/s)	H (cm)	e (cm)	L (cm)	$Clearanc$ (cm)	$shear\ rate$ (s^{-1})	$Viscosity$ $(poise)$	$P(\frac{dyne}{cm^2})$	$Q_d(\frac{cm^3}{s})$	$Q_p(\frac{cm^3}{s})$	$Q_T(\frac{cm^3}{s})$
6	*0.5*	*0.6*	*0.6*	*6*	*0.1*	*15.708*	*19237.84*	*0*	*15.404*	*0*	*15.404*
6	*0.75*	*0.6*	*0.6*	*6*	*0.1*	*23.5619*	*15988.36*	*0*	*23.106*	*0*	*23.106*
6	*1*	*0.6*	*0.6*	*6*	*0.1*	*31.4159*	*13864.42*	*0*	*30.808*	*0*	*30.808*
6	*1.25*	*0.6*	*0.6*	*6*	*0.1*	*39.2699*	*12333.4*	*0*	*38.510*	*0*	*38.510*
6	*1.5*	*0.6*	*0.6*	*6*	*0.1*	*47.1239*	*11162.23*	*0*	*46.212*	*0*	*46.212*

Table 4.22: Design point of extruder output and pressure in screw at different speed

1	Name	Update Order	P13 - e	P14 - H	P17 - Rr	P19 - Rb	P18 - L	P20 - flow rate	P21 - delta P
2	Units								dyne cm^-2
3	Current	30	0.6	0.6	2.4	3.1	6	10.146	4.8556E+06
*	Current	45	0.6	0.6	2.4	3.1	6	15.05	5.9447E+06
3	Current	60	0.6	0.6	2.4	3.1	6	19.896	6.7848E+06
3	Current	75	0.6	0.6	2.4	3.1	6	24.699	7.4692E+06
3	Current	90	0.6	0.6	2.4	3.1	6	29.465	8.0471E+06

Table 4.23: Design point of extruder output and pressure in nose at different speed

Table of Design Points

	A	B	C	D	E	F	G	H
1	Name	Update Order	P14 - e	P16 - Rb	P15 - Rr	P13 - H	P10 - flow rate	P11 - delta P
2	Units							dyne cm^-2
3	Current	30	0.6	3.1	2.4	0.6	10.203	5.4164E+06
3	Current	45	0.6	3.1	2.4	0.6	15.12	6.646E+06
3	Current	60	0.6	3.1	2.4	0.6	19.974	7.5966E+06
3	Current	75	0.6	3.1	2.4	0.6	24.779	8.3718E+06
3	Current	90	0.6	3.1	2.4	0.6	29.545	9.0254E+06

Table 4.24: Calculated maximum extruder output at different screw length

D (cm)	N (rev/s)	H (cm)	e (cm)	L (cm)	$Clearanc$ (cm)	$shear\ rate$ (s^{-1})	$Viscosity$ $(poise)$	$P(\frac{dyne}{cm^2})$	$Q_d(\frac{cm^3}{s})$	$Q_p(\frac{cm^3}{s})$	$Q_T(\frac{cm^3}{s})$
6	*1*	*0.6*	*0.6*	*6*	*0.1*	*31.4159*	*13864.42*	*0*	*30.808*	*0*	*30.808*
6	*1*	*0.6*	*0.6*	*12*	*0.1*	*31.4159*	*13864.42*	*0*	*30.808*	*0*	*30.808*
6	*1*	*0.6*	*0.6*	*18*	*0.1*	*31.4159*	*13864.42*	*0*	*30.808*	*0*	*30.808*
6	*1*	*0.6*	*0.6*	*24*	*0.1*	*31.4159*	*13864.42*	*0*	*30.808*	*0*	*30.808*
6	*1*	*0.6*	*0.6*	*30*	*0.1*	*31.4159*	*13864.42*	*0*	*30.808*	*0*	*30.808*

Table 4.25: Design point of extruder output and pressure in screw at different screw length

Table of Design Points

	A	B	C	D	E	F	G	H	I
1	Name	Update Order	P13 - e	P14 - H	P17 - Rr	P19 - Rb	P18 - L	P2 - extruder outpout	P1 - D pmax
2	Units								dyne cm^-2
3	Current	1	0.6	0.6	2.4	3.1	6	19.896	6.7848E+06
4	DP 1	2	0.6	0.6	2.4	3.1	12	21.714	8.8876E+06
5	DP 2	3	0.6	0.6	2.4	3.1	18	21.308	8.9769E+06
6	DP 3	4	0.6	0.6	2.4	3.1	24	15.769	2.7369E+07
7	DP 4	5	0.6	0.6	2.4	3.1	30	13.352	2.5564E+07

Table 4.26: Design point of extruder output and pressure in nose at different screw length

Table of Design Points

	A	B	C	D	E	F	G	H	I	J	K
1	Name	Update Order	P14 - e	P16 - Rb	P15 - Rr	P13 - H	P17 - XY... .H1	P18 - L	P19 - XYPlane .H37	P10 - flow rate	P11 - delta P
2	Units										dyne cm^-2
3	Current	1	0.6	3.1	2.4	0.6	6.6	7	6.6	19.974	7.5966E+06
4	DP 1	2	0.6	3.1	2.4	0.6	12.6	13	12.6	22.007	9.5676E+06
5	DP 2	3	0.6	3.1	2.4	0.6	18.6	19	18.6	21.514	9.9621E+06
6	DP 3	4	0.6	3.1	2.4	0.6	24.6	25	24.6	14.078	2.5168E+07
7	DP 4	5	0.6	3.1	2.4	0.6	30.6	31	30.6	13.254	2.4455E+07

Table 4.27: Nose and operating points at different die radii

	$Q(\frac{cm^3}{s})$	$P(\frac{dyne}{cm^2})$
Nose	***19.9736***	***7.5966E+06***
R1= 1	***17.8218***	***9.3801E+06***
R1=0.8	***16.7161***	***9.7526E+06***
R1=0.7	***15.7695***	***1.0426E+07***
R1=0.6	***14.3451***	***1.1623E+07***
R1=0.5	***12.5719***	***1.2794E+07***

Table 4.28: Design point of operating points at different die radii

Table of Design Points

	A	B	C	D	E	F	G	H	J	K
1	Name	Update Order	P14 - e	P16 - Rb	P15 - Rr	P13 - H	P19 - Ld	P18 - Rd	P10 - flow rate	P11 - delta P
2	Units									dyne cm^-2
3	Current	1	0.6	3.1	2.4	0.6	1	1	17.822	9.3801E+06
4	DP 1	2	0.6	3.1	2.4	0.6	1	0.8	16.716	9.7526E+06
5	DP 2	3	0.6	3.1	2.4	0.6	1	0.7	15.77	1.0426E+07
6	DP 3	4	0.6	3.1	2.4	0.6	1	0.6	14.345	1.1623E+07
7	DP 4	5	0.6	3.1	2.4	0.6	1	0.5	12.572	1.2794E+07

Table 4.29: Analytical extruder line and simulation at different die radii and flight width

Analytical extruder line	*e=0.6cm*	*e=0.4cm*	*e=0.2cm*

		Qmax	Pmax	Qmax	Pmax	Qmax	Pmax
		30.808	0	30.808	0	30.808	0
		0	2.22E+07	0	2.22E+07	0	2.22E+07
simulation	nose	19.9736	7.5966E+06	20.61	7.4556E+06	20.9821	7372710
	R1= 1	17.7933	9.2601E+06	18.0306	8835000	18.4191	9026550
	R1=0.8	16.6587	9.9008E+06	16.7448	10024700	17.0808	10154000
	R1=0.7	15.741	1.0669E+07	15.7909	10546900	15.8151	10896800
	R1=0.6	14.5679	1.1504E+07	14.3791	11371900	14.6757	11374300
	R1=0.5	12.5356	1.2485E+07	12.5443	12614700	12.6858	12712600

Table 4.30: Design point of operating points at different die radii and flight width

1	Name	Update Order	P14 - e	P16 - Rb	P15 - Rr	P13 - H	P19 - Ld	P18 - Rd	P20 - Angle	P10 - flow rate	P11 - delta P
2	Units										dyne cm^-2
3	Current	1	0.6	3.1	2.4	0.6	1	1	225	17.793	9.2601E+06
4	DP 1	2	0.6	3.1	2.4	0.6	1	0.8	225	16.659	9.9008E+06
5	DP 2	3	0.6	3.1	2.4	0.6	1	0.7	225	15.741	1.0669E+07
6	DP 3	4	0.6	3.1	2.4	0.6	1	0.6	225	14.568	1.1504E+07
7	DP 4	5	0.6	3.1	2.4	0.6	1	0.5	225	12.536	1.2485E+07
3	Current	1	0.4	3.1	2.4	0.6	1	1	225	18.031	8.835E+06
4	DP 1	2	0.4	3.1	2.4	0.6	1	0.8	225	16.745	1.0025E+07
5	DP 2	3	0.4	3.1	2.4	0.6	1	0.7	225	15.791	1.0547E+07
6	DP 3	4	0.4	3.1	2.4	0.6	1	0.6	225	14.379	1.1372E+07
7	DP 4	5	0.4	3.1	2.4	0.6	1	0.5	225	12.544	1.2615E+07
3	Current	1	0.2	3.1	2.4	0.6	1	1	225	18.419	9.0266E+06
4	DP 1	2	0.2	3.1	2.4	0.6	1	0.8	225	17.081	1.0154E+07
5	DP 2	3	0.2	3.1	2.4	0.6	1	0.7	225	15.815	1.0897E+07
6	DP 3	4	0.2	3.1	2.4	0.6	1	0.6	225	14.676	1.1374E+07
7	DP 4	5	0.2	3.1	2.4	0.6	1	0.5	225	12.686	1.2713E+07

Table 4.31: Analytical extruder line and simulation at different die radii and flight clearance

Analytical extruder line		clearance=0.1cm		clearance=0.08cm		clearance=0.06cm	
		Qmax	Pmax	Qmax	Pmax	Qmax	Pmax
		30.808	0	30.808	0	30.808	0
		0	2.22E+07	0	2.22E+07	0	2.22E+07
simulation	nose	19.9736	7.5966E+06	19.9883	8.1754E+06	20.0072	8795280
	R1= 1	17.7933	9.2601E+06	18.0954	1.0060E+07	18.4376	11319500
	R1=0.8	16.6587	9.9008E+06	17.0194	1.0896E+07	17.4809	12425700
	R1=0.7	15.8583	1.0420E+07	16.1627	1.1251E+07	16.7187	13210100
	R1=0.6	14.5723	1.1477E+07	15.1008	1.2587E+07	15.5708	14650900
	R1=0.5	12.6351	1.2739E+07	13.3081	1.3966E+07	14.026	15103600

Table 4.32: Design point of operating points at different die radii and flight clearance

Table of Design Points

	A	B	C	D	E	F	G	H	I	J	K
1	Name	Update Order	P14 - e	P16 - Rb	P15 - Rr	P13 - H	P19 - Ld	P18 - Rd	P20 - Angle	P10 - flow rate	P11 - delta P
2	Units										dyne cm^-2
3	Current	1	0.6	3.1	2.4	0.6	1	1	225	17.793	9.2601E+06
4	DP 1	2	0.6	3.1	2.4	0.6	1	0.8	225	16.659	9.9008E+06
5	DP 2	3	0.6	3.1	2.4	0.6	1	0.7	225	15.858	1.042E+07
6	DP 3	4	0.6	3.1	2.4	0.6	1	0.6	225	14.572	1.1477E+07
7	DP 4	5	0.6	3.1	2.4	0.6	1	0.5	225	12.635	1.2739E+07
3	Current	1	0.6	3.08	2.4	0.6	1	1	225	18.095	1.006E+07
4	DP 1	2	0.6	3.08	2.4	0.6	1	0.8	225	17.019	1.0896E+07
5	DP 2	3	0.6	3.08	2.4	0.6	1	0.7	225	16.163	1.1251E+07
6	DP 3	4	0.6	3.08	2.4	0.6	1	0.6	225	15.101	1.2587E+07
7	DP 4	5	0.6	3.08	2.4	0.6	1	0.5	225	13.308	1.3966E+07
3	Current	1	0.6	3.06	2.4	0.6	1	1	225	18.438	1.132E+07
4	DP 1	2	0.6	3.06	2.4	0.6	1	0.8	225	17.481	1.2426E+07
5	DP 2	3	0.6	3.06	2.4	0.6	1	0.7	225	16.719	1.321E+07
6	DP 3	4	0.6	3.06	2.4	0.6	1	0.6	225	15.571	1.4651E+07
7	DP 4	5	0.6	3.06	2.4	0.6	1	0.5	225	14.026	1.5104E+07

Table 4.33: Analytical extruder line and simulation at different die radii and screw depth

Analytical extruder line		*H=0.6cm*		*H=0.5cm*		*H=0.4cm*	
		Qmax	*Pmax*	*Qmax*	*Pmax*	*Qmax*	*Pmax*
		30.8077	*0*	*25.6731*	*0*	*20.5385*	*0*
		0.0000E+00	*2.2179E+07*	*0.0000E+00*	*3.6555E+07*	*0.0000E+00*	*6.7110E+07*
simulation	*nose*	*19.9736*	*7.5966E+06*	*16.2981*	*8.9284E+06*	*12.4539*	*1.1599E+07*
	R1= 1	*17.8218*	*9.3801E+06*	*14.7837*	*1.0581E+07*	*11.4304*	*1.1425E+07*
	R1=0.8	*16.7161*	*9.7526E+06*	*14.0448*	*1.1357E+07*	*10.9218*	*1.1979E+07*
	R1=0.7	*15.7695*	*1.0426E+07*	*13.3877*	*1.1817E+07*	*10.5432*	*1.2637E+07*
	R1=0.6	*14.3451*	*1.1623E+07*	*12.427*	*1.2593E+07*	*9.87833*	*1.3414E+07*
	R1=0.5	*12.5719*	*1.2794E+07*	*11.1949*	*1.3787E+07*	*8.97299*	*1.4684E+07*

Table 4.34: Design point of operating points at different die radii and screw depth

Table of Design Points

	A	B	C	D	E	F	G	H	I	J	K
1	Name	Update Order	P14 - e	P16 - Rb	P15 - Rr	P13 - H	P19 - Ld	P18 - Rd	P20 - Angle	P10 - flow rate	P11 - delta P
2	Units										dyne cm^-2
3	Current	1	0.6	3.1	2.4	0.6	1	1	225	17.822	9.3801E+06
4	DP 1	2	0.6	3.1	2.4	0.6	1	0.8	225	16.716	9.7526E+06
5	DP 2	3	0.6	3.1	2.4	0.6	1	0.7	225	15.77	1.0426E+07
6	DP 3	4	0.6	3.1	2.4	0.6	1	0.6	225	14.345	1.1623E+07
7	DP 4	5	0.6	3.1	2.4	0.6	1	0.5	225	12.572	1.2794E+07
3	Current	1	0.6	3.1	2.5	0.5	1	1	225	14.784	1.0581E+07
4	DP 1	2	0.6	3.1	2.5	0.5	1	0.8	225	14.045	1.1357E+07
5	DP 2	3	0.6	3.1	2.5	0.5	1	0.7	225	13.388	1.1817E+07
6	DP 3	4	0.6	3.1	2.5	0.5	1	0.6	225	12.427	1.2593E+07
7	DP 4	5	0.6	3.1	2.5	0.5	1	0.5	225	11.195	1.3787E+07
3	Current	1	0.6	3.1	2.6	0.4	1	1	225	11.43	1.1425E+07
4	DP 1	2	0.6	3.1	2.6	0.4	1	0.8	225	10.922	1.1979E+07
5	DP 2	3	0.6	3.1	2.6	0.4	1	0.7	225	10.543	1.2637E+07
6	DP 3	4	0.6	3.1	2.6	0.4	1	0.6	225	9.8783	1.3414E+07
7	DP 4	5	0.6	3.1	2.6	0.4	1	0.5	225	8.973	1.4684E+07

Table 4.35: Analytical extruder line and simulation at different die radii and screw speed

Analytical extruder line		N=30		N=60		N=90	
		Qmax	Pmax	Qmax	Pmax	Qmax	Pmax
		15.4039	0	30.80773	0	46.2115882	0
		0.00E+00	1.82E+07	0.00E+00	2.22E+07	0.00E+00	2.44E+07
simulation	nose	10.2027	5.4164E+06	19.9736	7.5966E+06	29.5447	9025390
	R1= 1	9.24941	6.5235E+06	17.7933	9.2601E+06	26.1526	10914700
	R1=0.8	8.62561	6.9238E+06	16.6587	9.9008E+06	24.4883	11729200
	R1=0.7	8.13246	7.5320E+06	15.8264	1.0543E+07	23.2241	12425000
	R1=0.6	7.5347	8.2544E+06	14.6871	1.1677E+07	21.4171	13963100
	R1=0.5	6.52543	9.6216E+06	12.6665	1.2977E+07	18.6249	15126800

Table 4.36: Design point of operating points at different die radii and screw depth

Table of Design Points

	A	B	C	D	E	F	G	H	I	J	K
1	Name	Update Order	P14 - e	P16 - Rb	P15 - Rr	P13 - H	P19 - Ld	P18 - Rd	P20 - Angle	P10 - flow rate	P11 - delta P
2	Units										dyne cm^-2
3	Current	1	0.6	3.1	2.4	0.6	1	1	225	9.2494	6.5235E+06
4	DP 1	2	0.6	3.1	2.4	0.6	1	0.8	225	8.6256	6.9238E+06
5	DP 2	3	0.6	3.1	2.4	0.6	1	0.7	225	8.1325	7.532E+06
6	DP 3	4	0.6	3.1	2.4	0.6	1	0.6	225	7.5347	8.2544E+06
7	DP 4	5	0.6	3.1	2.4	0.6	1	0.5	225	6.5254	9.6216E+06
3	Current	1	0.6	3.1	2.4	0.6	1	1	225	17.793	9.2601E+06
4	DP 1	2	0.6	3.1	2.4	0.6	1	0.8	225	16.659	9.9008E+06
5	DP 2	3	0.6	3.1	2.4	0.6	1	0.7	225	15.826	1.0543E+07
6	DP 3	4	0.6	3.1	2.4	0.6	1	0.6	225	14.687	1.1677E+07
7	DP 4	5	0.6	3.1	2.4	0.6	1	0.5	225	12.667	1.2977E+07
3	Current	1	0.6	3.1	2.4	0.6	1	1	225	26.153	1.0915E+07
4	DP 1	2	0.6	3.1	2.4	0.6	1	0.8	225	24.488	1.1729E+07
5	DP 2	3	0.6	3.1	2.4	0.6	1	0.7	225	23.224	1.2425E+07
6	DP 3	4	0.6	3.1	2.4	0.6	1	0.6	225	21.417	1.3963E+07
7	DP 4	5	0.6	3.1	2.4	0.6	1	0.5	225	18.625	1.5127E+07

Table 4.37: Analytical extruder line and simulation at different die radii and screw length

Analytical extruder line		L=7cm		L=13cm		L=19cm	
		Qmax	Pmax	Qmax	Pmax	Qmax	Pmax
		15.4039	0	30.80773	0	46.2115882	0
		0.00E+00	1.82E+07	0.00E+00	2.22E+07	0.00E+00	2.44E+07
simulation	nose	10.2027	5.4164E+06	19.9736	7.5966E+06	29.5447	9025390
	R1= 1	9.24941	6.5235E+06	17.7933	9.2601E+06	26.1526	10914700
	R1=0.8	8.62561	6.9238E+06	16.6587	9.9008E+06	24.4883	11729200
	R1=0.7	8.13246	7.5320E+06	15.8264	1.0543E+07	23.2241	12425000
	R1=0.6	7.5347	8.2544E+06	14.6871	1.1677E+07	21.4171	13963100
	R1=0.5	6.52543	9.6216E+06	12.6665	1.2977E+07	18.6249	15126800

Table 4.38: Design point of operating points at different die radii and screw length

Table of Design Points

	A	B	C	D	E	F	G	H	I	J	K	L
1	Name	Update Order	P14 - e	P16 - Rb	P15 - Rr	P13 - H	P19 - Ld	P18 - Rd	P20 - Angle	P21 - L	P10 - flow rate	P11 - delta P
2	Units											dyne cm^-2
3	Current	1	0.6	3.1	2.4	0.6	1	1	225	7	17.822	9.3801E+06
4	DP 1	2	0.6	3.1	2.4	0.6	1	0.8	225	7	16.716	9.7526E+06
5	DP 2	3	0.6	3.1	2.4	0.6	1	0.7	225	7	15.77	1.0426E+07
6	DP 3	4	0.6	3.1	2.4	0.6	1	0.6	225	7	14.345	1.1623E+07
7	DP 4	5	0.6	3.1	2.4	0.6	1	0.5	225	7	12.572	1.2794E+07
3	Current	1	0.6	3.1	2.4	0.6	1	1	225	13	20.987	1.0441E+07
4	DP 1	2	0.6	3.1	2.4	0.6	1	0.8	225	13	19.706	1.1091E+07
5	DP 2	3	0.6	3.1	2.4	0.6	1	0.7	225	13	19.165	1.1932E+07
6	DP 3	4	0.6	3.1	2.4	0.6	1	0.6	225	13	18.563	1.3095E+07
7	DP 4	5	0.6	3.1	2.4	0.6	1	0.5	225	13	17.313	1.4988E+07
3	Current	1	0.6	3.1	2.4	0.6	1	1	225	19	18.409	2.0982E+07
4	DP 1	2	0.6	3.1	2.4	0.6	1	0.8	225	19	17.563	2.28E+07
5	DP 2	3	0.6	3.1	2.4	0.6	1	0.7	225	19	17.343	2.3791E+07
6	DP 3	4	0.6	3.1	2.4	0.6	1	0.6	225	19	17.292	2.3946E+07
7	DP 4	5	0.6	3.1	2.4	0.6	1	0.5	225	19	16.562	2.6578E+07

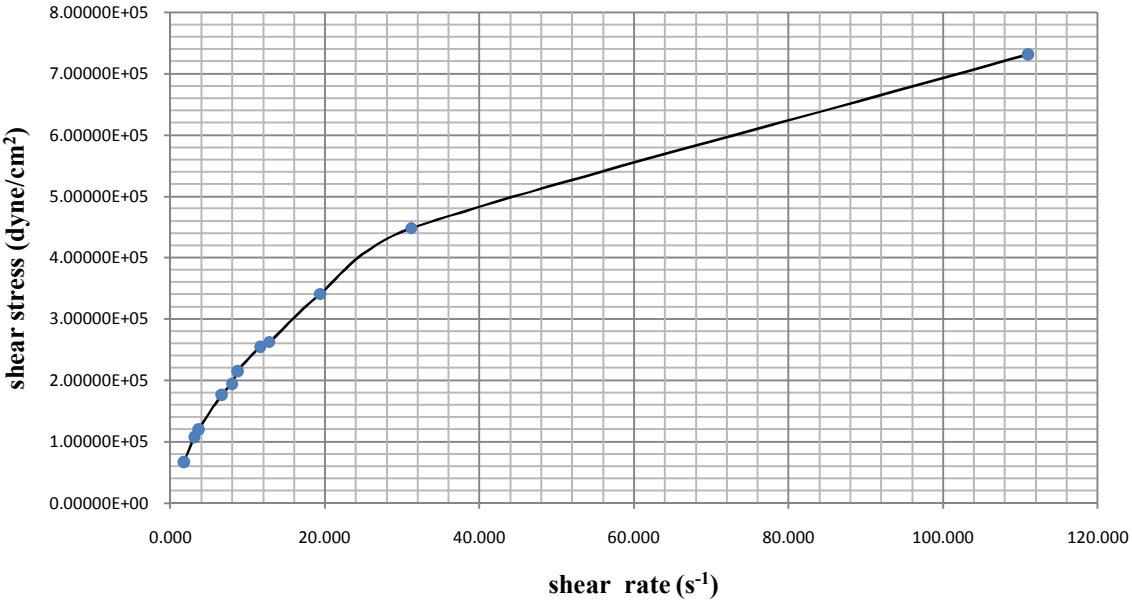

Fig. 4.1: Relation between shear stress and shear rate for (PP113)

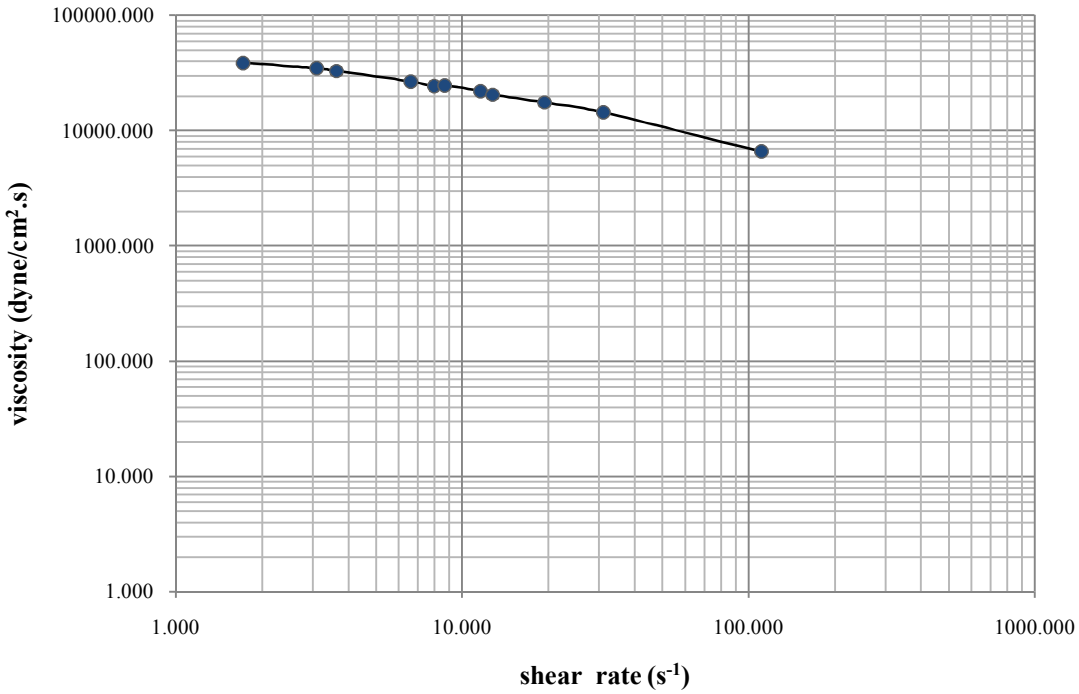

Fig. 4.2: Viscosity vs. shear rate curve for (PP113)

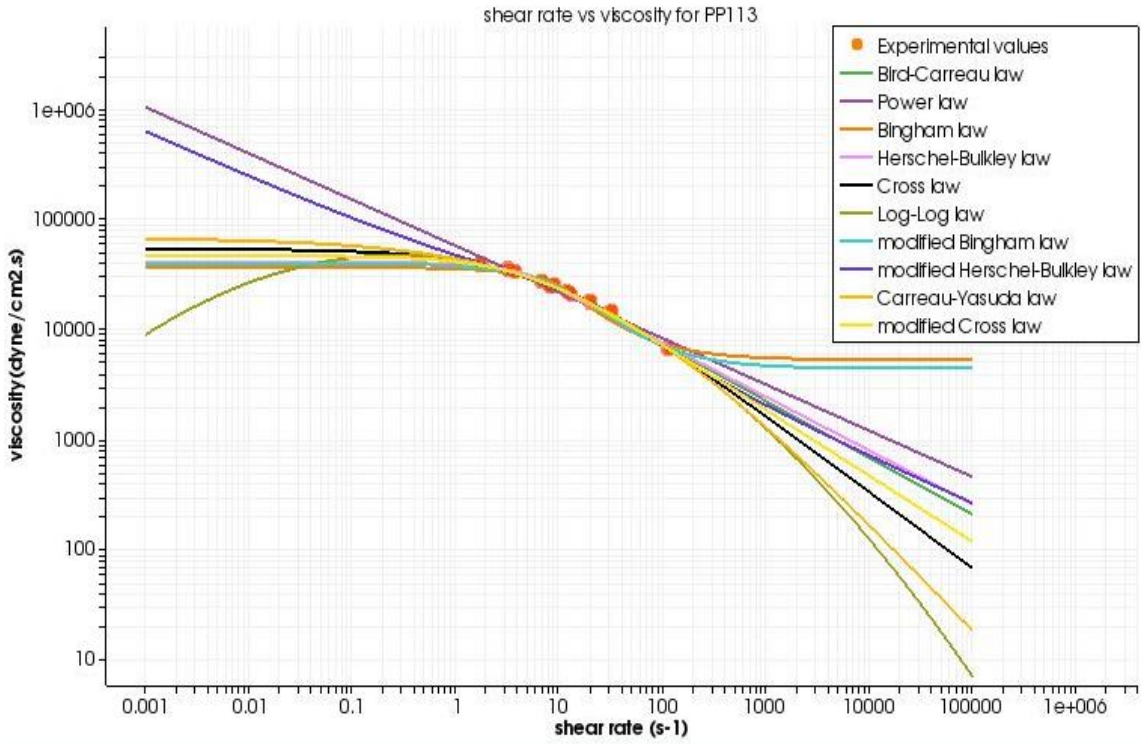

Fig. 4.3: Experimental viscosity (obs) and fitted viscosity (fit) for ten non Newton viscosity models in POLYMAT against experimental shear rate

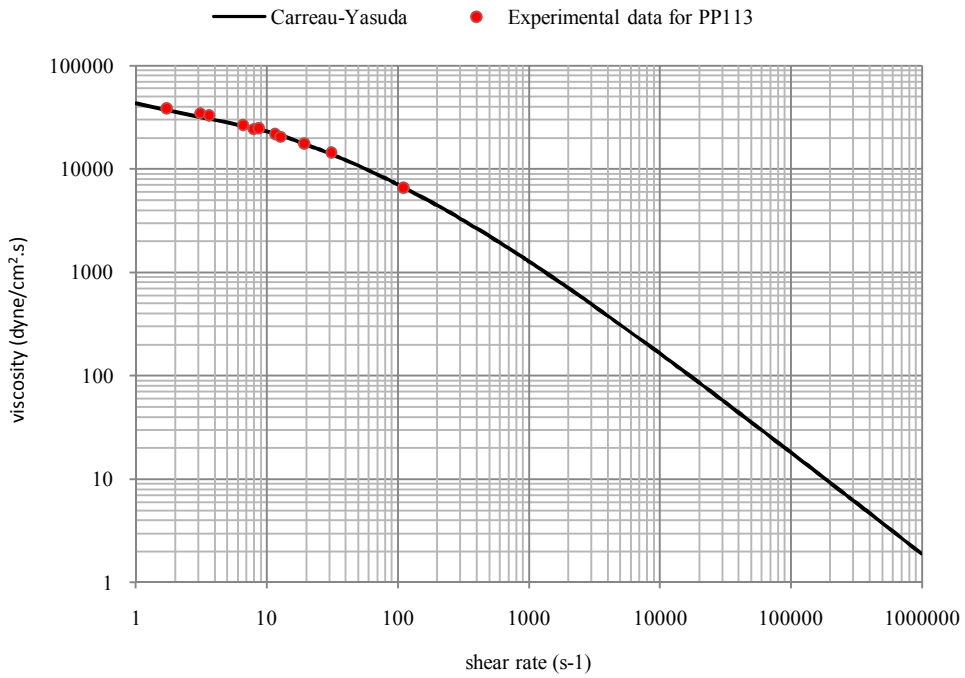

Fig. 4.4: Experimental viscosity (obs) with Carreau-Yasuda model

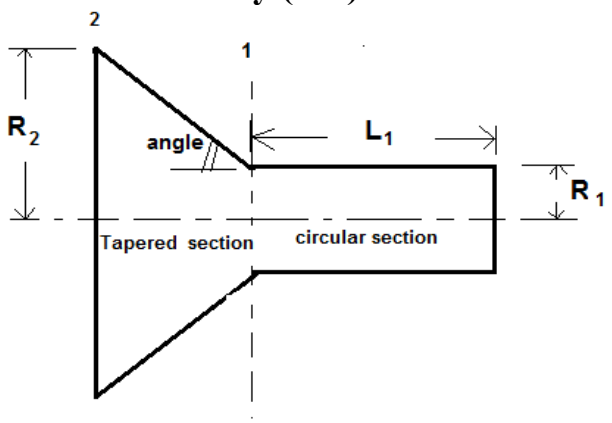

Fig. 4.5: Die section

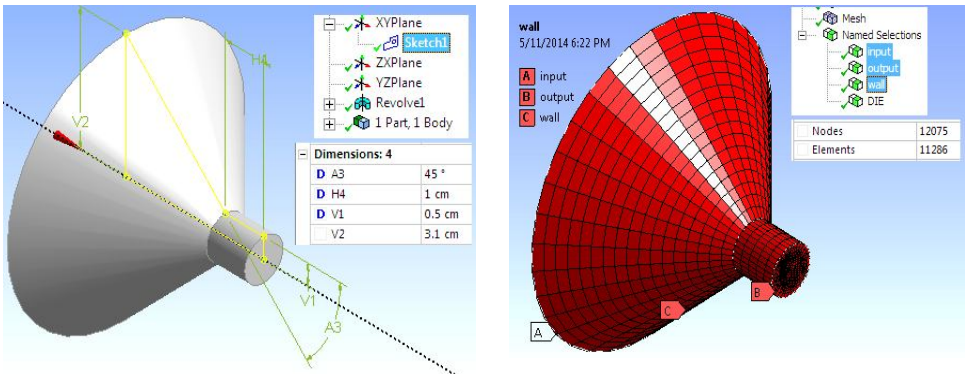

Fig. 4.6: Geometry and meshing for die

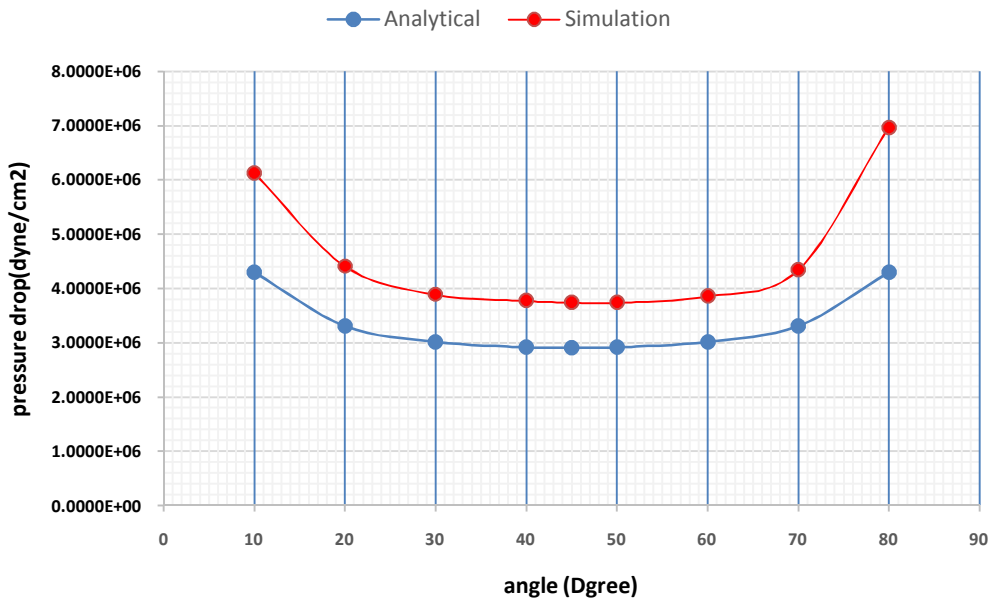

Fig. 4.7: Effect of angle on pressure drop

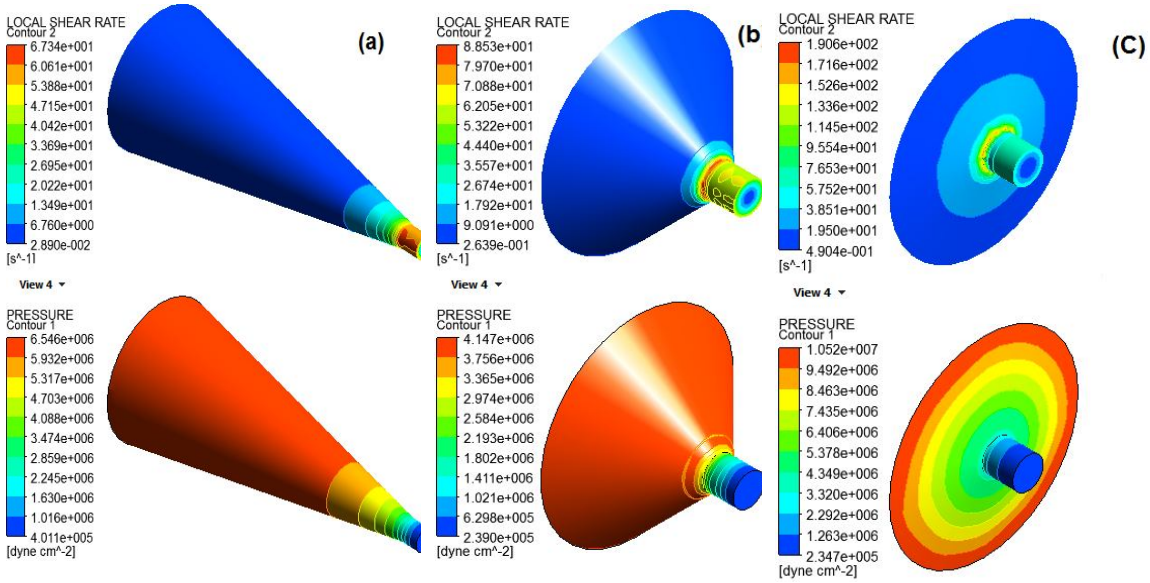

Fig. 4.8: Counters of shear rate and pressure in die a) angle=10^{o}, b) angle=45^{o}, c) angle=80^{o}

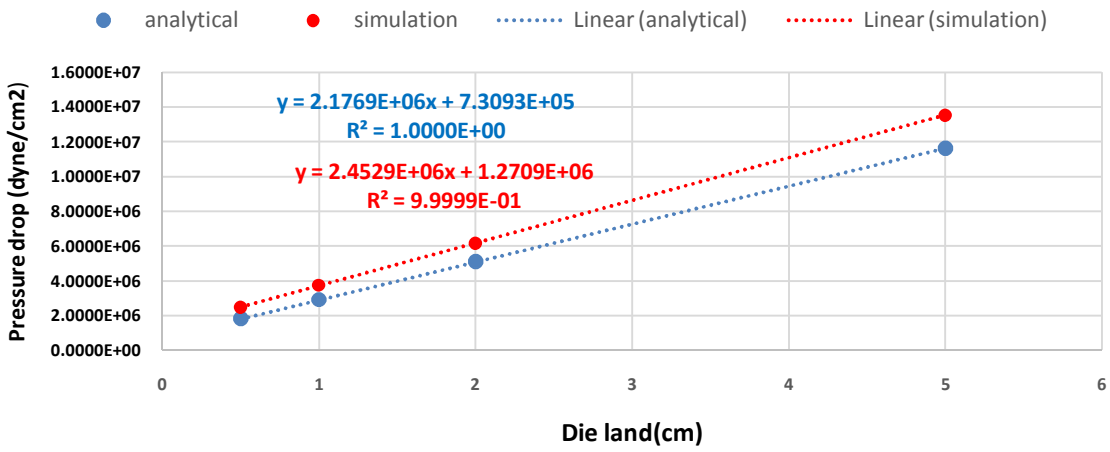

Fig. 4.9: Effect die land on pressure drop

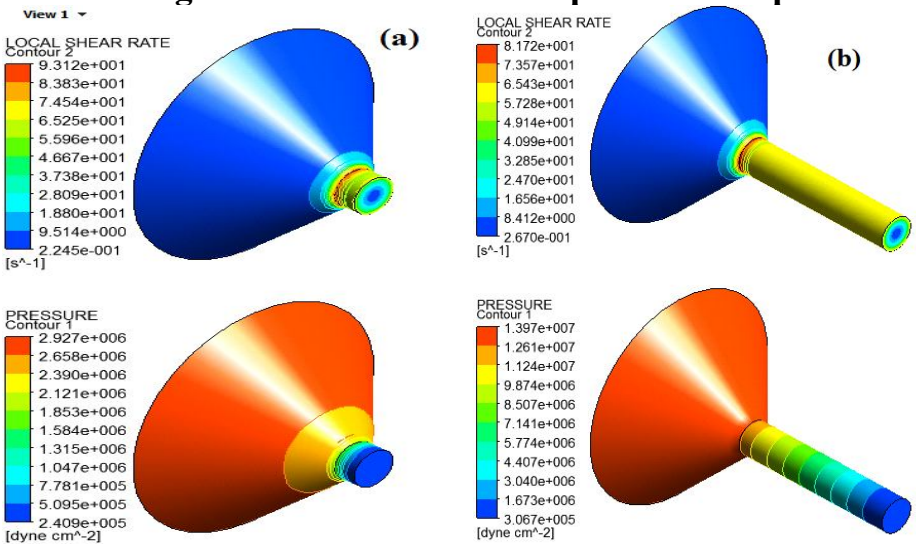

Fig. 4.10: Counters of shear rate and pressure in die a) length=0.5cm,b) length=5cm

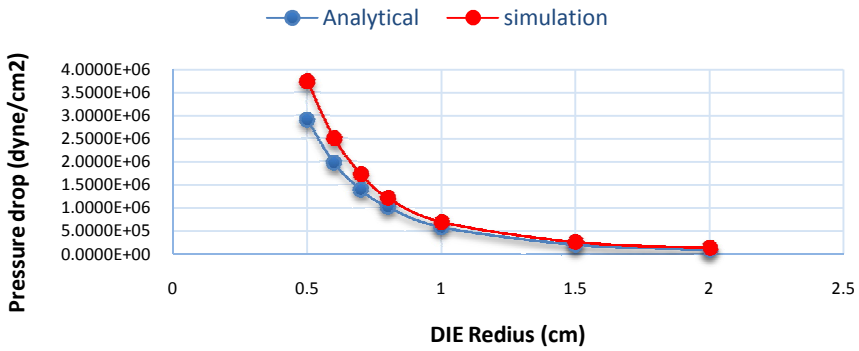

Fig. 4.11: Effect die radius on pressure drop

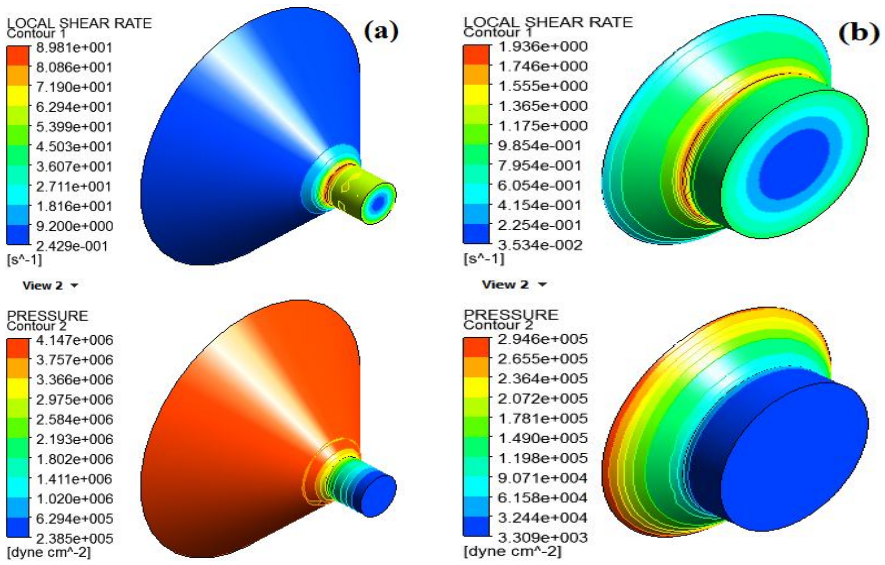

Fig. 4.12: Counters of shear rate and pressure in die a) radius=0.5 cm, b) radius=2 cm

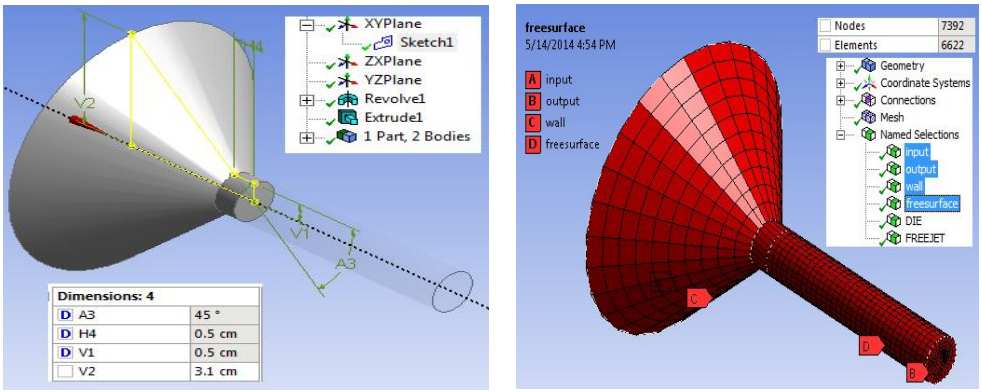

Fig. 4.13: Geometry and meshing for die and free jet

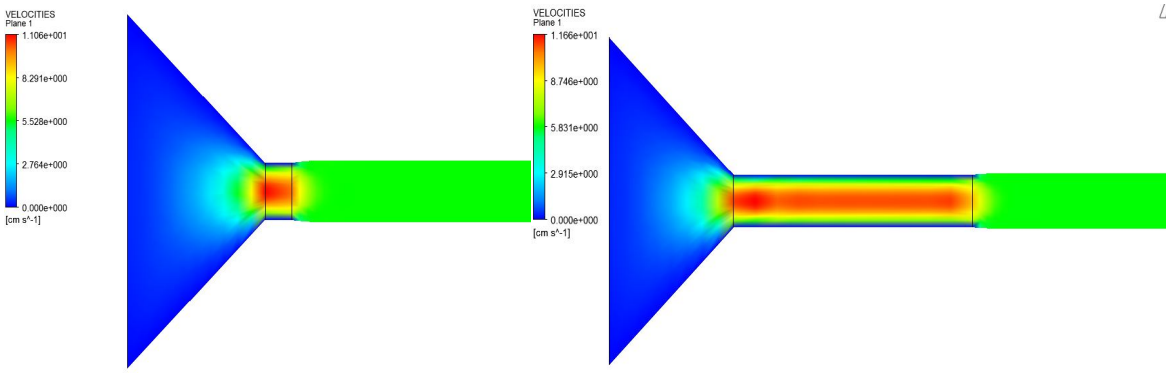

(A) **(B)**

Fig. 4.14: Velocity profiles and die swell at different die land A) L1=0.5cm, B) L1=5cm

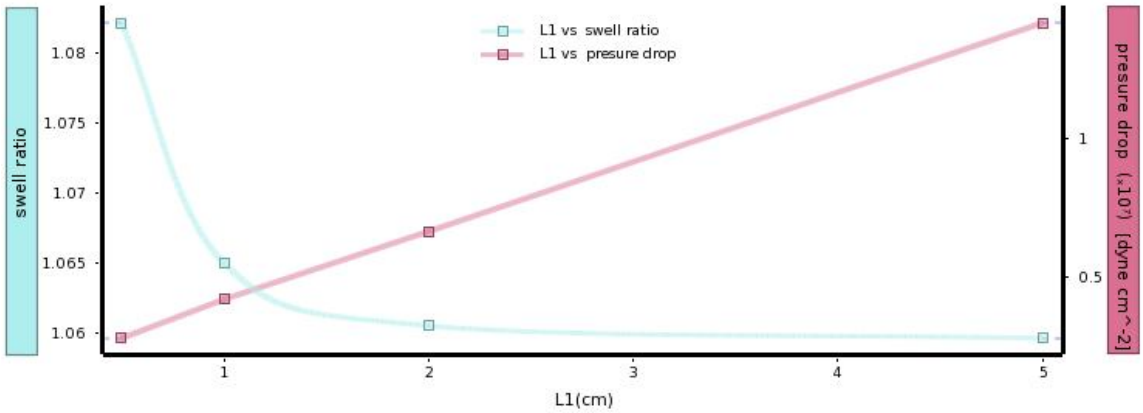

Fig. 4.15: Chart of swell ratio and pressure drop in the die at different die land values

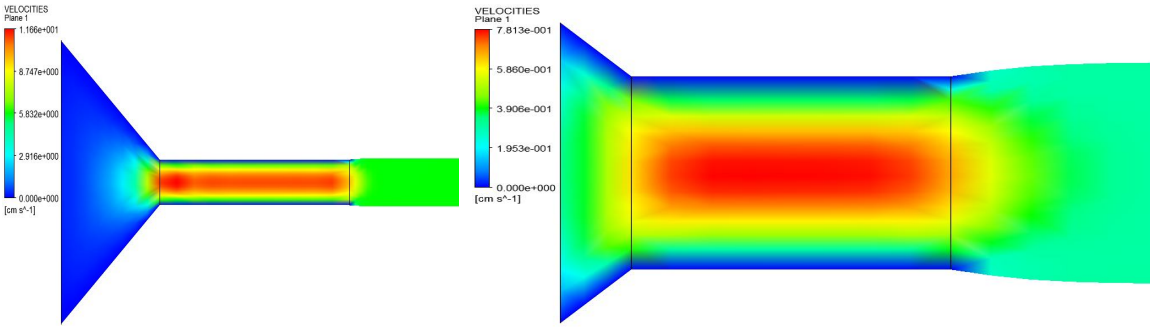

(A) (B)

Fig. 4.16: Velocity profiles and die swell at different Radius A) R1=0.5cm, B) R1=2cm

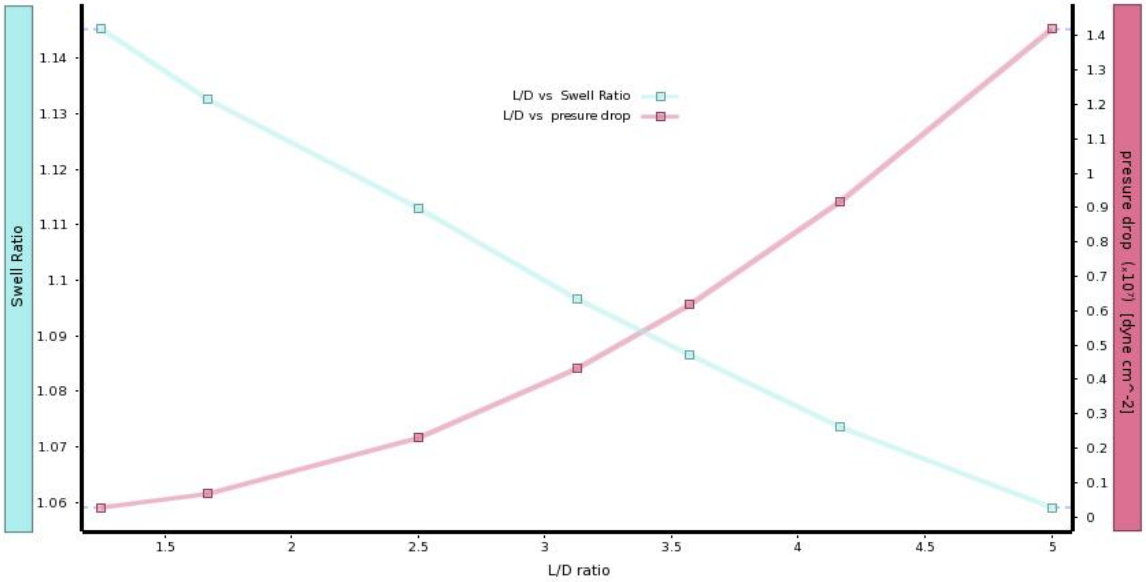

Fig. 4.17: Chart of swell ratio and pressure drop in the die at different L/D values

A B C

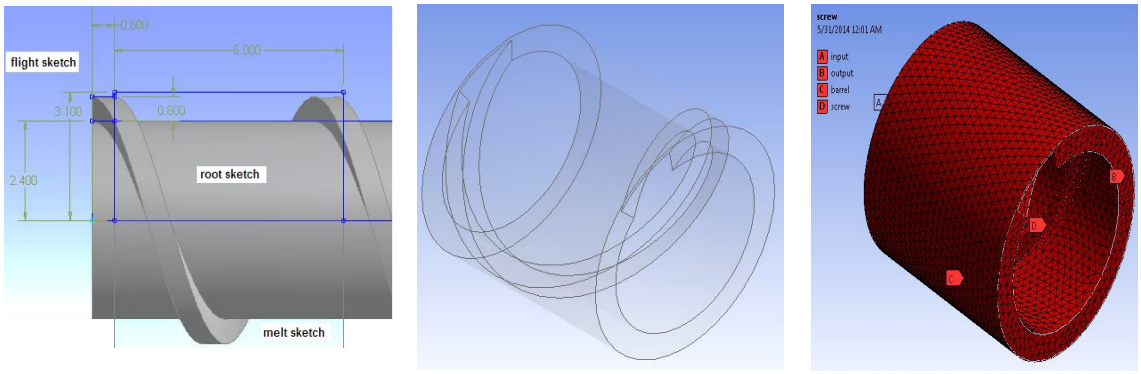

Fig. 4.18: Design one screw flight
A) Sketches and bodies, B) melt body C) meshing and boundaries

A B

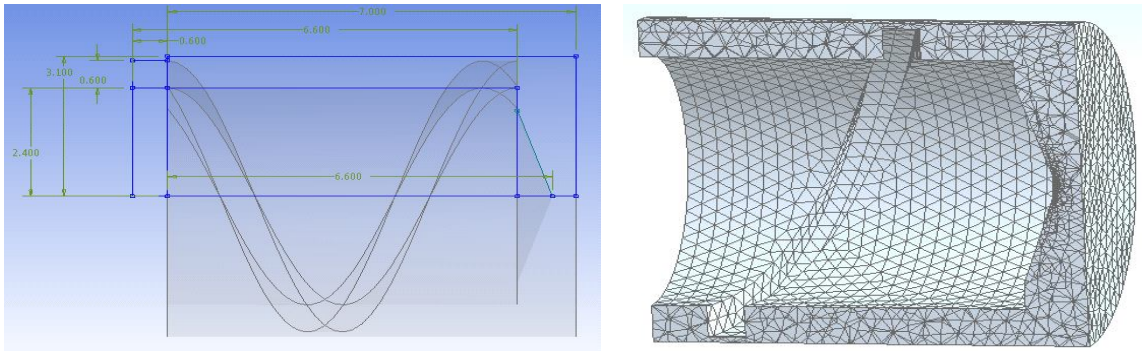

Fig. 4.19: Design one screw flight with nose A) melt body, B) meshing

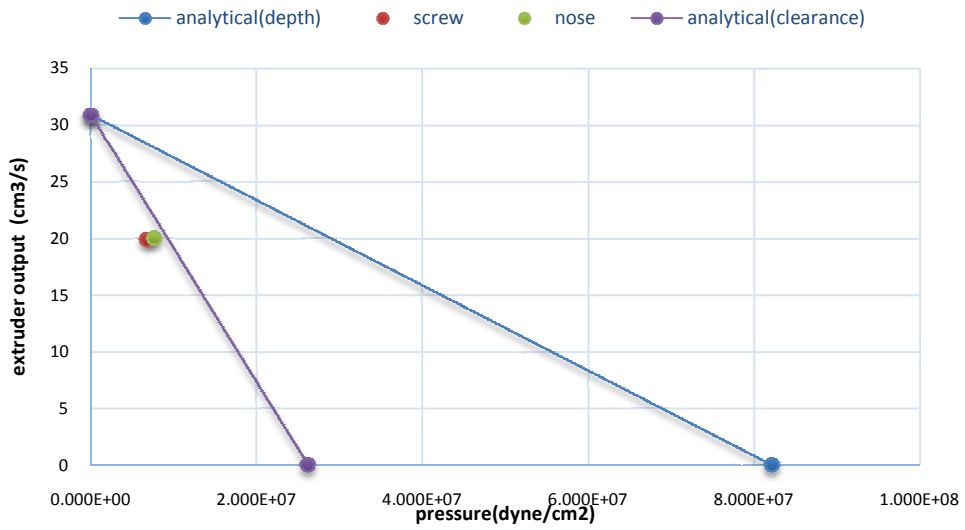

Fig. 4.20: Calculations extruder line at depth and clearance with screw and nose simulation

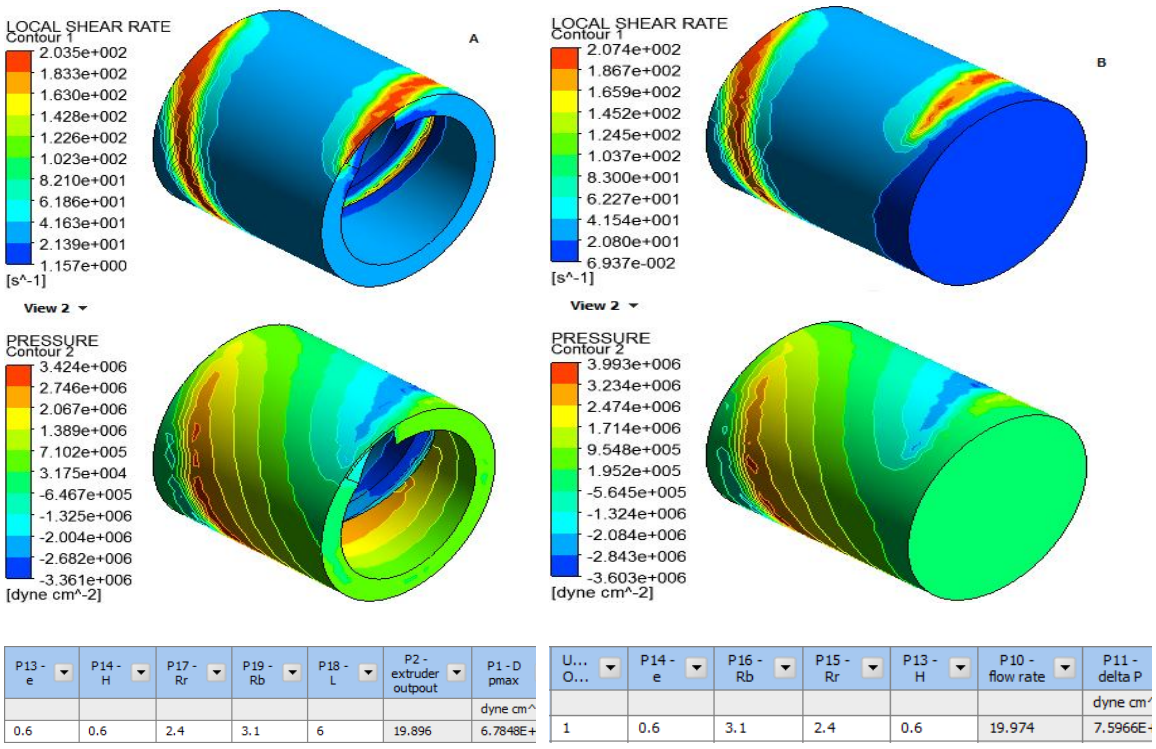

P13 - e	P14 - H	P17 - Rr	P19 - Rb	P18 - L	P2 - extruder outpout	P1 - D pmax
						dyne cm^
0.6	0.6	2.4	3.1	6	19.896	6.7848E+

U... O...	P14 - e	P16 - Rb	P15 - Rr	P13 - H	P10 - flow rate	P11 - delta P
						dyne cm^
1	0.6	3.1	2.4	0.6	19.974	7.5966E-

Fig. 4.21: Counters of shear rate and pressure A) Screw, B) Nose

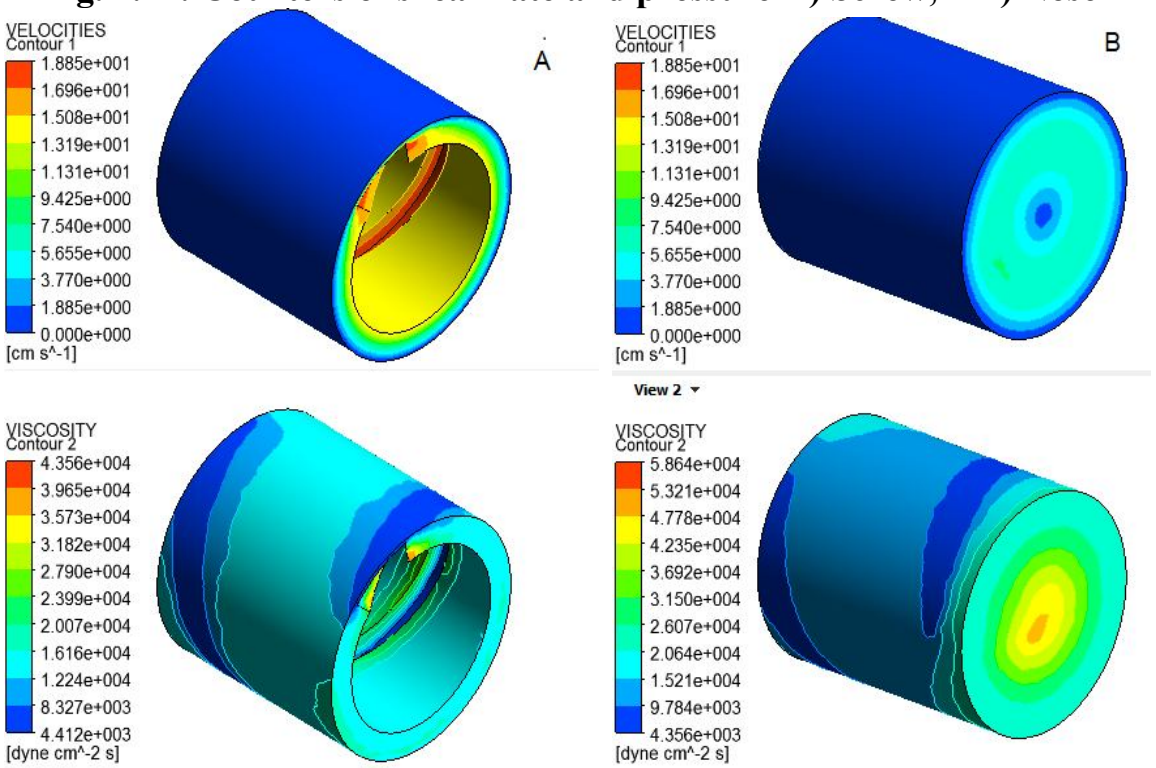

Fig. 4.22: Counters of velocity and viscosity A) Screw, B) Nose

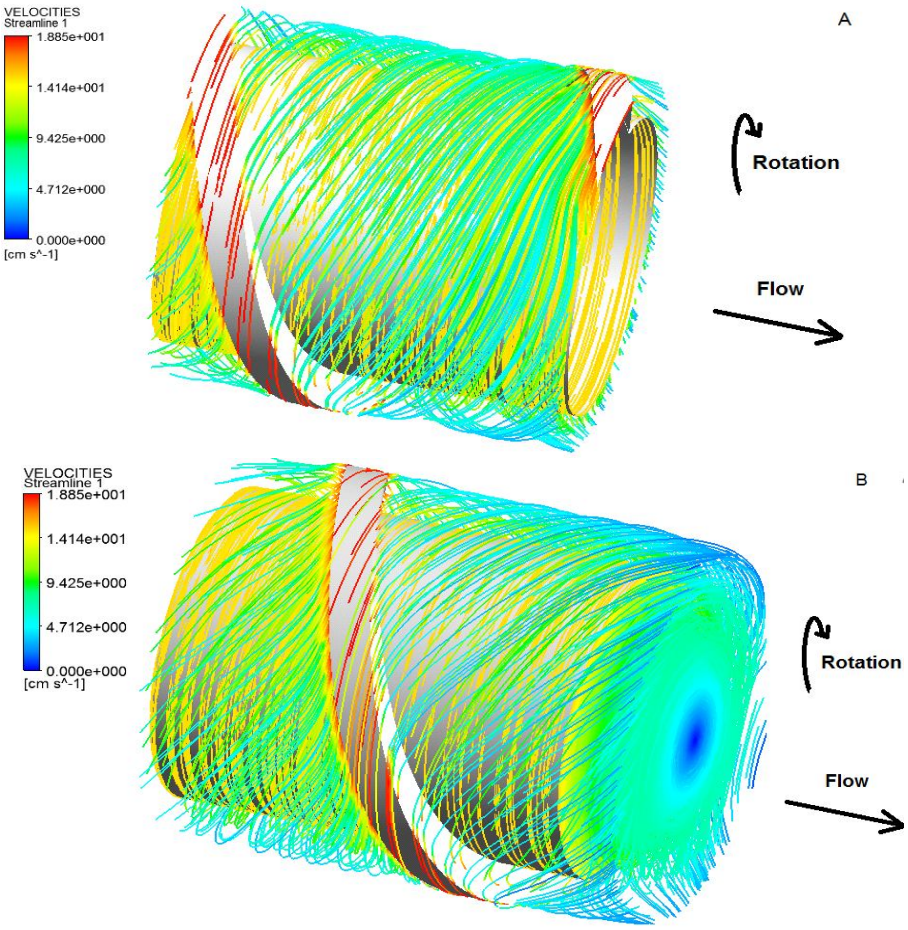

Fig. 4.23: Stream line A) Screw, B) Nose

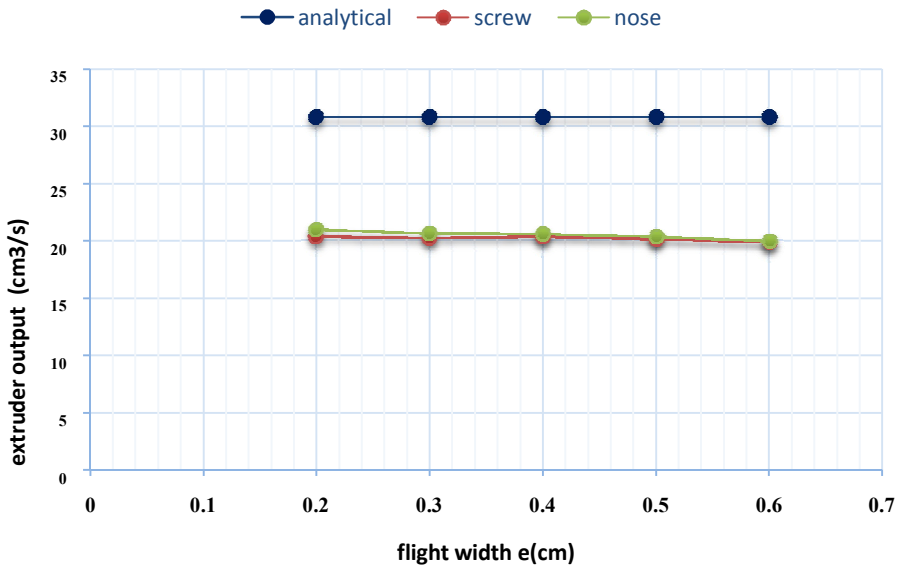

Fig. 4.24: Maximum output at different flight width analytically, screw and nose simulation

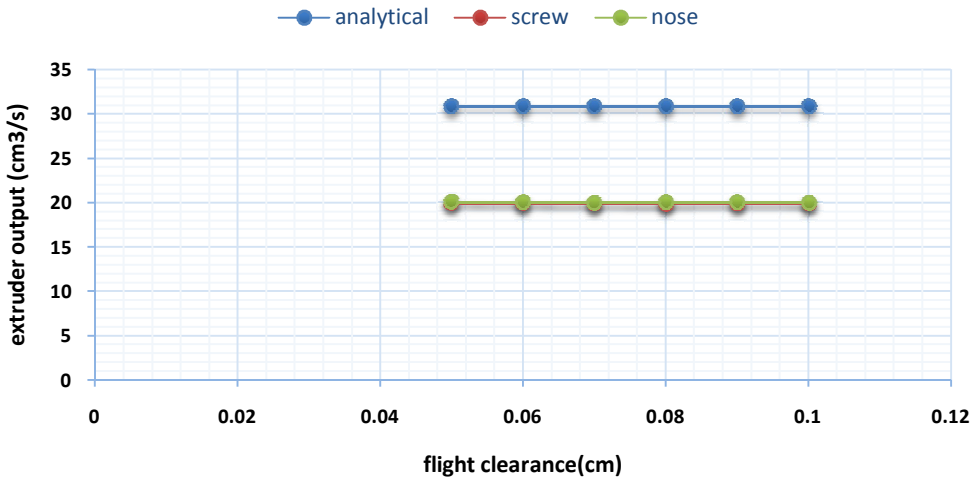

Fig. 4.25: Maximum output at different flight clearance analytically, screw and nose simulation

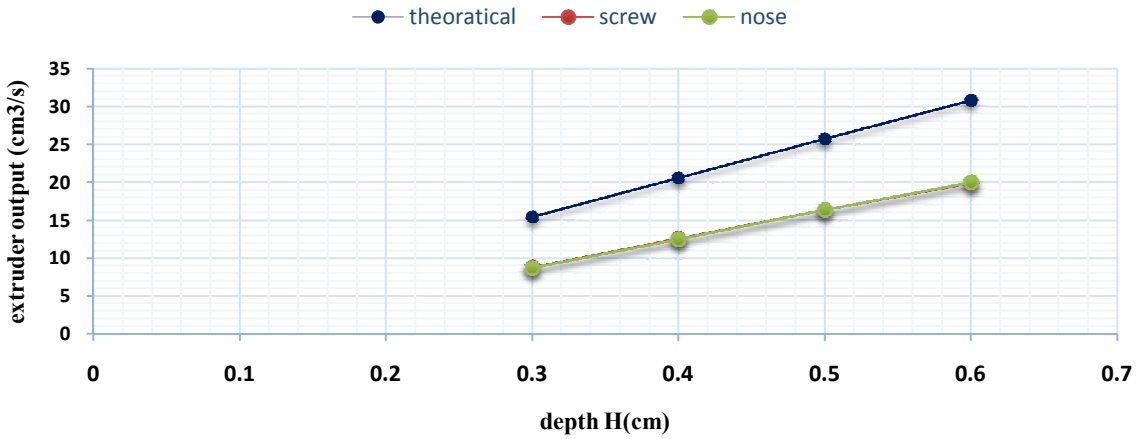

Fig. 4.26: Maximum output at different depth analytically, screw and nose simulation

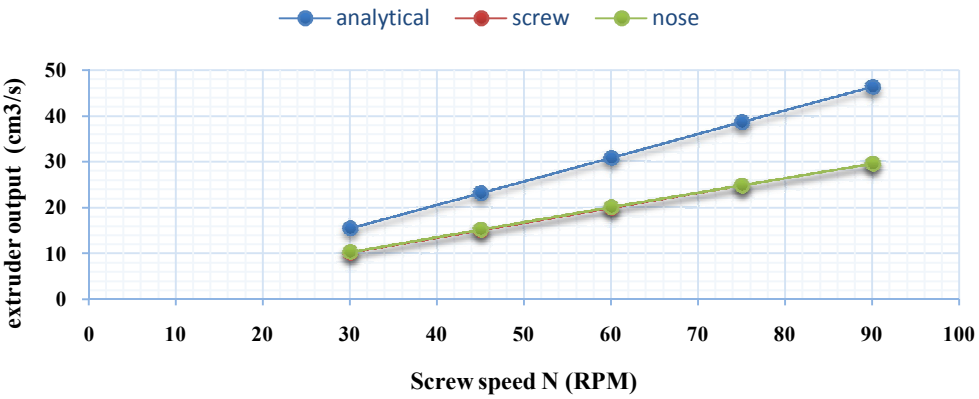

Fig. 4.27: Maximum output at different screw speed analytically, screw and nose simulation

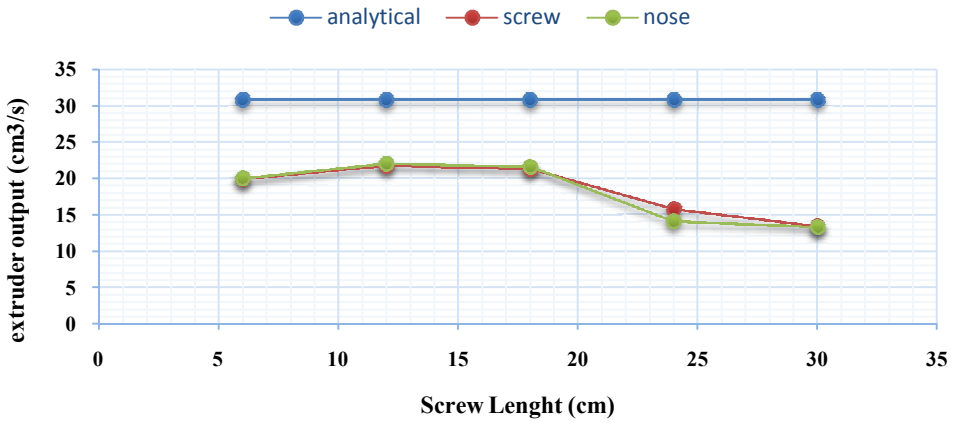

Fig. 4.28: Maximum output at different screw speed analytically, screw and nose simulation

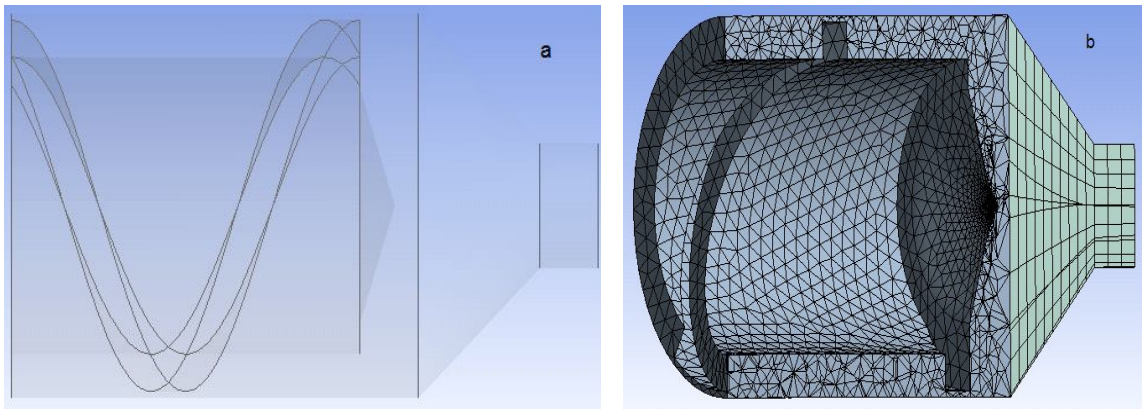

Fig. 4.29: Combine nose and die models a) melt body, b) meshing

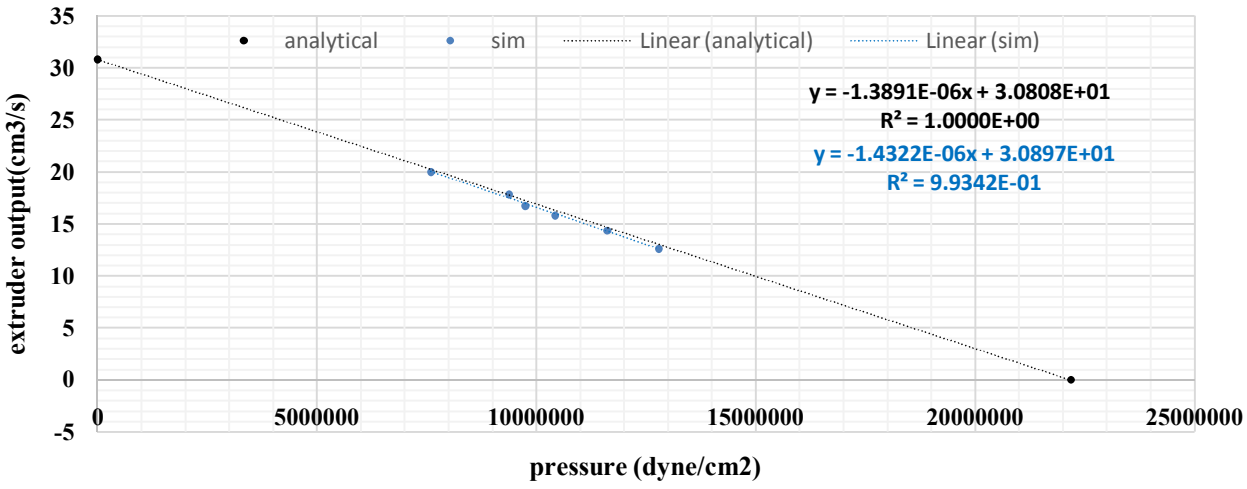

Fig. 4.30: Analytical extruder line and simulation operating points

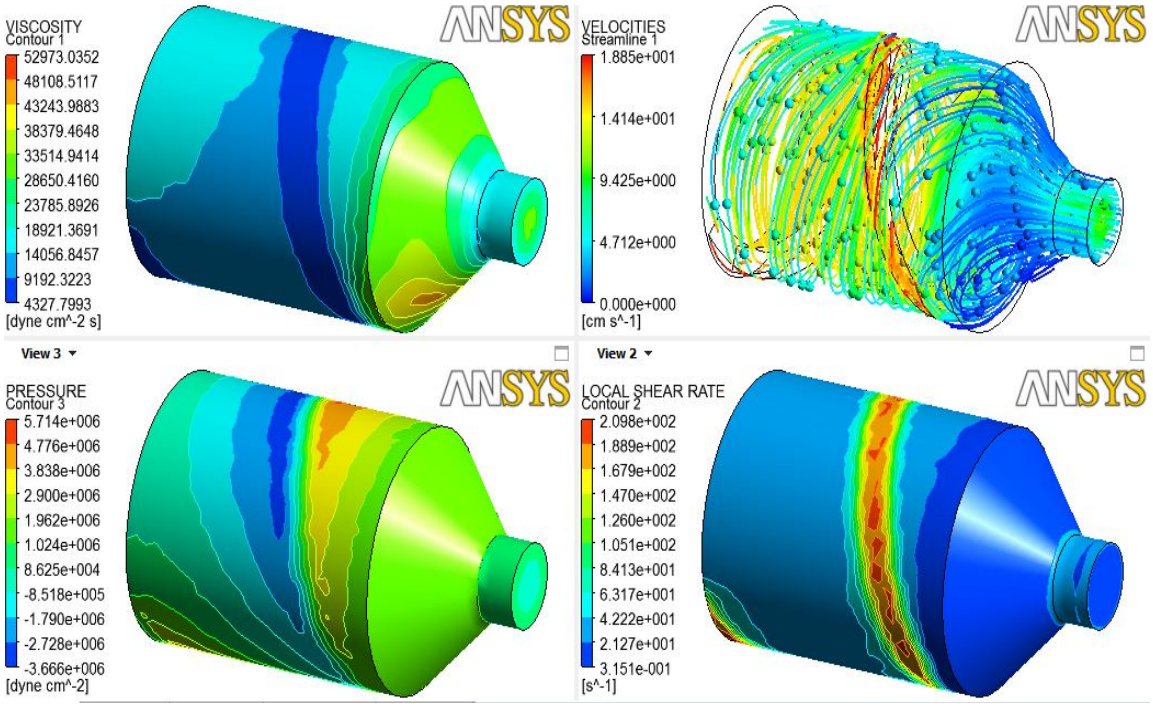

Fig. 4.31: Counters of simulation operating point at die radius 0.5cm

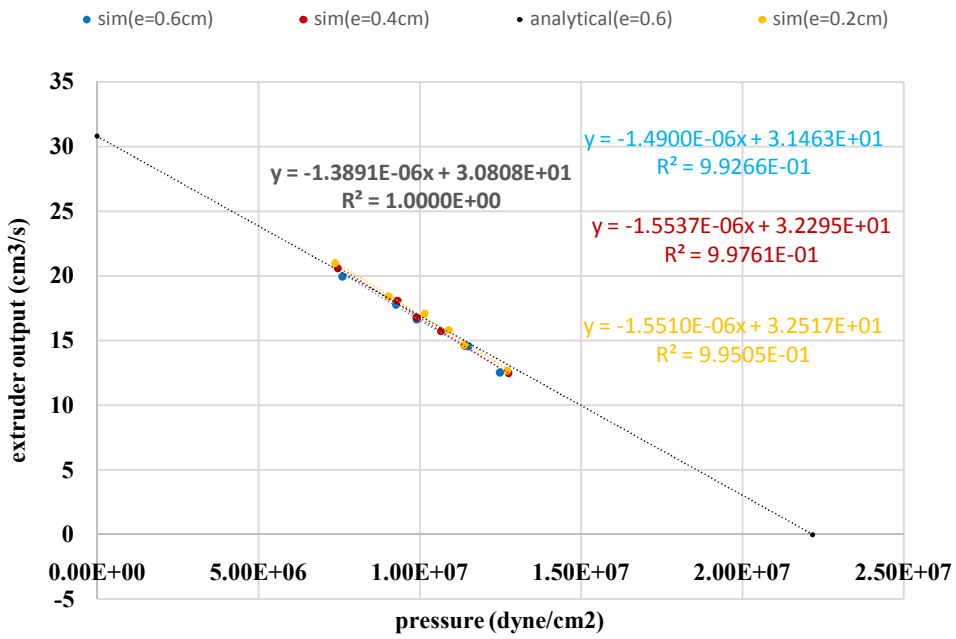

Fig. 4.32: Analytical extruder line and simulation operating points at different flight width

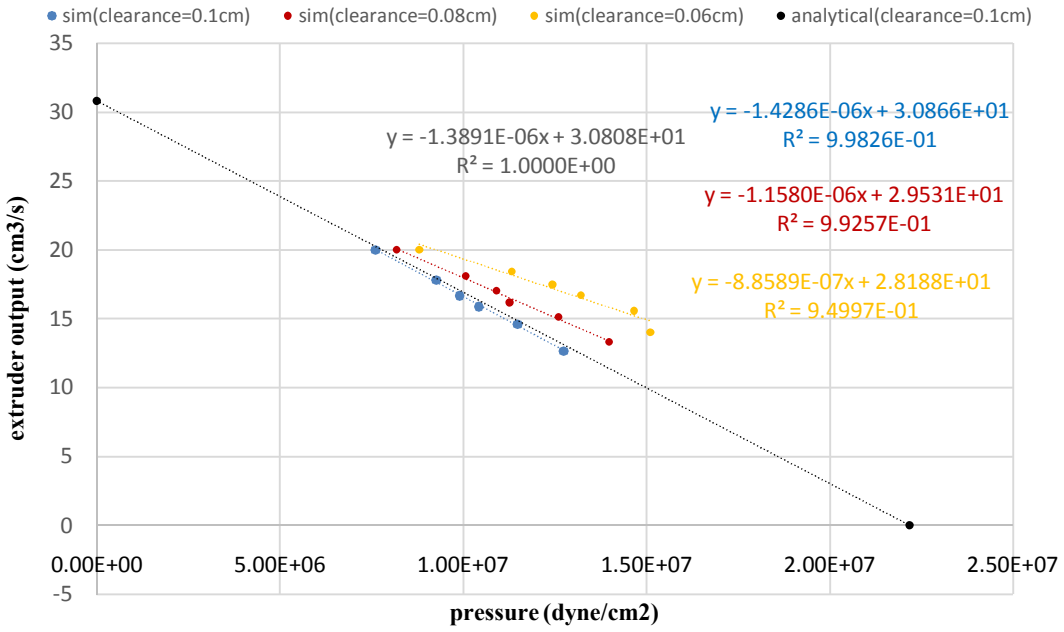

Fig. 4.33: Analytical extruder line and simulation operating points at different flight clearance

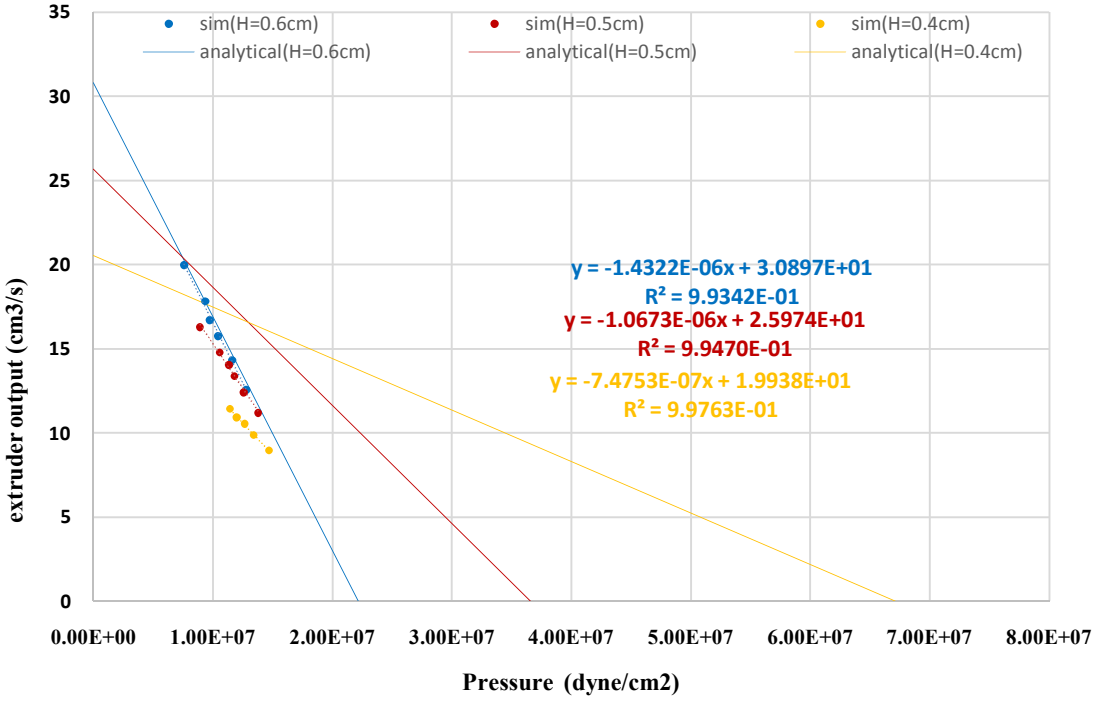

Fig. 4.34: Analytical extruder line and simulation operating points at different flight depth

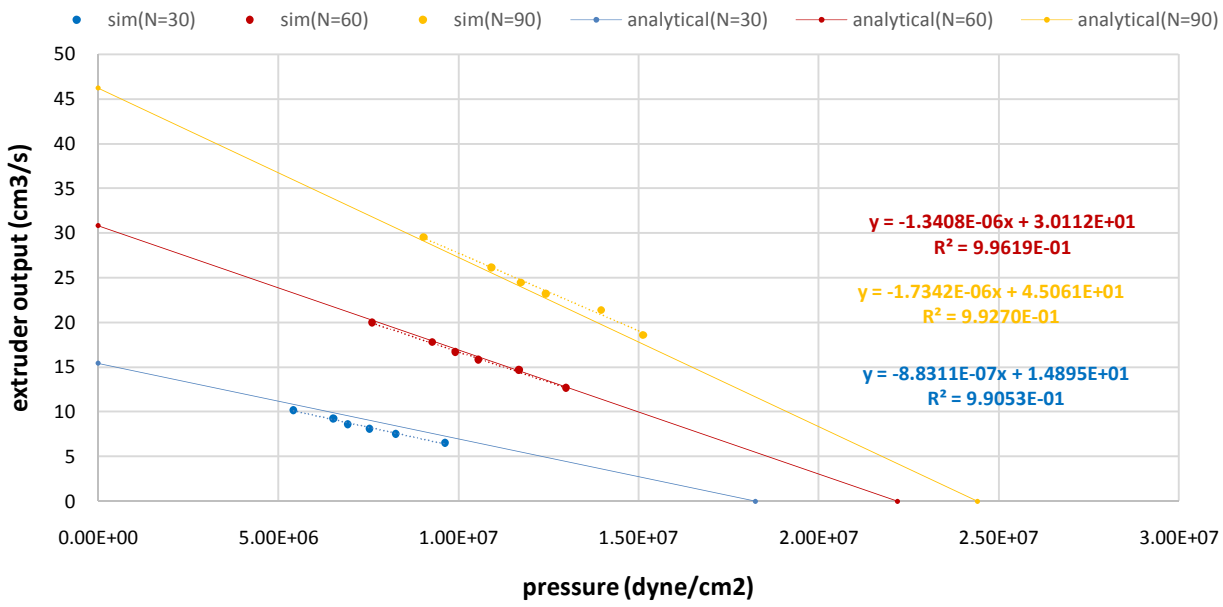

Fig. 4.35: Analytical extruder line and simulation operating points at different screw speed

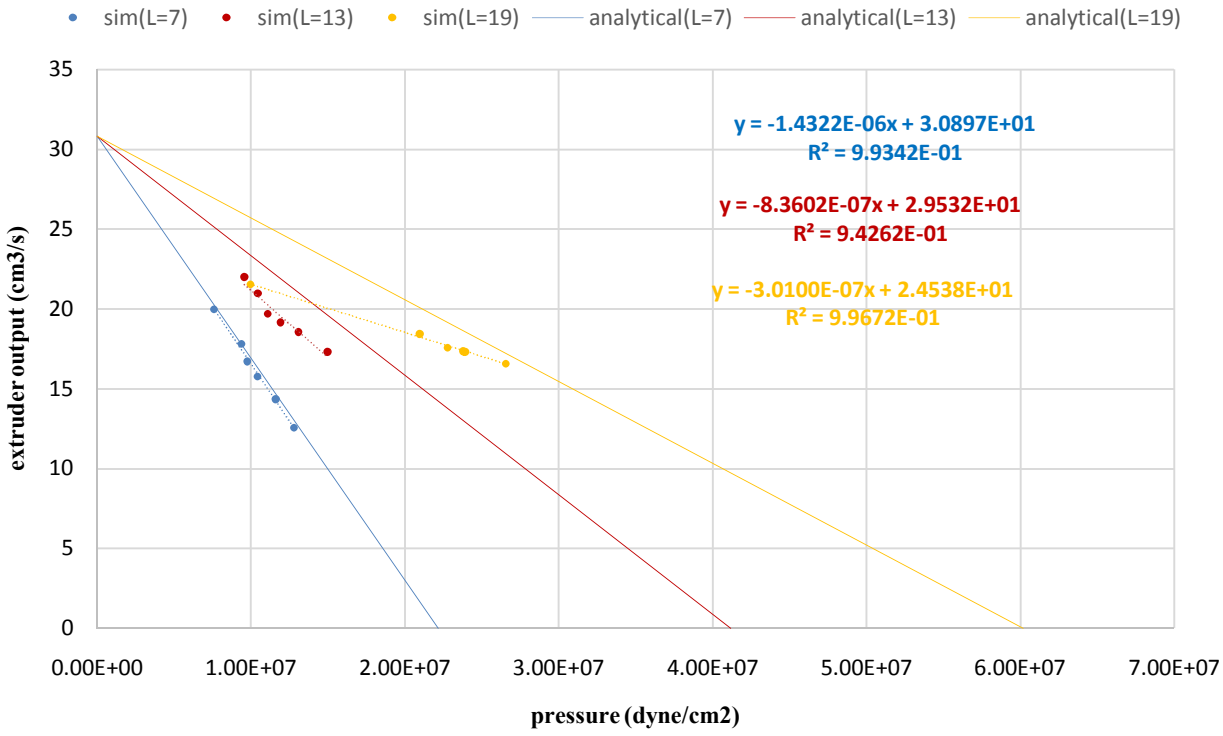

Fig. 4.36: Analytical extruder line and simulation operating points at different screw length

CHAPTER FIVE

CONCLUSIONS AND RECOMMENDATION

5.1. Conclusions

5.1.1 Material

The shear stress vs. shear rate for PP113 is non Newton model, the viscosity decreases with increasing shear rate. Polymat in Polyflow software was good fitting experimental data. PRMSE was easy method and accurate result obtained. Finally viscosity model Carreau-Yasuda was best fit model.

5.1.2 The combined die section (Tapered and non-tapered)

Die: The best taper angle for PP die that consist of circular section and tapered section is 45° .the highest shear rate was at the interface between the circular section and tapered section which gives the highest pressure drop .To prevent this the discontinuity between the two sections should be disappear .

Die and Free Jet: The swell ratio decreased for PP when land die was increase by slightly value than L/D was increased in the die.

5.1.3 The single screw extruder without and with nose models

The extruder line: The simulation of screw and nose gives single points with specified flow rate and pressure drop less than analytical value, the software describe the actual situation.

Flight width: The analytical was not consider flight width values, but simulation there small difference in flow rate between simulation screw and nose, the flow rate in simulation was increased and pressure

decreased at flight width decreased because the screw channel was increased and reduced friction area above flight .

Flight clearance: The analytical was not consider flight clearance values, but simulation there small difference in flow rate between simulation screw and nose, the flow rate in simulation and pressure were increased at flight clearance decreased because reduced back flow (leakage) and that increased the pressure according in small clearance (high shear rate).

Screw depth: The maximum extruder output and pressure in analytical and simulation was increased at screw depth increased, in simulation of screw and nose there was small difference in flow rate between them, the extruder output in simulation was increased at screw depth increased (deep channel) because the deep channel increased amount of melt flow and reduce pressure drop .

Screw speed: The maximum extruder output and pressure in analytical and simulation was increased at screw speed increased ,in simulation screw and nose there small difference in output between them, the output and pressure in simulation was increased at screw speed increased give increased amount of melt flow and shear rate .

Screw length: The analytical was constant value at length increased, in simulation screw and nose there are small difference in output and pressure between them, the best length of metering zone is (12cm) 2 flights this give high flow rate and suitable pressure drop.

5.1.4 The die characteristics at operating point

The extruder line: The constant linear relationship analytically and simulation that shown the maximum shear rate in die $303.80491 s^{-1}$of material pressure $2.17 \times 10^{7}\ dyne/cm^{2}$can be use analytically.

Flight width: The analytical extruder line was not affect by flight width values, but simulation the extruder output increase and pressure decrease at flight width decrease that allow wide flow channel and small friction area between flight and barrel .

Flight clearance: The maximum extruder output and pressure in analytical was not conceder flight clearance values, in simulation the output decrease and pressure increase at flight clearance decrease, the effect of clearance to the extrude with die is opposite to the extruder without die because the pressure (melting pressure) was considered in these is case.

Flight depth: The maximum extruder output and pressure in analytical and simulation was decreased at screw depth decreased, the analytical pressure high than simulation at flight depth decreased the assumption to design high shear rate in die was failed at small value of screw depth the new die radius less 0.5cm can be used experimentally small die at small depth .

Screw speed: The maximum extruder output and pressure in analytical and simulation was increased at screw speed increased, the effect of screw speed linearly high speed high shear rate, pressure, and output.

Screw length: The maximum output analytical was constant value at length increased, in simulation it was decreased because the long flow path and high pressure drop and that the actual situation in screw design.

5.2. Recommendation

- Estimate rheological properties at non-isothermal at different temperatures
- Estimate rheological properties for another Khartoum petrochemical company injection grid PP114.
- A parameters in pressure drop in tapered die must be study like type of meshing and its quality and curved sharp design in an interface between two sections.
- Simulated another parameters are the effect of in swell ratio
- Added mixing zone or design double flight screw.

REFERENCES

&D.R.SAIN, A. V. S. 2000. Thermoplastic melt rheology and Processing, ch, New York: Marcel Dekker, Inc.

ANSARI, M., ALABBAS, A., HATZIKIRIAKOS, S. & MITSOULIS, E. 2010. Entry flow of polyethylene melts in tapered dies. *International Polymer Processing,* 25.296-287 ,

ANSYS 2012. ANSYS POLYFLOW User's Guide

BAGLEY, E. 2004. End corrections in the capillary flow of polyethylene. *Journal of Applied Physics,* 28**,** 624-627.

BORG, T. & PÄÄKKÖNEN, E. J. 2009. Linear viscoelastic models: Part II. Recovery of the molecular weight distribution using viscosity data. *Journal of Non-Newtonian Fluid Mechanics,* 156**,** 129-138.

BUDAPEST UNIVERSITY OF TECHNOLOGY AND ECONOMICS, F. O. M. E., DEPARTMENT OF POLYMER ENGINEERING. 11. February 2007. MFI testing- viscosity measurementof thermoplastic polymers.

CORP, C. E. I. E. 2013. Melt Flow Rate Testing Instrument guide. SUST plastic laboratory.

CRAWFORD, R. J. 1998. *Plastics engineering*, Butterworth-Heinemann.

DOOLEY, J., KIM, H., LEE, P. C. & WRISLEY, R. THE EFFECT OF COATHANGERDIE MANIFOLD SYMMETRY ON LAYER UNIFORMITY IN MULTILAYER COEXTRUSION.

ENG, P. S. 2002. Extrusion lectures (MRC.(

FEDI-SOETAREDJO, F., NASHED, G., RUTGERS, R. & TORLEY, P. Numerical analysis of the effect of extrusion conditions on flow in slit die rheometer. 3rd International Conference on CFD in the Minerals and Process Industries. CSIRO: Melbourne, Australia, 2003.

FENG, Y. & QU, J. Numerical Simulation of Melting Process in Single Screw Extruder with Vibration Force Field.

GUPTA, S., UDAY, V., RAGHUWANSHI, A. S., CHOWKSHEY, S., DAS, S. N. & SURESH, S. 2013. Simulation of blow molding using ansys polyflOW. *APCBEE Procedia,* 5**,** 468-473.

HATZIKIRIAKOS, S. G. & MITSOULIS, E. 2009. Slip effects in tapered dies. *Polymer Engineering & Science,* 49**,** 1960-1969.

INC., F. August 26, 2003a. Chapter 8. Boundary Conditions.

INC., F. August 26, 2003b. Chapter 10. Generalized Newtonian Flow.

JUNHONG, W. 2003. POLYFLOW, the powerful simulation tool for Polymer Process,. *SVU/Academic Computing, Computer Centre, NUS*.

KOSTIC, M. & REIFSCHNEIDER, L. 2006. Design of extrusion dies. *Encyclopedia of Chemical Processing DOI,* 10.

LAFLEUR, P. G. & VERGNES, B. Single-Screw Extrusion. *Polymer Extrusion***,** 37-108.

MFI 2007. VISCOSITY MEASUREMENT OF THERMOPLASTIC POLYMERS.

MITSOULIS, E ,.KAZATCHKOV, I. B. & HATZIKIRIAKOS, S. G. 2005. The effect of slip in the flow of a branched PP melt: experiments and simulations. *Rheologica acta,* 44**,** 418-426.

MUCCIO, E. A. 1994. *Plastics processing technology*, ASM International.

MUSAMEH, S. & JODEH ,S. 2009. The effects of shear rate and capillary length-to-diameter ratio on isothermal extrudate swell of polymer melts.

OSSWALD, T. & HERNÁNDEZ-ORTIZ, J. P. 2006. Polymer processing. *Hanser, Munich*.

OSSWALD, T. A. & GRAMANN, P. 2001. Polymer processingsimulations trends. *Society for the Advancement of Material and Process Engineers*.

PATRICK C. LEE, L. D., JOSEPH DOOLEY 2011. Improving Film Die Flow Uniformity Using Optimization Methods.

PEPLIŃSKI, K. & MOZER, A. 2010. ANSYS-POLYFLOW SOFTWARE USE TO SELECT THE PARISON DIAMETER AND ITS THICKNES DISTRIBUTION IN BLOWING EXTRUSION. *parameters,* 3**,** 5.

PEPLIŃSKI, K. & MOZER, A. 2011. Design of extrusion die for plastic profile using ansys polyflow software. *Journal of Polish CIMAC,* 6**,** 221-226.

POLYMERS, F. O .Flow Through Simple Dies.

RAO, N. & O'BRIEN, K. 1998. Design data for plastics engineers.

RELEASE, A. I. 2012. Ansys polyflow user's guide.

SHENOY, A. V. & SAINI, D. 1996. *Thermoplastic melt rheology and processing*, Marcel Dekker New York.

SOMBATSOMPOP, N .1999 .Elastic properties of flowing polymer melts,Polymer PROcessing and Flow (P-PROF(

Materials Technology, School of Energy & Materials

King Mongkut's University of Technology Thonburi

STRUTT, J. V. D. 2001. The role of rheology in polymer extrusion ,department of chemical engineering& polydynamics, Inc, Hamilton, Ontario, Canada.

SULAIMAN, H. B. 2011. Polymer Technology II, EXTRUSION OF PLASTICS.

VADDIRAJU, S. R., KOSTIC, M., RYKALIN, V., REIFSCHNEIDER, L., PLA-DALMAU, A. & BROSS, A. Extrusion simulation and experimental validation to optimize precision die design. ANTEC-CONFERENCE PROCEEDINGS-. 2004. UNKNOWN, 76-80.

VLACHOPOULOS, J. & STRUTT, D. The role of rheology in polymer extrusion. New Technology for Extrusion Conference. Milan, Italy. Nov.21-20 .2003 ,

YAMSAENGSUNG, R. & NOOMUANG, C. Finite Element Modeling for the Design of a Single-Screw Extruder for Starch-Based Snack Products. Proceedings of the World Congress on Engineering, 2010.

YUNUS, M. & YUSRI, M. 2010. *Software development of concurrent design for manufacturing process selection of plastic materials.* Universiti Teknologi Malaysia, Faculty of Mechanical Engineering.

APPENDIXES

Appendix A: Isothermal flow through circular tube(Polymers)

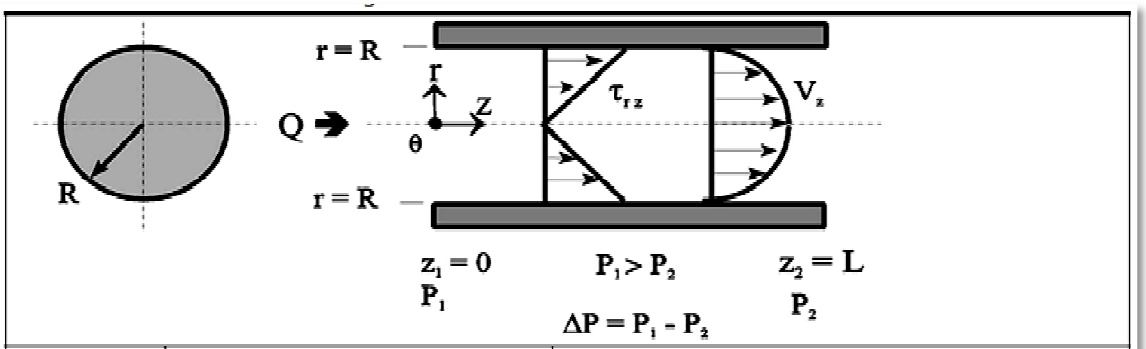

	Newtonian Fluid	Power-Law-Fluid
Viscosity	$\tau_w = \frac{\Delta P \cdot R}{2L}$	$\eta = \eta^o \cdot \left(\frac{\dot{\gamma}}{\dot{\gamma}^o}\right)^{(n-1)}$ with $\dot{\gamma}^o = 1.0\ s^{-1}$
Shear stress at the wall	$\tau_w = \frac{\Delta P \cdot R}{2L}$	$\tau_w = \frac{\Delta P \cdot R}{2L}$
Shear rate at the wall	$\dot{\gamma}_a = \frac{4Q}{\pi R^3}$	$\dot{\gamma}_w = \frac{\dot{\gamma}_a}{4} \cdot \left(3 + \frac{1}{n}\right)$
Maximum velocity at the tube center	$V_o = \frac{R^2 \cdot \Delta P}{4\mu L}$	$V_o = \left(\frac{R \cdot n \cdot \dot{\gamma}^o}{n+1}\right) \cdot \left(\frac{R \cdot \Delta P}{2\eta^o \cdot \dot{\gamma}^o \cdot L}\right)^{1/n}$
Average velocity	$V_{avg} = \frac{1}{2} V_o$	$V_{avg} = \left(\frac{n+1}{3n+1}\right) \cdot V_o$
Volumetric flow rate	$Q = \frac{\pi R^4 \cdot \Delta P}{8\mu L}$	$Q = \pi R^2 \cdot V_{avg}$
Pressure drop	$\Delta P = \frac{8\mu L \cdot Q}{\pi R^4}$	$\Delta P = \left[\frac{Q}{\pi R^3} \cdot \left(\frac{3n+1}{n \cdot \dot{\gamma}^o}\right)\right]^n \cdot \left(\frac{2\eta^o \cdot \dot{\gamma}^o \cdot L}{R}\right)$
Velocity profile	$V_z(r) = V_o \cdot \left[1 - \left(\frac{r}{R}\right)^2\right]$	$V_z(r) = V_o \cdot \left[1 - \left(\frac{r}{R}\right)^{(n+1)/n}\right]$
Shear rate profile	$\dot{\gamma}(r) = \left(\frac{2V_o}{R}\right) \cdot \left(\frac{r}{R}\right)$	$\dot{\gamma}(r) = \left(\frac{V_o}{R}\right) \cdot \left(\frac{n+1}{n}\right) \cdot \left(\frac{r}{R}\right)^{1/n}$

Appendix B: Reports from melt flow indexer instrument

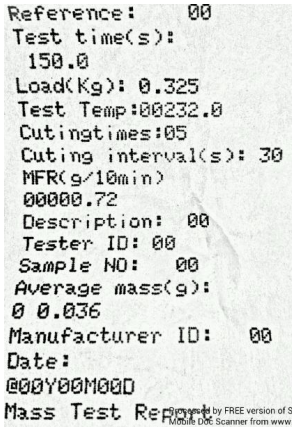
Reference: 00
Test time(s):
150.0
Load(Kg): 0.325
Test Temp:00232.0
Cutingtimes:05
Cuting interval(s): 30
MFR(g/10min)
00000.72
Description: 00
Tester ID: 00
Sample NO: 00
Average mass(g):
0 0.036
Manufacturer ID: 00
Date:
@00Y00M00D
Mass Test Report

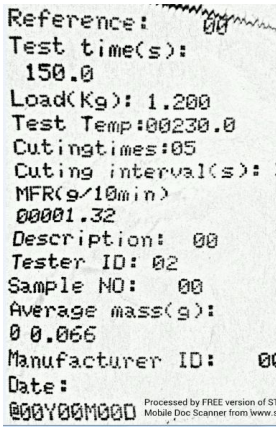
Reference: 00
Test time(s):
150.0
Load(Kg): 1.200
Test Temp:00230.0
Cutingtimes:05
Cuting interval(s):
MFR(g/10min)
00001.32
Description: 00
Tester ID: 02
Sample NO: 00
Average mass(g):
0 0.066
Manufacturer ID: 00
Date:
@00Y00M00D

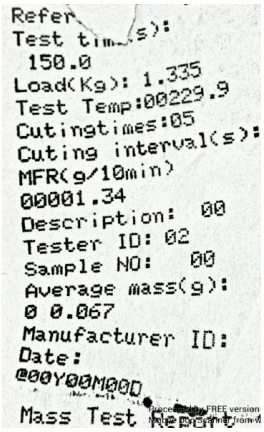
Refer
Test time(s):
150.0
Load(Kg): 1.335
Test Temp:00229.9
Cutingtimes:05
Cuting interval(s):
MFR(g/10min)
00001.34
Description: 00
Tester ID: 02
Sample NO: 00
Average mass(g):
0 0.067
Manufacturer ID:
Date:
@00Y00M00D
Mass Test Report

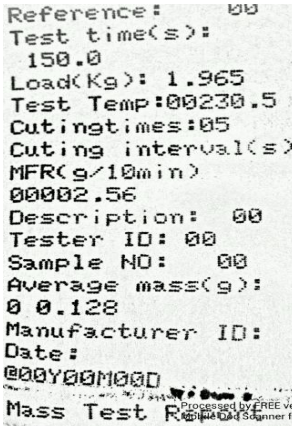
Reference: 00
Test time(s):
150.0
Load(Kg): 1.965
Test Temp:00230.5
Cutingtimes:05
Cuting interval(s)
MFR(g/10min)
00002.56
Description: 00
Tester ID: 00
Sample NO: 00
Average mass(g):
0 0.128
Manufacturer ID:
Date:
@00Y00M00D
Mass Test Report

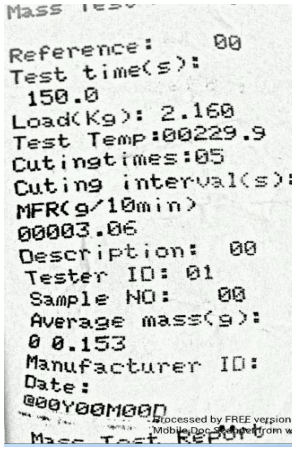
Reference: 00
Test time(s):
150.0
Load(Kg): 2.160
Test Temp:00229.9
Cutingtimes:05
Cuting interval(s):
MFR(g/10min)
00003.06
Description: 00
Tester ID: 01
Sample NO: 00
Average mass(g):
0 0.153
Manufacturer ID:
Date:
@00Y00M00D

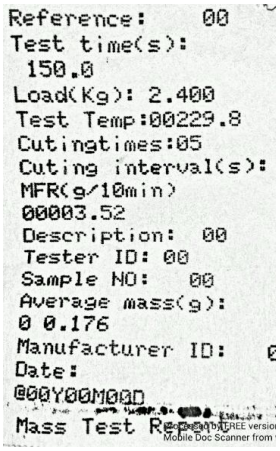
Reference: 00
Test time(s):
150.0
Load(Kg): 2.400
Test Temp:00229.8
Cutingtimes:05
Cuting interval(s):
MFR(g/10min)
00003.52
Description: 00
Tester ID: 00
Sample NO: 00
Average mass(g):
0 0.176
Manufacturer ID:
Date:
@00Y00M00D
Mass Test Report

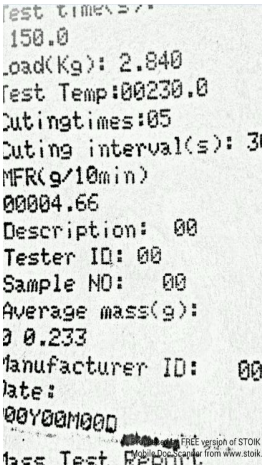
150.0
Load(Kg): 2.840
Test Temp:00230.0
Cutingtimes:05
Cuting interval(s):
MFR(g/10min)
00004.66
Description: 00
Tester ID: 00
Sample NO: 00
Average mass(g):
0 0.233
Manufacturer ID: 00
Date:
@00Y00M00D

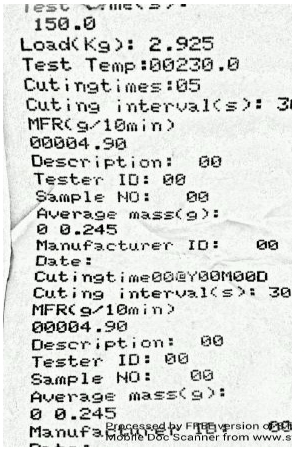
150.0
Load(Kg): 2.925
Test Temp:00230.0
Cutingtimes:05
Cuting interval(s):
MFR(g/10min)
00004.90
Description: 00
Tester ID: 00
Sample NO: 00
Average mass(g):
0 0.245
Manufacturer ID: 00
Date:
Cutingtime00@Y00M00D
Cuting interval(s): 30
MFR(g/10min)
00004.90
Description: 00
Tester ID: 00
Sample NO: 00
Average mass(g):
0 0.245

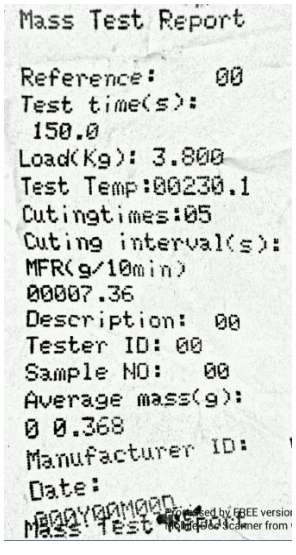
Mass Test Report
Reference: 00
Test time(s):
150.0
Load(Kg): 3.800
Test Temp:00230.1
Cutingtimes:05
Cuting interval(s):
MFR(g/10min)
00007.36
Description: 00
Tester ID: 00
Sample NO: 00
Average mass(g):
0 0.368
Manufacturer ID:
Date:

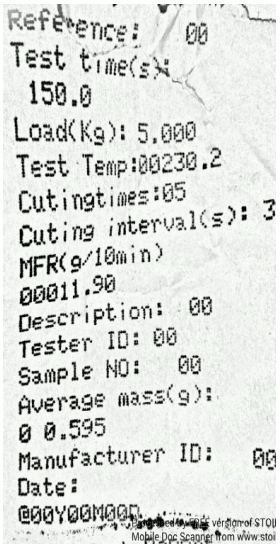
Reference: 00
Test time(s):
150.0
Load(Kg): 5.000
Test Temp:00230.2
Cutingtimes:05
Cuting interval(s): 3
MFR(g/10min)
00011.90
Description: 00
Tester ID: 00
Sample NO: 00
Average mass(g):
0 0.595
Manufacturer ID: 00
Date:
@00Y00M00D

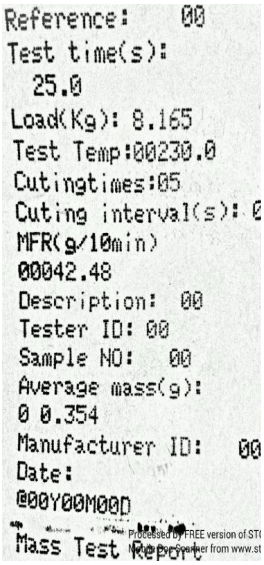
Reference: 00
Test time(s):
25.0
Load(Kg): 8.165
Test Temp:00230.0
Cutingtimes:05
Cuting interval(s): 0
MFR(g/10min)
00042.48
Description: 00
Tester ID: 00
Sample NO: 00
Average mass(g):
0 0.354
Manufacturer ID: 00
Date:
@00Y00M00D
Mass Test Report

Appendix C: Equations and parameters from Polymat software

Power Low	Bird-Carreau Law
Power law f(g) = fac * (tnat*g)**(expo-1) fac = 0.1807456E+05 [auto] tnat = 0.6480288E-01 [auto] expo = 0.5802489E+00 [auto]	Bird-Carreau law f(g) = facinf + (fac-facinf) * [1+(tnat*g)**2]**((expo-1)/2) fac = 0.3939230E+05 [auto] tnat = 0.2607249E+00 [auto] expo = 0.4833018E+00 [auto] facinf = 0.3273708E-02 [auto]
Cross Law	**Log log law**
Cross law f(g) = fac/ (1 + (tnat*g)**expom) fac = 0.5356631E+05 [auto] tnat = 0.1473487E+00 [auto] expom = 0.6964472E+00 [auto]	Log-Log law f(g) = fac * 10**(a0 +a1*log(g/gcrit) +a11*log(g/gcrit)**2) a0 = -0.3965743E+00 [auto] a1 = 0.5546945E+00 [auto] a11 = -0.1229601E+00 [auto] fac = 0.2771846E+05 [auto] gcrit = 0.1456364E-02 [auto]
Bingham law	**Herschel-Bulkley law**
Bingham law f(g) = fac + ystr/g when g >= gcrit = fac + ystr/gcrit*(2-g/gcrit) when g <gcrit fac = 0.5279988E+04 [auto] ystr = 0.2095891E+06 [auto] gcrit = 0.1341293E+02 [auto]	Herschel-Bulkley law f(g) = fac1 / g + fac2 * (g/gcrit) ** (expo-1) when g >gcrit = fac1 * [2 - g/gcrit] / gcrit + fac2 * [(2-expo) + (expo-1) * g/gcrit] when g <gcrit fac1 = 0.5191806E-02 [auto] fac2 = 0.2746237E+05 [auto] expo = 0.5120642E+00 [auto] gcrit = 0.6912179E+01 [auto]
modified Cross law	**modified Bingham law**
modified Bingham law f(g) = fac + ystr*(1-exp(-m*g))/g where m = 3/gcrit fac = 0.4399646E+04 [auto] ystr = 0.2670147E+06 [auto] gcrit = 0.2265015E+02 [auto]	modified Bingham law f(g) = fac + ystr*(1-exp(-m*g))/g where m = 3/gcrit fac = 0.4399646E+04 [auto] ystr = 0.2670147E+06 [auto] gcrit = 0.2265015E+02 [auto]
modified Herschel-Bulkley law	**Carreau Yasuda law**
modified Herschel-Bulkley law f(g) = fac1 * (1 - exp(-3 * g / gcrit)) / g + fac2 * (g / gcrit) ** (expo-1) fac1 = 0.2262428E+06 [auto] fac2 = 0.6511587E+04 [auto] expo = 0.5786505E+00 [auto] gcrit = 0.4817822E+02 [auto]	Carreau-Yasuda law f(g) = facinf + (fac-facinf) * [1+(tnat*g)**expoa]**((expo-1)/expoa) fac = 0.6738002E+05 [auto] tnat = 0.3531332E-01 [auto] expo = 0.5375814E-05 [auto] facinf = 0.1445808E-01 [auto] expoa = 0.4534786E+00 [auto]

Appendix D: Basic equation and Shear-Rate temperatures -Dependent Viscosity Laws(Inc., August 26, 2003b)

Basic Equations

For a GNF, POLYFLOW solves the momentum equations, the incompressibility equation, and (for non-isothermal lows) the energy equation.

- The form of the momentum equations is

$$\nabla p + \nabla . \mathrm{T} + f = \rho a - - - (D.1)$$

where

$p = pressure$

$T = extra - stress\ tensor$

$f = volumetric\ force$

$\rho = density$

$a = acceleration$

- The incompressibility equation is

$$\nabla . v = 0 - - - (D.2)$$

where

$v = velocity.$

- The energy equation

$$\mathrm{T} = 2\mu \mathrm{D} - - - (\mathrm{D}.3)$$

Where D is the rate-of-deformation tensor and μ can be a function of local shear rate $\dot{\gamma}$ temperature T, or both.

- The local shear rate

$$\dot{\gamma} = \sqrt{2(\mathrm{D}^2)} - - - (D.4)$$

In a simple shear $\dot{\gamma}$ reduces to the velocity gradient.

When non-isothermal low is modeled, POLYFLOW calculates the temperature, velocity,and pressure fields simultaneously (i.e., fully coupled, unless otherwise specified by a change in the default numerical parameters).

1) Shear-Rate-Dependent Viscosity Laws

The isothermal viscosity laws will be presented in this section

I. Constant : For Newtonian fluids, a constant viscosity Can be specified

$$\eta = \eta_0 - - - (D.5)$$

$\eta_0$is referred to as the Newtonian or zero-shear-rate viscosity.

II. Power Law:

$$\eta = K(\lambda\dot{\gamma})^{n-1} - - - (D.6)$$

Where K is the consistency factor, λ is the natural time, and n is the power-law index, which is a property of a given material.

It is commonly used to describe the viscous behavior of polymeric materials, with shear rates greater than 2 or 3 decades. If the behavior at low shear rates needs to betted as well, the Bird-Carreau or Cross law

III. Bird-Carreau Law:

$$\eta = \eta_\infty + (\eta_0 - \eta_\infty)(1 + \lambda^2\dot{\gamma}^2)^{\frac{n-1}{2}} - - - (D.7)$$

Where

η_∞= infinite-shear-rate viscosity

η_0= zero-shear-rate viscosity

λ = natural time (i.e., inverse of the shear rate at which the fluid changes from Newtonian to power-law behavior) and n = power-law index

IV. Cross Law

$$\eta = \frac{\eta_0}{1 + (\lambda\dot{\gamma})^m} - - - (D.8)$$

Where

η_0= zero-shear-rate viscosity

λ = natural time (i.e., inverse of the shear rate at which the fluid changes from Newtonian to power-law behavior)

m = Cross-law index (= 1 - n for large shear rates)

V. Modified Cross law

$$\eta = \frac{\eta_0}{1 + (\lambda\dot{\gamma})^m} - - - (D.9)$$

VI. Bingham Law

$$\eta = \begin{cases} \eta_0 + \dfrac{\tau_0}{\dot{\gamma}}, & \dot{\gamma} \geq \dot{\gamma}_c \\ \eta_0 + \dfrac{\tau_0\left(2 - \frac{\dot{\gamma}}{\dot{\gamma}_c}\right)}{\dot{\gamma}_c}, & \dot{\gamma} < \dot{\gamma}_c \end{cases} - - - (D.10)$$

Where

τ_0 is the yield stress and $\dot{\gamma}_c$ is the critical shear rate, beyond which Bingham's constitutive equation is applied. For shear rates less than $\dot{\gamma}_c$, the behavior of the fluid is normalized in order to guarantee appropriate continuity properties in the viscosity curve.

The Bingham law is commonly used to describe materials such as concrete, mud, dough, and toothpaste, for which a constant viscosity after a critical shear stress is a reasonable assumption, typically at rather low shear rates.

VII. Modified Bingham Law

$$\eta = \eta_0 + \tau_0 \left(\frac{1 - \exp(-m\dot{\gamma})}{\dot{\gamma}} \right) - - - (D.11)$$

Where $m = 3/\dot{\gamma}_c$

Compared to the standard Bingham law, the modified Bingham law is an analytic expression, which means that it may be easier for POLYFLOW to calculate, leading to a more stable solution.

VIII. Herschel-Bulkley Law

$$\eta = \begin{cases} \eta_0 + \frac{\tau_0}{\dot{\gamma}} + K(\frac{\dot{\gamma}}{\dot{\gamma}_c})^{n-1}, & \dot{\gamma} > \dot{\gamma}_c \\ \frac{\tau_0 \left(2 - \frac{\dot{\gamma}}{\dot{\gamma}_c}\right)}{\dot{\gamma}_c} + K\left[((2-n) + (n-1)\frac{\dot{\gamma}}{\dot{\gamma}_c}\right], \dot{\gamma} \leq \dot{\gamma}_c \end{cases} - - - (D.12)$$

Where

τ_0 is the yield stress, $\dot{\gamma}_c$is the critical shear rate, *K* is the consistency factor, and

n is the power-law index. Like the Bingham law, the Herschel-Bulkley law is commonly used to describe materials such as concrete, mud, dough, and toothpaste, for which a power-law viscosity after a critical shear stress is a reasonable assumption.

IX. Modified Herschel-Bulkley Law

$$\eta = \tau_0 \left(\frac{1 - \exp(\frac{3\dot{\gamma}}{\dot{\gamma}_c})}{\dot{\gamma}} \right) + K(\frac{\dot{\gamma}}{\dot{\gamma}_c})^{n-1} - - - (D.13)$$

Compared to the standard Herschel-Bulkley law, the modified Herschel-Bulkley law is an analytic expression, which means that it may be easier for POLYFLOW to calculate, leading to a more stable solution.

X. Log-Log Law

$$\eta = \eta_0 10^{a_0 + a_1\left[\log(\frac{\dot{\gamma}}{\dot{\gamma}_c}) + a_{11}\log(\frac{\dot{\gamma}}{\dot{\gamma}_c})^2\right]} - - - (D.14)$$

Where

$\eta_0$is the zero-shear-rate viscosity and a_0, a_1, and $a_{11}$are the coefficients of the polynomial expression. This viscosity law is purely empirical, but sometimes provides a better t to experimental data than the others.

XI. Carreau-Yasuda Law

$$\eta = \eta_\infty + (\eta_0 - \eta_\infty)(1 + (\lambda\dot{\gamma})^a)^{\frac{n-1}{a}} - - - (D.15)$$

Where
η_∞= infinite-shear-rate viscosity
η_0= zero-shear-rate viscosity
λ = natural time (i.e., inverse of the shear rate at which the fluid changes from Newtonian to power-law behavior)
a = index that controls the transition from the Newtonian plateau to the power-law region
n = power-law index

The Carreau-Yasuda law is a slight variation on the Bird-Carreau law (Equation 10.2-7).The addition of the exponent a allows for control of the transition from the Newtonian plateau to the power-law region. A low value (a < 1) lengthens the transition, and a high value (a > 1) results in an abrupt transition.

2) Temperature-Dependent Viscosity Laws

If the flow is non-isothermal, the temperature dependence of the viscosity must be taken into account along with the shear-rate dependence. The viscosity law can be factorized as follows:

$$\eta = H(T)\eta_0(\dot{\gamma}) - - - (D.16)$$

Where
$H(T)$is the Arrhenius law (or one of the other available laws) and $\eta_0(\dot{\gamma})$is the viscosity law at some reference temperature T (as computed by one of the shear-rate dependent laws described above)

I. Arrhenius Law

$$H(T) = exp\left[\alpha\left(\frac{1}{T - T_0} - \frac{1}{T_\alpha - T_0}\right)\right] - - - (D.17)$$

Where
α is the energy of activation and T_α is a reference temperature for which $H(T) = 1$.
The reference temperature T_0 is set to 0 by default, so T and T_α are absolute temperatures. They can also be defined relative to a non-zero reference temperature.

II. Approximate Arrhenius Law

$$H(T) = exp[\alpha(T - T_\alpha)] - - - (D.18)$$

The behavior described by Equation 10.2-19 is similar to that described by Equation 10.2-17 in the neighborhood of T_α . Equation 10.2-19 is valid as long as the temperature difference $T - T_\alpha$ is not too large.

III. Fulcher Law

$$H(T) = 10^{-f_1 + \frac{f_2}{T - f_3}} - - - (D.19)$$

Where

f_1, f_2, and f_3 are the Fulcher constants. The Fulcher law is used mainly for glass.

IV. WLF Law

The Williams-Landel-Ferry (WLF) equation is a temperature-dependent viscosity law that fits experimental data better than the Arrhenius law for a wide range of temperatures, especially close to the glass transition temperature:

$$Ln\big(H(T)\big) = \frac{c_1(T_r - T_a)}{c_2 + (T_r - T_a)} - \frac{c_1(T - T_a)}{c_2 + (T - T_a)} - - - (D.20)$$

Where

c_1 And $c_2$are the WLF constants, and T_r and T_a are reference temperatures.

Appendix E: Boundary conditions in ansys Polyflow**(Inc., August 26, 2003a)**

Solving a problem in POLYFLOW requires that you prescribe information about the low along the boundary of the computational domain for each sub-task. Solving a time dependent low also requires that you prescribe initial conditions within the domain, as Time-Dependent Flows. In addition, for viscoelastic lows, boundary conditions for the viscoelastic part of the constitutive equation are required at inlets. These represent the contribution to the constitutive equation from the past history of material particles entering the low domain.

The domain of the sub-task is surrounded by closed curves (in 2D) or surfaces (in 3D) consisting of boundary sets and intersections with adjacent sub domains that are not included in the sub-task. Each of these curves or surfaces is referred to as a boundary. The boundary conditions available in POLYDATA are as follows:

i. Interface

It is condition establishes the continuity between the two sides of an intersection between different sub-tasks. For the momentum equation, the interface condition guarantees continuity of the velocity yield and of the contact forces.

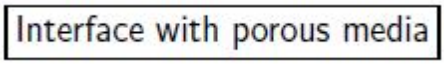

ii. normal and tangential velocity imposed

The normal and tangential velocity condition allows you to specify the normal and tangential velocity components on the boundary section. The normal velocity component is denoted by v_n and the tangential component byv_s. The default condition corresponds to$v_n = v_s = 0$, but you can assign non-zero values for one or both of the components.

iii. normal and tangential force imposed

It is similar to the normal and tangential velocity condition was described before, this condition is typically used for exit sections of free surface problems. And fn and fs are surface force densities expressed, for example, in Pa. A traction force on the boundary section produces a

positive fn. A counterclockwise tangential force produces a positive value of fs (in 2D). In 3D, due to orientation conventions (as is the case for the tangential velocity component), it is difficult to assign a non-zero value for fs. If the tangential force in a 3D problem is non-zero, you should use the global force condition instead.

Normal and tangential forces imposed (fn, fs)

iv. normal velocity and tangential force imposed

Use of this condition is for the upper free surface of a basin with zero normal velocity and zero shear forces (or full slip along a wall). Another example is a moving boundary with an imposed uniform value of vn and, in case of slip, a zero value of fs. As mentioned in the previous sections, zero values for vn and fs are most common, but non-zero values are also possible (although not a non-zero value for fs in 3D). If the tangential force in a 3D problem is non-zero, you should use the global force condition instead.

Normal velocity and tangential force imposed (vn, fs)

v. normal force and tangential velocity imposed

Use of this condition is for an exit section where the normal force is zero and the tangential.

Normal force and tangential velocity imposed (fn, vs)

vi. slip conditions

For the slip condition in POLYFLOW, a zero normal velocity component is imposed simultaneously with one of three relationships between the shear force and the tangential relative velocity.

$$f_s = F_{\text{slip}}(v_{wall} - v_s)|v_s - v_{wall}|^{e_{\text{slip}}-1}$$

Where v_s the tangential velocity of the fluid, v_{wall} is the tangential velocity of the wall, and F_{slip} and e_{slip} are material parameters. v_{wall} is assumed to be zero, by default. Note that full slip is obtained when $F_{\text{slip}} = 0$. Eq () is either linear, with $e_{\text{slip}} = 1$, or of the full power law type with $0 < e_{\text{slip}} < 1$.

User Inputs for the Slip Condition

1. Select the Slip conditions menu item in the list of boundary condition choices.

Slip conditions

2. Set the value for the velocity of the wall (v_{wall}).

Define v_wall, the velocity of the wall

To assign a rotational velocity in 3D, specify the 1st point of the axis, 2nd point of the axis, and angular velocity.

vii. Symmetry

The symmetry condition is equivalent to imposing zero values for the normal velocity and tangential force.

Plane of symmetry (fs=0, vn=0)

viii. Inflow

The inflow condition allows you to specify a volumetric flow rate across a boundary section surrounded by other boundary sections with well-defined adhesion conditions (slip, no slip, symmetry, etc.).

ix. Outflow

The outflow condition in POLYFLOW is different for generalized Newtonian low and
Viscoelastic low.

- Outflow Condition for Generalized Newtonian Flow

The outflow condition for generalized Newtonian low is similar to the normal force and tangential velocity condition described above, Normal Force and Tangential Velocity Condition, with $f_n = 0$ and $v_s = 0$. It replaces a long channel at the exit of the flow domain by a single boundary condition. Note that an outflow condition can take into account deformations of the flow domain in the downstream channel.

x. free surface

POLYFLOW it has advanced features for the calculation of free surfaces. Along such boundary sections, surface forces are imposed while the liquid cannot cross the free surface.